

1-1-2002

Preparation of ordered nanocomposites in polymeric templates swollen by supercritical carbon dioxide.

Garth D. Brown

University of Massachusetts Amherst

Follow this and additional works at: https://scholarworks.umass.edu/dissertations_1

Recommended Citation

Brown, Garth D., "Preparation of ordered nanocomposites in polymeric templates swollen by supercritical carbon dioxide." (2002).
Doctoral Dissertations 1896 - February 2014. 1040.
https://scholarworks.umass.edu/dissertations_1/1040

This Open Access Dissertation is brought to you for free and open access by ScholarWorks@UMass Amherst. It has been accepted for inclusion in Doctoral Dissertations 1896 - February 2014 by an authorized administrator of ScholarWorks@UMass Amherst. For more information, please contact scholarworks@library.umass.edu.



312066 0288 0651 5

**PREPARATION OF ORDERED NANOCOMPOSITES IN POLYMERIC
TEMPLATES SWOLLEN BY SUPERCRITICAL CARBON DIOXIDE**

A Dissertation Presented

by

GARTH D. BROWN

Submitted to the Graduate School of the
University of Massachusetts Amherst in partial fulfillment
of the requirements for the degree of

DOCTOR OF PHILOSOPHY

September 2002

Polymer Science and Engineering

PREPARATION OF ORDERED NANOCOMPOSITES IN POLYMERIC
TEMPLATES SWOLLEN BY SUPERCRITICAL CARBON DIOXIDE

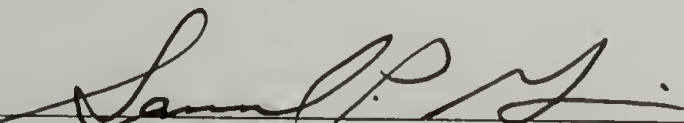
A Dissertation Presented

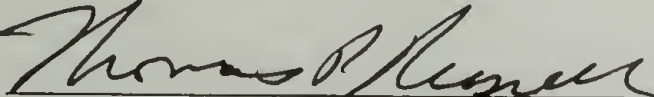
by

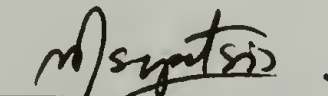
GARTH D. BROWN


Approved as to style and content by:


James J. Watkins, Chair


Samuel P. Gido, Member


Thomas P. Russell, Member


Michael Tsapatsis, Member


Thomas J. McCarthy, Department Head
Department of Polymer Science and Engineering

DEDICATION

I want to dedicate this to my family and my friends that have made my time here at UMass enjoyable.

ACKNOWLEDGEMENTS

I have to first and foremost acknowledge my advisor Dr. James J. Watkins. I am glad that I have had the chance to work with him and must thank him more than probably is realized for supporting me during a difficult time in the fall of 2001. The research directions that the group is heading are in new and exciting directions for industry. I also want to thank my committee for the input on my dissertation, Dr. Sam Gido, Dr. Tom Russell, and Dr. Michael Tsapatsis.

I also have to thank Paul, Gary and Joe of the Chemical Engineering Shop. They have been an incredible group of guys to talk with, advise me on fixing my truck, and an amazing resource for building lab equipment, such as Gary's ability to build a melt press out of some scrap metal, heating cartridges and a C-clamp. I also must thank the help that was received from other people, such as Dr. Alan Waddon for his help with the X-ray equipment and analysis, Eileen Besse who I think the PSE department would crumble without, Lou Raboin for his help with the electron microscopes. I also must thank the members of the Watkins group. It has been a pleasure to work with, especially the more "senior" members and people that I've worked closely with VJ, Bryan, Jason B., Danielle, Dave, Jason L., Albertina, Scott, Ravi, and the rest of the group.

I must also acknowledge some other good friends from school. Mike P., who was always there to go sledding in a snowstorm, Doug for being a great roommate and friend, Mike L. for being a great friend and running partner, Lou for introducing me to winter mountaineering, Ben who still needs to learn where the town lines are and should also not quit his day job to pursue a career in singing, and Amanda for getting me up so many mornings for swimming.

I also want to thank people whom I gotten to know that have nothing to do with school, including Mark, Dave, Rich, John's, Chris's, Pete, Elissa, Adam, and Doug from the Northampton Cycling Club and the countless other riders out there in NCC blue, members of Troop 504, especially Don, Gabe, and Bill, the Masters swim team especially Ed, John, and Laura.

Finally, I have to thank the "gang," Dan, Ludi, Jack, Chris, Scott, and Jen. I could go on for days, talking about experiences, such as the 1999 Lake Placid Ironman Triathlon, with them and I can't image the number of thousands of miles that we've ridden together. I'm at a complete loss of words to describe how much this group has meant to me and affected my life. I can just say that its been a privilege to know them.

ABSTRACT

PREPARATION OF ORDERED NANOCOMPOSITES IN POLYMERIC TEMPLATES SWOLLEN BY SUPERCRITICAL CARBON DIOXIDE

SEPTEMBER 2002

GARTH D. BROWN,

B.S., UNIVERSITY OF MISSOURI – ROLLA

M.S., UNIVERSITY OF MASSACHUSETTS AMHERST

Ph.D., UNIVERSITY OF MASSACHUSETTS AMHERST

Directed by: Professor James J. Watkins

Nanocomposites are of interest for numerous applications such as catalysis, photonic band gap materials, and waveguides. Ionomers and diblock copolymers have previously been used as templates for ordered nanocomposites. However, these processes have been limited to reactions within thin films or coprecipitation methods from solution due to mass transport limitations of ceramic and metallic precursors within the solid templates. This issue has been addressed by fabricating ordered nanocomposites using phase selective deposition of precursors into supercritical carbon dioxide (SC-CO₂) swollen polymeric templates. SC-CO₂ is an effective plasticizing agent for most polymers and enhances mass transport of the precursors into polymeric templates while preserving the initial template morphology. By proper choice of template material, the precursor can be selectively bound within one phase of the template and reacted to produce the desired material. The resulting composite contains nanoparticles arranged in an ordered morphology dictated by the template over bulk

dimensions. Polymer/ceramic and polymer/metal nanocomposites have been successfully synthesized using this technique.

TABLE OF CONTENTS

	Page
ACKNOWLEDGEMENTS.....	v
ABSTRACT.....	vii
LIST OF TABLES.....	xii
LIST OF FIGURES.....	xiii
CHAPTER	
1. INTRODUCTION.....	1
1.1 Project Overview.....	1
1.2 Overview of Nanocomposite Materials.....	3
1.2.1 Applications of Nanocomposite.....	3
1.2.1.1 Active Nanoparticles.....	4
1.2.1.2 Collections of Nanoparticles.....	6
1.2.1.3 Polymer Modification.....	7
1.2.2 Nanoparticle Chemistry.....	8
1.2.2.1 Ceramic Nanoparticles.....	8
1.2.2.2 Metal Nanoparticles.....	12
1.2.2.3 Metal Sulfide Nanoparticles.....	13
1.2.3 Nanocomposite Fabrication Methods.....	13
1.2.3.1 Disordered Nanocomposites.....	15
1.2.3.1.1 Disordered Polymer/Ceramic Nanocomposites.....	15
1.2.3.1.2 Disordered Polymer/Metal Nanocomposites.....	17
1.2.3.1.3 Disordered Polymer/Metal Sulfide Nanocomposites.....	18
1.2.3.2 Ordered Nanocomposites.....	18
1.2.3.2.1 Natural Nanocomposites.....	19
1.2.3.2.2 Surfactant Templates.....	19
1.2.3.2.3 Liquid Crystal Templates.....	21
1.2.3.2.4 Polymeric Ionomer Templates.....	22
1.2.3.2.5 Block Copolymer Templates.....	24

1.2.4 Nanoparticle Size and Aggregation	31
1.3 Background on Supercritical Fluids.....	37
1.3.1 Use of SCF's in Polymers	38
1.3.2 Small Molecules in SCF-Swollen Polymers	40
1.3.3 SCF – Polymer Phase Behavior	41
1.3.4 Supercritical Fluids and Nanoparticles	42
2. POLYMER / CERAMIC NANOCOMPOSITES.....	44
2.1 Introduction.....	44
2.2 Experimental Section	44
2.2.1 Materials.....	45
2.2.2 TEOS/CO ₂ Phase Behavior.....	45
2.2.3 Silicon Dioxide Deposition.....	48
2.2.4 Nafion/Ceramic Nanocomposites	50
2.2.4.1 Water Uptake into Nafion	50
2.2.4.2 Nafion Pretreatment	52
2.2.4.3 TEOS Reactions in Nafion.....	53
3. POLY(STYRENE)- <i>BLOCK</i> -POLY(ACRYLIC ACID) NANOCOMPOSITES.....	61
3.1 Introduction.....	61
3.2 Experimental Section	62
3.2.1 Materials.....	62
3.2.2 Polystyrene/Platinum Metal Nanocomposites	64
3.2.3 PS- <i>b</i> -PAA / Metal Nanocomposites	68
3.2.3.1 PS- <i>b</i> -PAA / Platinum Nanocomposites.....	70
3.2.3.2 PS- <i>b</i> -PAA / Silver Nanocomposites	76
3.2.3.3 Other Metals in PS- <i>b</i> -PAA.....	78
3.2.4 Metal Sulfides into PS- <i>b</i> -PAA.....	80
4. POLYSTYRENE- <i>BLOCK</i> -POLY(VINYL PYRIDINE) NANOCOMPOSITES.....	83
4.1 Introduction.....	83
4.2 Experimental Section	84
4.2.1 Materials.....	84
4.2.2 Platinum Precursor Partitioning Between Polystyrene and CO ₂	87
4.2.3 Phase Selectivity of the Organometallics.....	90

4.2.4 PS- <i>b</i> -PVP / Platinum Nanocomposites	93
4.2.4.1 PS- <i>b</i> -P4VP Copolymer	94
4.2.4.2 PS- <i>b</i> -P2VP Copolymer	98
4.2.5 PS- <i>b</i> -P2VP / Silver Nanocomposites	103
CONCLUSIONS AND FUTURE DIRECTIONS.....	110
APPENDIX: NANOPARTICLE MOVEMENT	115
BIBLIOGRAPHY	118

LIST OF TABLES

Table	Page
1.1 Selected Disordered Polymer Nanocomposites.....	14
1.2 Selected Ordered Polymer Nanocomposites.....	15
1.3 Physical Properties of Liquids, Gases and SCF's.....	38
2.1 Reaction Condition of Deposited Silicon Dioxide Films	49
3.1 Preparation of Platinum Nanoparticles in Polystyrene	68
3.2 Various Reduction Conditions of Platinum precursor in PS- <i>b</i> -PAA.....	71
4.1 PS- <i>b</i> -PVP Copolymers Used as Templates	85
4.2 Distribution of Ag(COD)hfac Between PS and P2VP	90

LIST OF FIGURES

Figure	Page
1.1 Reaction scheme for the fabrication of ordered nanocomposites using SC-CO ₂ swollen polymeric templates.....	2
1.2 General reaction scheme for sol-gel chemistry.....	9
1.3 Sol-gel chemistry of tetraethylorthosilicate.....	10
1.4 Structure of two silicon dioxide network modifiers, DEDMS and GLYMOS.....	11
1.5 Reduction of (1,5-cyclooctadiene) dimethylplatinum with hydrogen.....	13
1.6 Schematic of the cooperative organization of silicate-surfactant mesophases.....	21
1.7 Chemical structure of protonated Nafion.....	23
1.8 Model of Nafion ionomer.....	23
1.9 Generic block copolymer morphology.....	25
1.10 Phase diagram of a poly(isoprene- <i>b</i> -styrene) copolymers ^{132, 134}	27
1.11 Diffusion of 20 nm gold nanoparticles in poly(2-vinyl pyridine) ¹⁴⁸	36
1.12 SC-CO ₂ density isotherms ¹⁵⁹	38
1.13 Block copolymer phase diagram.....	41
2.1 Schematic of variable volume view cell used to determine solubility.....	46
2.2 Phase behavior of TEOS in SC-CO ₂	48
2.3 Deposition of silicon dioxide films on silicon wafers.....	49
2.4 Uptake of neat water into Nafion.....	51
2.5 Nafion uptake of water from humidified SC-CO ₂	52
2.6 Weight percent increase of SiO ₂ in Nafion nanocomposites upon reaction in a TEOS/ <i>n</i> -propanol solution.....	54
2.7 Weight percent increase of SiO ₂ in Nafion nanocomposites upon reaction of TEOS/SC-CO ₂	55

2.8 TEM micrograph of unmodified Nafion.....	56
2.9 TEM micrograph of 7 weight percent SiO ₂ Nafion/ceramic nanocomposite	57
2.10 WAXS of Nafion and Nafion/silica nanocomposites	58
2.11 SAXS of Nafion/ceramic nanocomposites	59
3.1 Polystyrene- <i>block</i> -poly(acrylic acid) copolymer.....	63
3.2 Metal precursors for nanoparticle formation	64
3.3 H ₂ reduction to produce ~10 nm Pt nanoclusters in PS	66
3.4 CO ₂ /H ₂ reduction to produce ~30 nm Pt nanoclusters in PS	67
3.5 WAXS of platinum nanoparticles in polystyrene	67
3.6 Copolymer templating process	69
3.7 Platinum precursor in PS- <i>b</i> -PAA before reduction	72
3.8 Platinum/PS- <i>b</i> -PAA nanocomposite subjected to Reduction A.....	73
3.9 Platinum/PS- <i>b</i> -PAA nanocomposite subjected to Reduction B	74
3.10 Platinum/PS- <i>b</i> -PAA nanocomposite subjected to Reduction C	75
3.11 Silver precursor in PS- <i>b</i> -PAA before reduction	77
3.12 Silver/PS- <i>b</i> -PAA nanocomposite after reduction.....	78
3.13 Various Metal/PS- <i>b</i> -PAA Nanocomposites.....	79
3.14 Lead Sulfide in polystyrene- <i>block</i> -Poly(acrylic Acid)	82
4.1 Polystyrene- <i>block</i> -poly(vinyl pyridine) copolymers	85
4.2 Platinum and silver precursors.....	86
4.3 Mass uptake of Pt(COD)Me ₂ within PS infused with CO ₂ at 60 °C and different pressures.....	88
4.4 Mass uptake of Pt(COD)Me ₂ within PS infused with CO ₂ at 60 °C and different densities.....	89

4.5 SEM image indicating strong silver – P2VP binding	91
4.6 Close-up of interface between silver and neat P2VP	92
4.7 WAXS of silver nanoparticles within homopolymer P2VP prepared at 40 °C	93
4.8 PS- <i>b</i> -P4VP copolymer stained with iodine	94
4.9 Platinum infused PS- <i>b</i> -P4VP before H ₂ reduction	96
4.10 Platinum infused PS- <i>b</i> -P4VP after H ₂ reduction	97
4.11 Platinum nanoparticles in PS- <i>b</i> -P2VP	99
4.12 Electron diffraction of a PS- <i>b</i> -P2VP/platinum nanocomposite	101
4.13 WAXS of a PS- <i>b</i> -P2VP/platinum nanocomposite	102
4.14 Evolution of platinum peak observed in WAXS in a PS- <i>b</i> -P2VP copolymer	103
4.15 Silver nanoparticles within cylindrical P2VP domains of PS- <i>b</i> -P2VP prepared using reactions at 60 °C	105
4.16 Silver precursor within PS- <i>b</i> -P2VP prior to the addition of hydrogen prepared using reactions at 40 °C	106
4.17 Silver nanoparticles within cylindrical P2VP domains of PS- <i>b</i> -P2VP prepared using reactions at 40 °C	107
4.18 TEM of silver interface within PS- <i>b</i> -P2VP prepared using reactions at 40 °C	108
4.19 Close-up of interface TEM of silver interface within PS- <i>b</i> -P2VP from reactions at 40 °C	109
A.1 Silver nanoparticles within P2VP	116
A.2 Silver nanoparticles within P2VP after heating at 120 °C	117

CHAPTER 1

INTRODUCTION

1.1 Project Overview

This dissertation describes the preparation of ordered nanocomposites in polymeric templates swollen by supercritical carbon dioxide (SC-CO₂) using the general approach summarized in Figure 1.1. Polymer ionomers and block copolymers have controllable morphologies that can be used as structure-directing templates. Ceramic and metallic precursors were infused into specific domains within polymeric systems from SC-CO₂ solution. Sorption of the SC-CO₂ solution into the polymer matrix mitigates the mass transport limitations for delivering precursors. CO₂ sorption can be controlled at modest levels which can have the added benefit of preserving the long-range order of a block copolymer, which is often not the case with traditional solvents. Upon CO₂ infusion, precursors were selectively bound within an ionic cluster or one phase of the block copolymer, which is the key to the templating process. Under proper reaction conditions, nanoparticles are produced with a morphology dictated by the polymeric template. Nanocomposites composed of the polymeric template containing ceramics, metals, or metal sulfides were prepared in this manner.

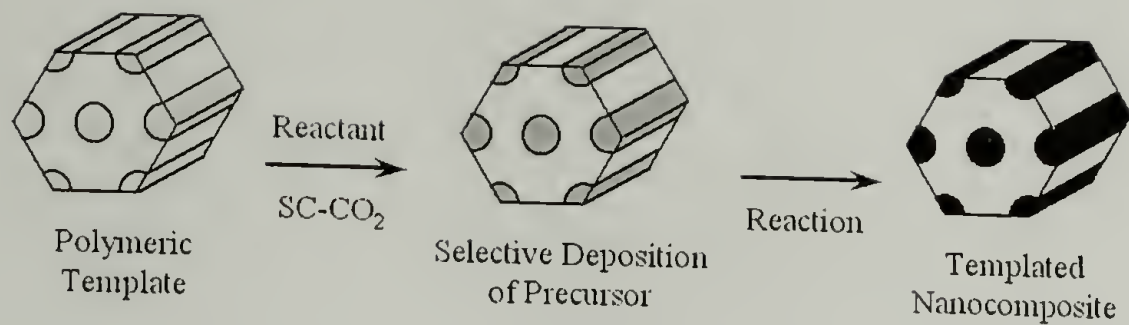


Figure 1.1 Reaction scheme for the fabrication of ordered nanocomposites using SC-CO₂ swollen polymeric templates

The first part of the research project was the formation of templated polymer/ceramic nanocomposites by the *in-situ* sol-gel chemistry within an acidic polymer, Nafion. This is a ionomer that has a fluorinated carbon backbone with pendent sulfonic acid groups organized into ionic clusters. SC-CO₂ was used to deliver a ceramic precursor, tetraethylorthosilicate (TEOS), into the polymer film. Condensation of the precursor via sol-gel chemistry within the acidic ionic cluster of the polymer produced a silicon dioxide (SiO₂) network structure. The next two sections of the research project focused largely on the formation of templated metal/polymer nanocomposites using block copolymers templates. The copolymers investigated in the second and third sections were polystyrene-*block*-poly(acrylic acid) and polystyrene-*block*-poly(vinyl pyridines). Each of these copolymer systems has one phase which is able to undergo chemical binding with an organometallic. Upon dissolving the organometallic in SC-CO₂, it is infused into the polymer systems and metallic nanoclusters are produced upon reduction. The nanocomposites were characterized by several methods, including transmission electron microscopy and wide angle X-ray scattering.

1.2 Overview of Nanocomposite Materials

Nanocomposites are materials composed of two or more components in which the size scale of at least one of the domains is on the order of 1 to 100's of nanometers. These materials are often polymer matrices filled with a second inorganic phase of ceramics, metals or metal sulfides. The applications of nanocomposites are varied depending on the functionality of the minor component. For example, mechanical properties of polymers can be improved with ceramic fillers¹ and polymers filled with specific sizes of metal nanoparticles can yield optical devices.²⁻⁴

Three levels of control are critical for dictating nanocluster properties: composition, size and ordering. Nanoparticle chemistry controls the chemical makeup of the second phase which is commonly ceramic, metal, or metal sulfide nanoparticles. Discrete clusters with well defined properties can be produced by a number of techniques involving molecular self-assembly of structure directing agents including surfactants,^{5, 6} liquid crystals,^{6, 7} ionomers,⁸⁻¹⁵ and block copolymers.^{2, 4, 16-54} These self-assembled materials are often commensurate with the size of desired nanoparticles and can direct their architecture. However, to fabricate many practical devices, the long-range order of nanoparticles must be controlled over bulk dimensions. The limitations of current methods results from the nature of the template, including mass transport limitations of reactants through solid templates such as block copolymers and the fragility of bicontinuous surfactant phases in solution.⁵⁵

1.2.1 Applications of Nanocomposite

The applications of polymer-based nanocomposites arise from the functionality imparted by the formation of a second domain. These applications can be broken down into

three different classes depending on the functionality of nanoparticles. The first case is that in which the small nanoparticles themselves give rise to the desired properties. An example is a quantum dot. The second case includes applications in which the nanoparticles as a group collectively impart functionality. An example is modifying the refractive index of a copolymer phase for potential optical applications. The third case arises when the nanoparticles impart modification of the entire polymer, such as fillers providing improved mechanical properties.

1.2.1.1 Active Nanoparticles

Nanoparticles can be prepared and encapsulated within supports, such as polymers, to produce nanocomposites in which the nanoparticles themselves impart active functionality. Applications for nanocomposites of polymers containing nanosized metal and semiconductor particles arises from quantum effects and large surface to volume ratios of the active nanoparticles. Extremely small nanoparticles, often less than 1 nanometer in size, are often called quantum dots, consisting of a few hundred atoms to less than ten with properties between that of a single atom and bulk material.^{31, 56, 57} This unique region of ultra-small sizes gives an incompletely developed electronic band-gap structure, that are tunable with particle size. The large surface/volume ratios of nanoparticles also have been used to explain the different properties compared to bulk material, which have low surface/volume ratios.^{31, 56-58} For example, a 2 nm platinum nanoparticle consists of about 280 atoms with about 100 in the 'bulk like' interior. In contrast, a 0.7 nm platinum nanoparticle consists of about 12 atoms, all on the surface.⁵⁸

Lack of a fully developed electronic structure gives rise to the unusual size-dependent optical properties, such as an absorption spectrum that is "blue shifted" as particles become smaller, leading to applications for optical devices.^{2, 3, 56, 59-62} By controlling the size of small nanoparticles, the wavelength of light transmitted or reflected, from infrared to ultraviolet, can be precisely controlled. This leads to devices such as optical filters, where only one wavelength of light is allowed to pass through the sample.⁶³⁻⁶⁵ Specific absorbances could make it possible to produce nanocomposite films in a wide range of colors.

Nanoparticles with unusual magnetic properties have been prepared within polymer supports and investigated by various research groups.^{4, 62, 66, 67} These nanocomposites have particles small enough such that each one acts as a single magnetic domain and can exhibit phenomena such as superparamagnetism, where the domains are small enough to lose their magnetic field due to thermal fluctuations.⁵⁷ An example of a magnetic nanocomposite produced in a copolymer is an optically transparent film containing magnetic nanoparticles of ferric oxide, with magnetic properties different from that of the bulk ferric oxide.⁴ Other magnetic nanocomposites have been prepared with cobalt nanoparticles in poly(acrylonitrile)⁶⁷ and with non-polymeric materials such as nickel within a silica support.⁶⁶

The preparation of nanoparticles for catalytic applications has been studied by numerous groups.^{21, 25, 26, 33, 34, 36, 37, 68-70} The majority of work has been in the area of palladium and platinum nanoparticles stabilized within polymeric supports. Examples of catalytic studies using nanocomposites include catalytic cracking of ¹³C-labeled 2-methylpentane⁶⁸ and hydrogenation of ethylene and propylene.²⁵ Studies have shown that the smaller sized nanoparticles had a greater catalytic activity due to the larger surface area.²⁵

The polymer matrix also influences the catalytic activity,^{34, 36, 37} and the shape of the nanoparticle is important.⁷¹ Polymers play an important role in nanocomposites with active nanoparticles. Nonconductive, transparent, permeable and easily processable polymers are frequently used as the matrix for nanoclusters.^{28, 29, 62} The polymer matrix serves several purposes including: 1) stabilization of the colloidal dispersion and prevention of the agglomeration of the nanoparticles, 2) protection of surfaces from contaminate deactivation, and 3) tailoring the surface properties of the particles.^{33, 35} Nanoparticles in matrices other than polymers such as water microemulsions and aluminum oxide have also been prepared and investigated.⁶⁸

1.2.1.2 Collections of Nanoparticles

The presences of nanoparticles can influence the bulk properties of the matrix in which they are distributed, such as in dielectrics and optical materials. Optical devices produced from nanocomposites in which one component collectively adds functionality is potentially one very important application. An example of this is the preparation of photonic crystals using emulsion templates.⁶⁴ In this example, colloidal crystals of oil droplets acted as a template for titania, which was subsequently calcined, to produce inorganic optical material.⁶⁴

Ordered nanocomposites fabricated in the manner presented in this dissertation can be used for optical applications. First a film of a high molecular weight lamellar block copolymer could be annealed in SC-CO₂ with spacings that are on the order of the wavelength of light.⁷² Modification of the film, by methods presented here (Figure 1.1),

could alter the refractive index of one phase to fabricate highly ordered nanocomposites. These could be capable of interacting with light to produce devices such as optical mirrors.

1.2.1.3 Polymer Modification

Nanocomposites can also be prepared for applications in which nanoparticles modify the mechanical properties of a second phase. The most common example of this are polymeric materials filled with ceramic nanoparticles. The fillers have been placed into polymeric matrixes by one of two basic methods: 1) mechanical mixing of different components or 2) *in-situ* formation of one or both of the phases.

Polymer-ceramic nanocomposites have been prepared by annealing a mixture of silicates and polymers statically or under shear.⁷³⁻⁷⁵ Intercalation of the polymer chains between silicate layers produced the nanocomposite. The polymer-silicate nanocomposites exhibited improved modulus, reduced gas permeability, increased solvent resistance, decreased thermal expansion coefficient, and enhanced ionic conductivity over the unmodified polymer.⁷³⁻⁷⁵

Nanocomposites have also been prepared by the *in-situ* formation of ceramic phases within polymers for improved mechanical properties. Surface hardening of clear plastic windows has been achieved by subsequently carrying out sol-gel chemistry on the polymer surface.^{76, 77} This process produced a silicon dioxide film on the surface that interpenetrated into the top layers of polymer chains. Conversely, ceramic windows have been surface modified with monomers that can undergo both sol-gel chemistry and vinyl polymerization, providing color and decreasing reflectance of glass.⁷⁶

1.2.2 Nanoparticle Chemistry

Different classes of nanoparticles can be produced by different chemistries to control their chemical makeup. These nanoparticles are commonly composed of ceramics, metals, or metal sulfides.

1.2.2.1 Ceramic Nanoparticles

Ceramic nanoparticles can be produced by sol-gel chemistry. This is a widely used and industrially important method for producing high purity ceramics at temperatures much lower than traditional ceramic processing.^{78, 79} The sol-gel process starts with the formation of a colloidal suspension (sol) and gelation of the sol into a continuous liquid or semi-solid phase (gel). The precursors are metals or metalloids with reactive ligands, most commonly metal alkoxides because they readily react with water to further produce an inorganic network structure.

Sol-gel chemistry can be described by three general reactions (Figure 1.2). The first step is hydrolysis of a metal alkoxide by water usually with acid or base catalysis. The subsequent two reactions produce the inorganic network: two hydrolyzed species react to produce metal oxide while liberating water (water condensation) or one hydrolyzed species reacts with the original starting material to yield a metal oxide and alcohol (alcohol condensation). The characteristics and properties of a particular sol-gel inorganic network are related to a number of factors that affect the rate of hydrolysis and condensation reactions such as pH, temperature, time, alkoxide composition, water composition, and catalyst.^{78, 79}

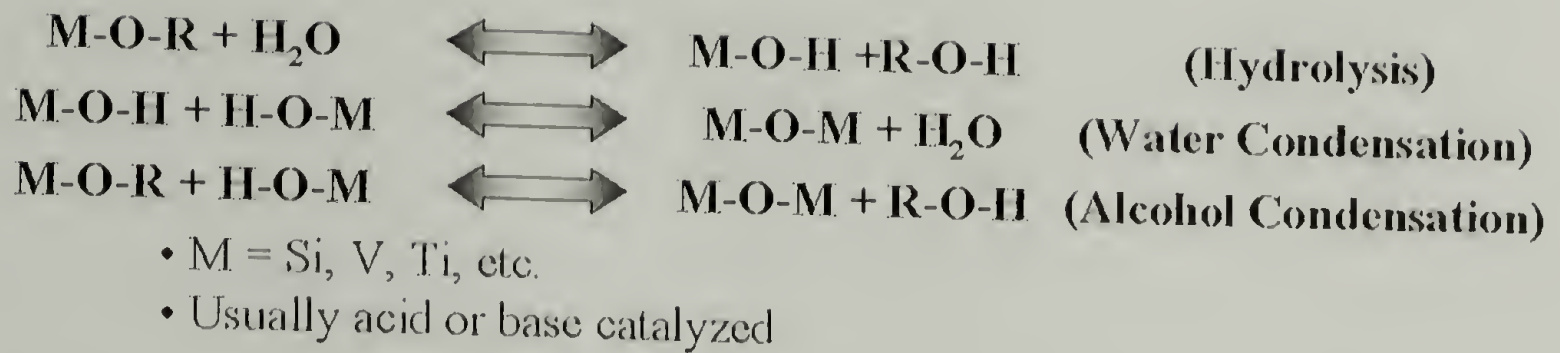
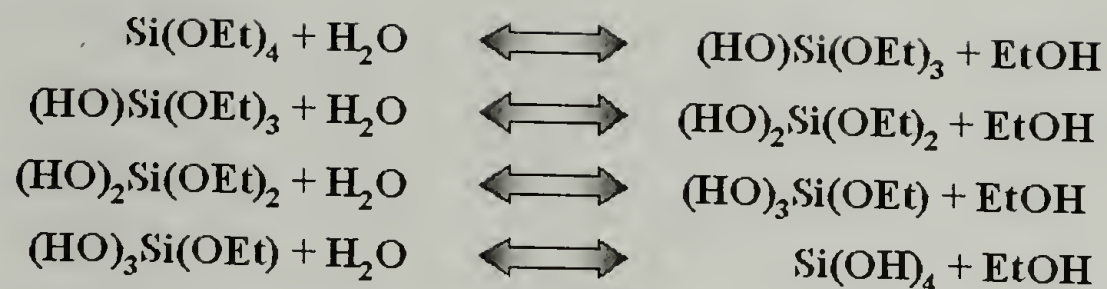


Figure 1.2 General reaction scheme for sol-gel chemistry

The most widely used metal alkoxide is tetraethylorthosilicate (TEOS), which yields silicon dioxide (SiO_2) networks upon condensation (Figure 1.3). The network structure is highly dependent on the pH of reaction. Networks produced under acid-catalyzed conditions yield primarily linear or random branched polymers which entangle upon gelation to form additional branches.⁷⁹ Networks derived under base-catalyzed conditions yield more highly branched clusters that do not interpenetrate prior to gelation and thus behave as discrete clusters.⁷⁹ Tetramethylorthosilicate (TMOS) is structurally similar to TEOS, except the ethoxy side groups are replaced with the shorter methoxy groups. TMOS has similar chemistry to TEOS, but is not as widely used due to its increased reactivity and toxicity.¹ Sol-gel chemistry can be used to produce other metal oxide networks, such as aluminum oxide (Al_2O_3) with the proper choice of precursors such as aluminum butoxide ($Al(OC_4H_9)_3$).^{16, 78}

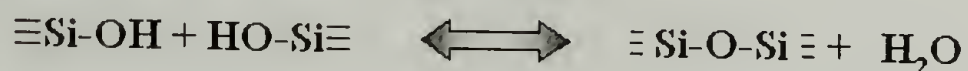
Hydrolysis



Alcohol Condensation (Alcoxolation)



Water Condensation (Oxolation)



Overall Reaction



SiO₂ Network

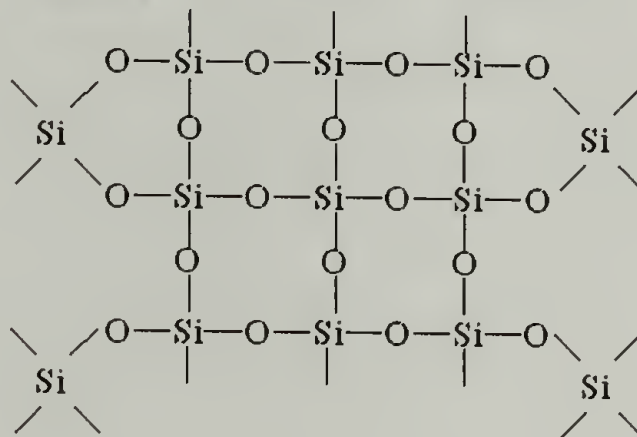


Figure 1.3 Sol-gel chemistry of tetraethylorthosilicate

Sol-gel reactions are also advantageous with respect to versatile functionalities that can be exploited to chemically modify the inorganic network structure.^{11, 12, 16, 78, 80, 81} Diethoxydimethylsilane (DEDMS) is an example of a TEOS derivative in which two ethoxide groups are replaced with two methyl groups (Figure 1.4), resulting in methyl groups within the SiO₂ network structure when co-reacted with TEOS.¹⁰ 3-(Glycidyloxypropyl)trimethoxysilane (GLYMOS) is a modified TMOS and when copolymerized with TEOS, polymerizable epoxide groups are placed within the SiO₂

network structure (Figure 1.4). Temperature sensitive molecules have also been incorporated into the SiO₂ network as a method to make optically transparent biological and chemical sensors.⁸⁰

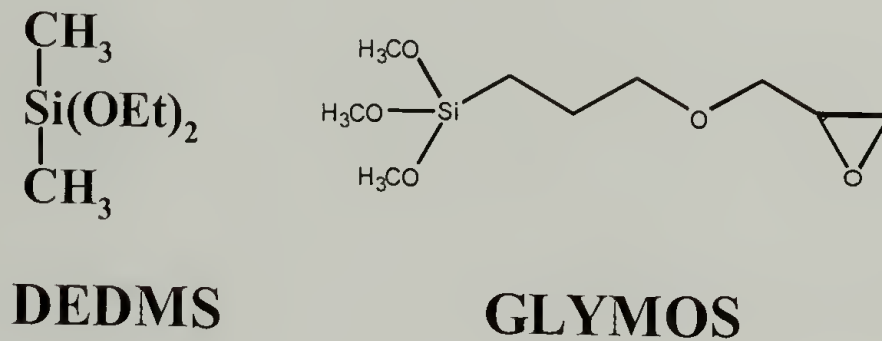


Figure 1.4 Structure of two silicon dioxide network modifiers, DEDMS and GLYMOS

Sol-gel chemistry has been used to make ultra-low density SiO₂ networks called aerogels.^{82, 83} In traditional sol-gel chemistry, solvent removal by evaporation gives rise to large capillary forces within pores which causes a shrinking of the network, potentially leading to cracking and mechanical failure of the xerogel. To prevent collapse due to surface tension, solvent can be removed by heating it above its critical temperature and pressure. The supercritical solvent has zero surface tension and is removed without collapse of the porous network. Sol-gel chemistry is typically conducted in traditional solvents, such as ethanol, followed by exchange by a solvent with more accessible critical conditions, such as carbon dioxide. The CO₂ is then heated into the supercritical state where it was slowly removed to leave behind the highly porous silica network.⁸⁴

1.2.2.2 Metal Nanoparticles

Metal nanoparticles have been prepared by various chemical reactions that involve the reduction of metal ions or organometallics using thermal, photolytic, or chemical means such as reaction with hydrazine or hydrogen. One of the most straightforward ways to make nanoclusters is by the thermal reduction of metal salts within refluxing solvents. For example, palladium acetate was reduced to palladium metal in refluxing methyl isobutyl ketone.^{69, 85} Thermal reduction of (1,5-cyclooctadiene) silver (hexafluoroacetylacetonate) has been used to produce silver nanoclusters.^{22, 86} Gold salts have been photolytically reduced with a laser.^{51, 54} Silver halide can be photolytically reduced with visible light, which is the basis for traditional photography.⁸⁷

Metal nanoparticles have also been produced by the chemical reduction of metal salts or organometallics. For example, hydrazine has been used for the reduction of metal salts for the formation of platinum and palladium alloys.⁶⁸ One of the most common ways to produce metal clusters is the reduction of metal ions or organometallics with hydrogen.^{21-23, 25, 27-29, 34-37, 88-97}

Diolefin dialkylplatinum complexes, such as (1,5-cyclooctadiene) dimethylplatinum (II) [Pt(COD)Me₂], are rapidly reduced by hydrogen to produce platinum metal in an autocatalytic reaction (Figure 1.5).^{90-92, 98} The generated platinum is incorporated into the surface of the platinum particle and the reduction rate is strongly influenced by mass transport and by the surface area of the catalyst. This platinum precursor is also very useful for composite synthesis as it has been reacted with hydrogen to produce platinum nanoclusters within poly(4-methyl-1-pentene)⁹⁶ and platinum films from SC-CO₂ solutions.⁹⁵

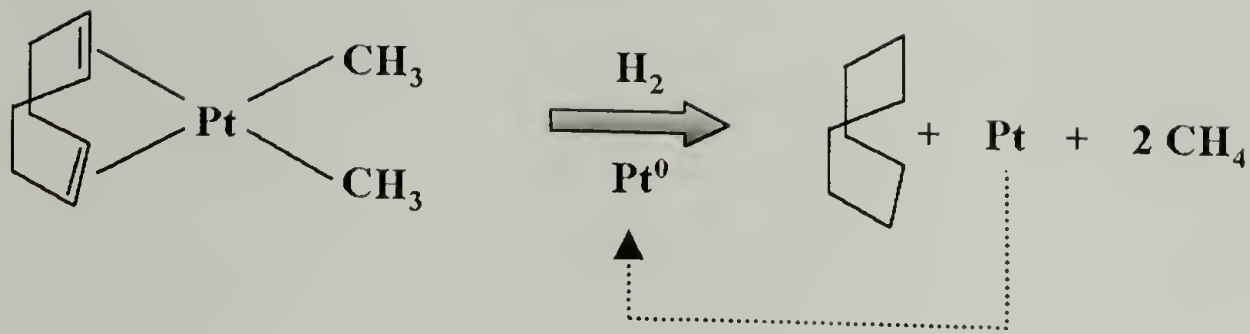


Figure 1.5 Reduction of (1,5-cyclooctadiene) dimethylplatinum with hydrogen

1.2.2.3 Metal Sulfide Nanoparticles

Metal sulfide nanoparticles have been prepared by the reactions of metal salts or organometallics with hydrogen sulfide (H_2S). Most of this work has involved metal sulfide nanocomposites prepared by reacting hydrogen sulfide with metal salts or organometallics within polymeric systems.^{30, 44, 92, 99-104} The precursors can be loaded into polymer systems by solvent casting with the precursors^{30, 44, 99, 102-104} or by mixing the precursors with a monomer solutions followed by polymerization.¹⁰⁰ Volatile metal sulfide precursors, such as diethyl zinc and dimethyl cadmium, have been infused into thin polymeric films directly from the vapor phase.⁹⁹ Once the precursors were loaded into the polymeric systems, treatment with H_2S produced the metal sulfide nanoparticles.

1.2.3 Nanocomposite Fabrication Methods

The fabrication of nanocomposites can be broadly divided into two different categories depending on the final organization of the components, either disordered or ordered. Disordered nanocomposites exhibit a random spatial distribution of nanoparticles, but can have a narrow size distribution. Numerous techniques have been used for fabrication

of randomly distributed nanoparticles within a host matrix. These include polymer/ceramic nanocomposites prepared by melt-pressing polystyrene with silicates fillers,⁷³⁻⁷⁵ polymer/metal nanocomposites prepared by the evaporation of gold nanoparticles into monomers later polymerized,^{89, 105} or by the incorporation of a metal precursor into SC-CO₂ swollen homopolymer followed by hydrogen reduction.⁹⁶ Ordered nanocomposites have been fabricated using molecular self-assembly to produce a template. These self-assembled materials can be commensurate with the size of desired nanoparticles. Examples of self-assembled materials used previously as templates include surfactants,^{5, 6} liquid crystals,^{6, 7} ionomers,⁸⁻¹⁵ and block copolymers.^{2, 4, 16-54} Several examples of disordered and ordered nanocomposites are given in Table 1.1 and Table 1.2 respectively.

Table 1.1 Selected Disordered Polymer Nanocomposites

Polymer	Nanoparticle	Preparation Method
Poly(methyl methacrylate)	SiO ₂	Simultaneous polymerization ¹
Polystyrene	Silicate	Melt pressed ⁷⁴
Polystyrene	Gold	Evaporation of metal into liquid monomer, ¹⁰⁵
Carbon Fiber	Cobalt	Thermal reduction of cobalt precursor ⁶⁷
Nylon 11	Gold	Evaporation of metal onto Nylon 11. ^{106, 107}
PMP	Platinum	Infusion of precursor into homopolymer with SC-CO ₂ ⁹⁶
Polystyrene	Cadmium Sulfide	Simultaneous formation in an emulsion. ¹⁰⁸

Table 1.2 Selected Ordered Polymer Nanocomposites

Polymer	Nanoparticle	Preparation Method
Nafion	SiO ₂	<i>In-situ</i> sol-gel chemistry within Nafion ⁸⁻¹⁵
PS- <i>b</i> -P2VP	Silver	Soaking crosslinked polymer in silver iodide ¹⁰⁹
PS- <i>b</i> -P2VP	Gold	Coprecipitation of precursors and copolymer from solution ⁵¹
PS- <i>b</i> -PEO	Palladium	Coprecipitation of precursors and copolymer from solution ³⁵
PI- <i>b</i> -P2VP	Palladium	Reduction of solution in benzyl alcohol ³²
PS- <i>b</i> -PAA	Cadmium Sulfide	Simultaneous formation in an emulsion ^{102, 103}
MTD Copolymer	Numcrous Mctals	Uptake of metal precursors from solution into thin films followed by reaction ^{27, 28, 99}

1.2.3.1 Disordered Nanocomposites

Disordered nanocomposites are materials fabricated in which one component encapsulates a second nanosized component with no spatial ordering. However, some of the disordered nanocomposites can exhibit narrow size distributions of the particles. This section reviews some of the work on disorder nanocomposites in which one phase is ceramic, metal, or metal sulfide.

1.2.3.1.1 Disordered Polymer/Ceramic Nanocomposites

Disordered polymer/ceramic nanocomposites have been fabricated within different polymers either by mixing polymers with nanosized ceramic fillers or by the preparation of the ceramic phase through sol-gel chemistry for improved mechanical properties of the composite.^{1, 76} Examples of a disordered polymer/ceramic nanocomposites include polymers filled with organically modified silicates.⁷³⁻⁷⁵ Fabrication involved directly annealing a mixture of the silicate and polymer statically or under shear. Intercalation of the polymer

chains between the silicate layers gave rise to the nanocomposite, with improved mechanical properties over the unfilled polymer.⁷⁴

Disordered polymer/ceramic composites have been prepared by forming interpenetrating structures either by sol-gel chemistry within a polymer matrix or by sol-gel reactions during polymerization rather than just a mechanical mixing of a ceramic filler and polymer.¹ The use of sol-gel chemistry in the formation of these composites is important because functionalized ceramic precursors can be commercially obtained, allowing for direct covalent bonds with the polymer chains. The ceramic/organic materials can be divided into two major groups where the two phases are either connected by strong covalent bonds or embedded together with weak bonds.^{76, 110}

An example of an interpenetrating polymer ceramic nanocomposite without strong covalent bonds between the two phases is clear ceramic reinforced plastic windows. These are fabricated by first solvent casting TEOS with poly(methyl methacrylate). Following heating, sol-gel chemistry produced ceramic nanoparticles dispersed throughout the polymer.⁷⁷ In a similar manner, surface properties of polymers have also been modified with polymer/ceramic structures. The surface of clear plastic windows have been hardened by subsequently conducting sol-gel chemistry on the surface.⁷⁶ Ceramic windows have been surface modified with monomers that can undergo both sol-gel chemistry and vinyl polymerization to provide color or to decrease reflectance of glass.⁷⁶

Disordered polymer/ceramic nanocomposites have been prepared in which the ceramic and polymer phases are covalently bound together. One method for this was conducting TEOS sol-gel chemistry within polyethersulfone.⁸¹ Polyethersulfone contains hydroxyl groups that are able to react with TEOS. During sol-gel chemistry, the silicon

dioxide network becomes chemically bound to polymer chain ends. Linking of the polymer chains was demonstrated by the increase in molecular weight as shown by gel permeation chromatography.⁸¹ Other examples of silicon dioxide ceramic structures bound to polymers are those with poly(silsesquioxane),¹¹¹ isocyanate functionalized poly(tetramethylene oxide),¹¹⁰ poly(caprolactone)¹¹², and hyperbranched polymers.⁸⁴

1.2.3.1.2 Disordered Polymer/Metal Nanocomposites

Polymer/metal nanocomposites have been prepared by various methods such as the incorporation of metal nanocluster directly into polymeric systems or the incorporation of metal precursors into polymers. An example of a disordered polymer/metal nanocomposite involved the deposition of metal vapor into liquid monomer. Upon polymerization, gold nanoparticles were trapped within a polymeric network of polystyrene,¹⁰⁵ poly(methyl methacrylate),¹⁰⁵ and poly(isobutylene).⁸⁹ Another example of a disordered polymer/metal nanocomposites was the chemical vapor deposition of gold onto Nylon 11. Upon heating above the glass transition temperature of nylon, relaxation of the polymer chains occurred and the metal clusters were distributed throughout the polymer films.^{106, 107} An example of a polymer/metal nanocomposite was the loading of cobalt precursors into poly(acrylonitrile) during solvent casting. Upon thermolysis, cobalt nanoparticle were produced by reduction within a carbon fiber matrix.⁶⁷ A more elegant and direct method was the diffusion of a platinum organometallic into SC-CO₂ swollen poly(4-methyl-1-pentene).⁹⁶ Upon reduction with hydrogen, platinum nanoclusters were produced and stabilized by the polymer matrix.

1.2.3.1.3 Disordered Polymer/Metal Sulfide Nanocomposites

Disordered polymer/metal sulfide nanocomposites have been fabricated by mixing metal sulfide precursors with monomers followed by polymerization. An example of this is the mixing of cadmium salts with a styrene emulsion.¹⁰⁸ Upon introduction of hydrogen sulfide, the salts were reduced to yield cadmium sulfide followed by emulsion polymerization of a styrene network. This technique has been extended with other salts to prepare nanoparticles of copper sulfide and zinc sulfide within polystyrene.¹⁰⁰

Disordered polymer/metal sulfide nanocomposites have been fabricated by the reaction of metal sulfide precursors within polymeric systems. Examples of these are random copolymer films of polystyrene and poly(acrylic acid) cast onto films and immersed into aqueous solutions containing cadmium or lead salts.^{102, 103, 113} Upon subjecting the dried slides to hydrogen sulfide, metal sulfides in copolymers were produced. Optical properties of these nanoparticles were investigated and control of nanoparticle size was dictated by the random copolymer.¹¹³

1.2.3.2 Ordered Nanocomposites

For numerous applications, three dimensional ordering of nanoparticles within a second matrix is critical. Nature has perfected the fabrication of ordered nanocomposites through the self-assembly of a bio molecule template which directs the formation of a second inorganic phase. To obtain nanoparticles with controlled architectures on the size scale of interest, many research groups have attempted to mimic nature with self-assembled templates. Examples of self-assembled templates include surfactants,^{5, 6} liquid crystals,^{6, 7} ionomers,⁸⁻¹⁵ and block copolymers.^{2, 4, 16-54}

1.2.3.2.1 Natural Nanocomposites

Nature consistently produces ordered ceramic/polymer nanocomposites, such as abalone sea shells,¹¹⁴ radiolarian microskeletons,¹¹⁵ cartilage, eggshells, mollusk shells, teeth, and bone.¹¹⁶ These naturally fabricated bioceramics are composites prepared from self-assembled templates at ambient conditions in aqueous media from readily available natural materials.⁵⁵ Bone is an elegant example of a natural nanocomposite whose structure has been perfected at both small and large scales, which provides for the desired mechanical properties. Organic collagen fibers first self-assemble forming a template structure. This fibrous framework is then filled with minerals, primarily calcium phosphate, producing a structure with roughly 67% ceramic and 33% organic materials. Bulk composites are made while domain sizes are controlled down to the micron level as the mineral adopts a structure directed by an organic matrix. This process for the fabrication of ordered polymer/ceramic nanocomposites through elegant chemistry at low temperatures is referred to as biomineralization.^{115, 117, 118}

1.2.3.2.2 Surfactant Templates

Ordered nanocomposites have been prepared by surfactant templates which contain two antagonistic parts and are the simplest molecules to undergo self-assembly.¹¹⁹ When surfactants have been used as templates for ceramics nanocomposites, the process has been called "biomimetic," in reference to similar processes in nature.^{6, 55, 101, 114, 117, 120-122}

Surfactant self-assembly occurs in water with amphiphilic surfactants consisting of a hydrophobic organic tail and a hydrophilic ionic head. Above a critical micelle concentration (CMC), the organic tails associate with the tails of other surfactants forming a sphere surrounded by the polar head group, which is exposed to the water. Changing variables, such as the surfactant concentration, temperature, solvent, and the surfactant itself can give rise to different non-robust structures, such as cylinders, lamellae, and bicontinuous structures.^{6, 123} Switching to a non-polar solvent can result in an inversion of the micellar structure, where the polar head groups will associate away from the non-polar solvent. Examples of larger molecules that can also undergo similar self-assembly are liquid crystals, protein chains, and block copolymers. Block copolymers can also exhibit a CMC in solution, but this occurs at a much lower concentration than that for low molecular weight surfactants. CMC for a surfactant is about 10^{-3} to 10^{-1} Mol/L, whereas for a copolymer CMC is in the range of 10^{-9} to 10^{-4} Mol/L.¹¹⁹

The structure directivity of surfactant templates is illustrated in Figure 1.6.^{5, 6} The first step is the formation of a surfactant structure in a suitable non-polar solvent above the CMC, which can take on several different morphologies such as spheres, cylinders, lamella, and bicontinuous systems. Mixing with the inorganic precursor, such as TEOS, can lead to self-assembly where the inorganic networks can start to form. After sol-gel chemical reaction of precursor, an ordered structure will be produced with a morphology directed by the surfactant.⁶ Surfactant structures have also been used to produce ordered structures with metal nanoparticles. Metal salts were added to the surfactant structure and reduced with hydrazine to produce palladium and platinum alloys.⁶⁸ The particles were collected on a solid alumina support.

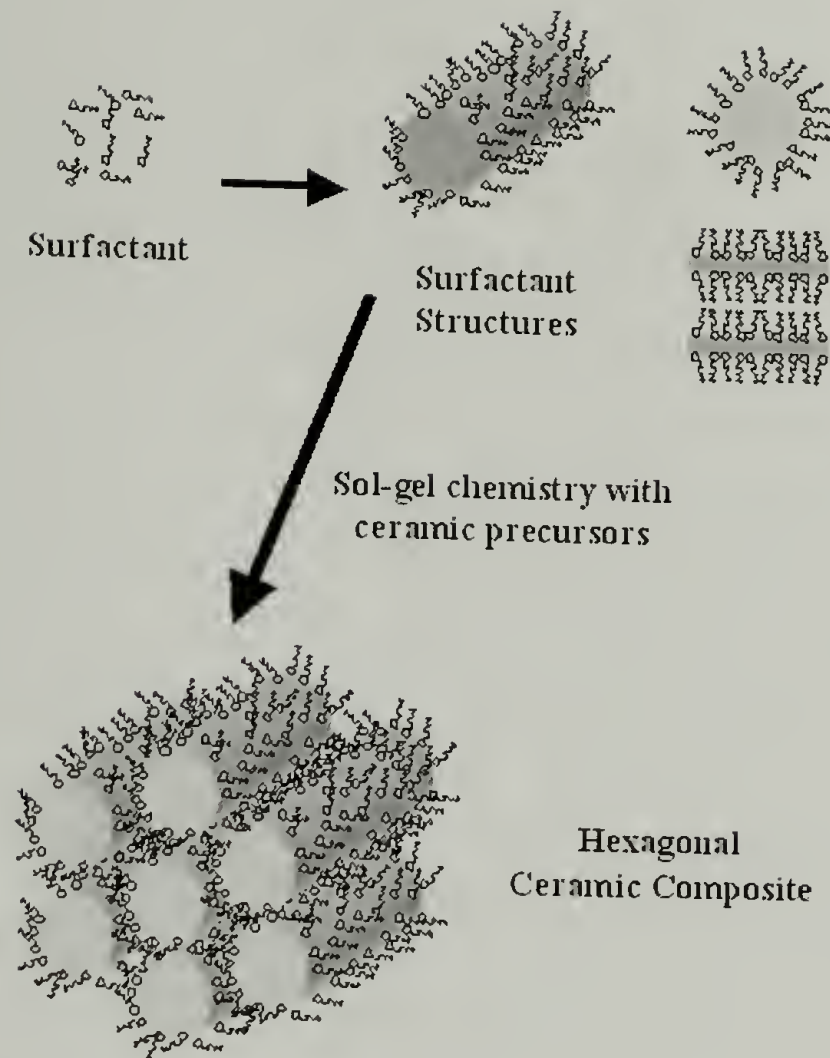


Figure 1.6 Schematic of the cooperative organization of silicate-surfactant mesophases

1.2.3.2.3 Liquid Crystal Templates

Liquid crystals are molecules that undergo molecular self-assembly and some have been used as templates for ordered nanocomposites. Lyotropic liquid crystals are larger, more complex than simple surfactants with numerous structures available to prepare nanocomposites.^{7, 124} In one example, lyotropic liquid crystals containing unsaturated links self-assembled into a hexagonal pattern. Upon cross-linking with UV light, TEOS was introduced into the structures. Reduction of TEOS produced a templated structure of SiO₂.⁷

1.2.3.2.4 Polymeric Ionomer Templates

Polymeric ionomers have been used as templates to prepare ordered nanocomposites. Ionomers are copolymers in which one of the blocks contains an ionic functionality and aggregate into a quasi three-dimensional order. Nafion is the most widely used ionomer. It contains small segments of sulfonic acid functional groups, and has been used as an acid catalyst for TEOS sol-gel reactions.^{8-13, 125} Nafion was developed in the 1960's by DuPont and has been used in numerous applications such as catalysts, gas separation, liquid separation, and fuel cells.^{14, 15, 126} These applications are enabled by Nafion's thermal and chemical resistance, ion-exchange properties, selectivity, mechanical strength, hydrophilic nature, and insolubility in water.¹²⁷

The chemical structure of protonated Nafion ionomer consists of a fluorinated carbon backbone with pendant sulfonic acid functional groups (Figure 1.7). This semicrystalline material ($T_m = 270$ °C and ~12% crystallinity) is structurally complex and the exact structure of the ionic group aggregation is not fully known.^{127, 128} Analysis by small angle X-ray scattering (SAXS) and neutron scattering indicate that the ionic groups tend to aggregated to form tightly packed ionic clusters from strong electrostatic interactions.¹²⁷ From this information and other studies such as ion transport through films, a structural model has been developed that suggests that the ionic groups are dispersed in a quasi-order fashion throughout a hydrophobic semicrystalline perfluorocarbon matrix (Figure 1.8). The approximate center to center spacing of the ionic clusters is about 5 nm.¹²⁹

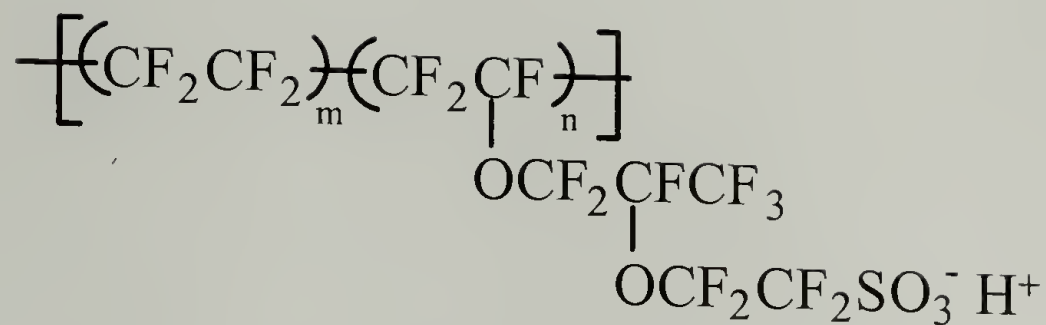


Figure 1.7 Chemical structure of protonated Nafion

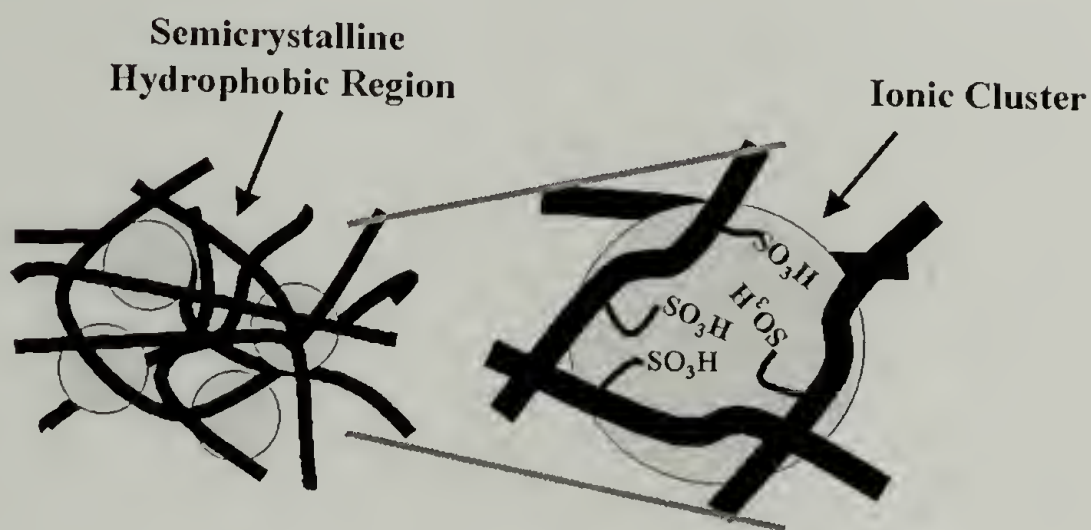


Figure 1.8 Model of Nafion ionomer

Nafion has been extensively studied as solid acid catalyst for the preparation of polymer/ceramic nanocomposites based on sol-gel chemistry within sulfonic acid ($-\text{SO}_3\text{H}$) catalytic sites.^{8-12, 125, 128, 129} The polar clusters within Nafion and other ionomers act as an interactive template that directs the reaction of metal oxide precursor and the disposition of the final metal oxide network, most commonly SiO_2 from TEOS. Upon high loading of the SiO_2 phase, percolation of the inorganic occurs, as suggested by brittle fracture in mechanical tests.¹²⁹

The templating capability of Nafion has been verified by SAXS on the Nafion film before reaction and of the nanocomposite following reaction.^{10, 12} In one example, untreated Nafion showed a broad scattering maximum of $q_{\text{max}} \sim 2.0 \text{ nm}^{-1}$, attributed to a quasi-ordered

array of clusters with a spacing of $\sim 50 \text{ \AA}$.¹⁰ Upon TEOS infusion and subsequent reactions, the nanocomposites showed a scattering peak at the same location, supporting the templating theory.¹²⁸ The silicon dioxide network within Nafion has been modified by adding different ratios of TEOS and DEDMS (Figure 1.4).¹⁰ These organically modified ceramics within Nafion have been shown by SAXS to have similarly sized inorganic network structures.

Pretreatment of Nafion prior to any chemical impregnation has been shown to have a large effect on the final product.¹³⁰ The pretreatment involved soaking the films in hydrochloric acid to oxidize dimethyl sulfoxide and other impurities left over from polymer processing, followed by rinsing with doubly distilled water. Nafion was then treated with nitric acid to fully protonate the acid groups and to “initialize” the membrane. The films were then treated with water to remove excess acid. This last step was repeated until a neutral pH of the water was obtained ($6.5 < \text{pH} < 7.0$).¹³⁰

After pretreatment of the films, the general reaction procedure was as follows.¹⁰ Nafion films were first soaked in a stirred solution of 5:1 (V/V) methanol:water at room temperature for 24 hours. This swelling facilitates subsequent permeation of TEOS into the films. Premixed solutions of TEOS/methanol were then added to keep the water/TEOS ratio at 4:1. After 10 minutes in the solutions, the films were removed and washed with methanol and dried at $100 \text{ }^\circ\text{C}$ for 48 hours to further promote the reaction and remove volatile material.

1.2.3.2.5 Block Copolymer Templates

Block copolymers can encompass a wide range of phase separated morphologies and can be used as structure directing templates to produce ordered nanocomposites.^{2, 4, 16-54} Block copolymers are the polymeric analogue of liquid crystals and surfactants with

morphologies more stable than those of their low molecular weight counterparts. Block copolymers are made by the linking of two (or more) different segments of homopolymers. If two homopolymers of the same molecular weight are mixed together, phase separation will occur if the product of the Flory-Huggins segment-segment interaction (χ) and degree of polymerization (N) is sufficient ($\chi N > 2$).¹³¹ Linking the chain ends forms a block copolymer, limiting the size scale upon which phase separation can occur. Segment connectivity raises the penalty for phase separation ($\chi N > 10.5$) for two blocks of equal volume fraction.¹³¹ The morphology for a given phase separated block copolymer is dictated by minimizing both interfacial area and stretching of the coil governed by χ , N , and f , the volume fraction of each block. If one considers a simple block copolymer composed of two immiscible homopolymers, Poly(A) and Poly(B), phase separation will occur forming the morphologies shown in Figure 1.9.

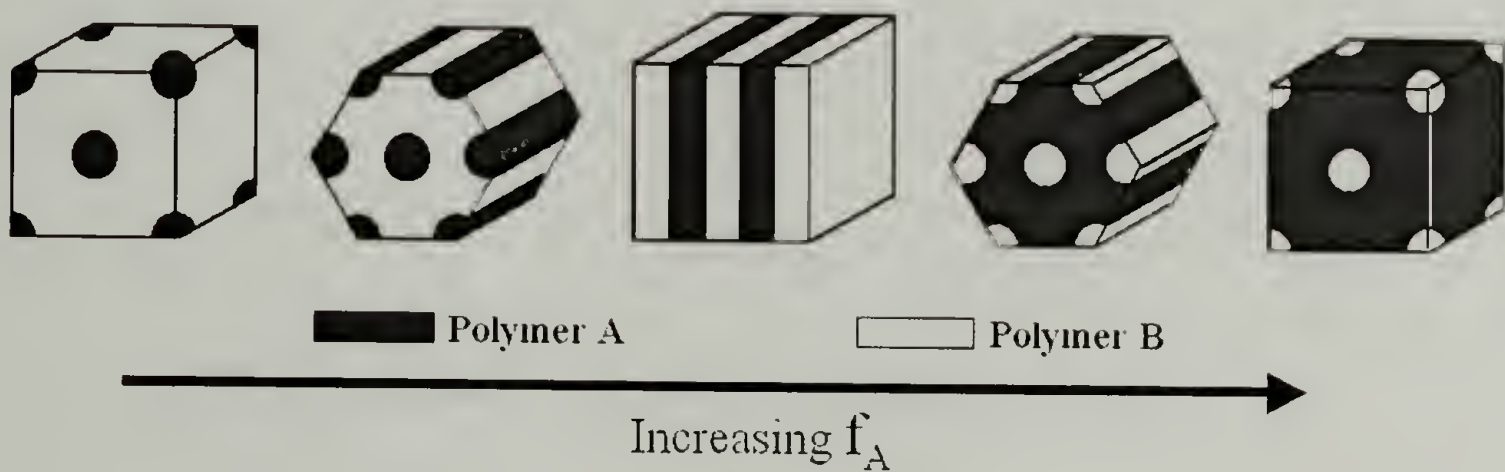


Figure 1.9 Generic block copolymer morphology

If one of the phases, Poly(A), represents a small volume fraction, it will aggregate into spheres of Poly(A) surrounded by Poly(B), akin to spherical surfactant micelles. An increase in the volume fraction of the minor phase will increase the surface area of the

interface. The copolymer system will attempt to minimize this surface area and upon reaching a critical value, a lower surface area is achieved by forming cylinders of Poly(A) surrounded by a continuous phase of Poly(B). Further increase in the volume fraction of Poly(A) will result in a lamellar structure of alternating blocks followed by the inversion of the phases.

The actual morphologies of block copolymers are more complex and have been studied in detail for several copolymer systems, most extensively for polystyrene-*block*-polyisoprene. Examples of more complex structures include bicontinuous phases and metastable perforated lamellae and modulated lamellae, shown in a compilation of data (Figure 1.10).^{31, 132-134} This work has also shown the block copolymer phase behavior can be further defined by the strength of segregation.^{31, 132-134} The block copolymer is in the weak segregation limit with poorly defined interfaces close to the critical χN , which is 10.5 for lamellar systems. A much larger χN drives the system in the strong segregation limit giving a sharper interface.¹³³

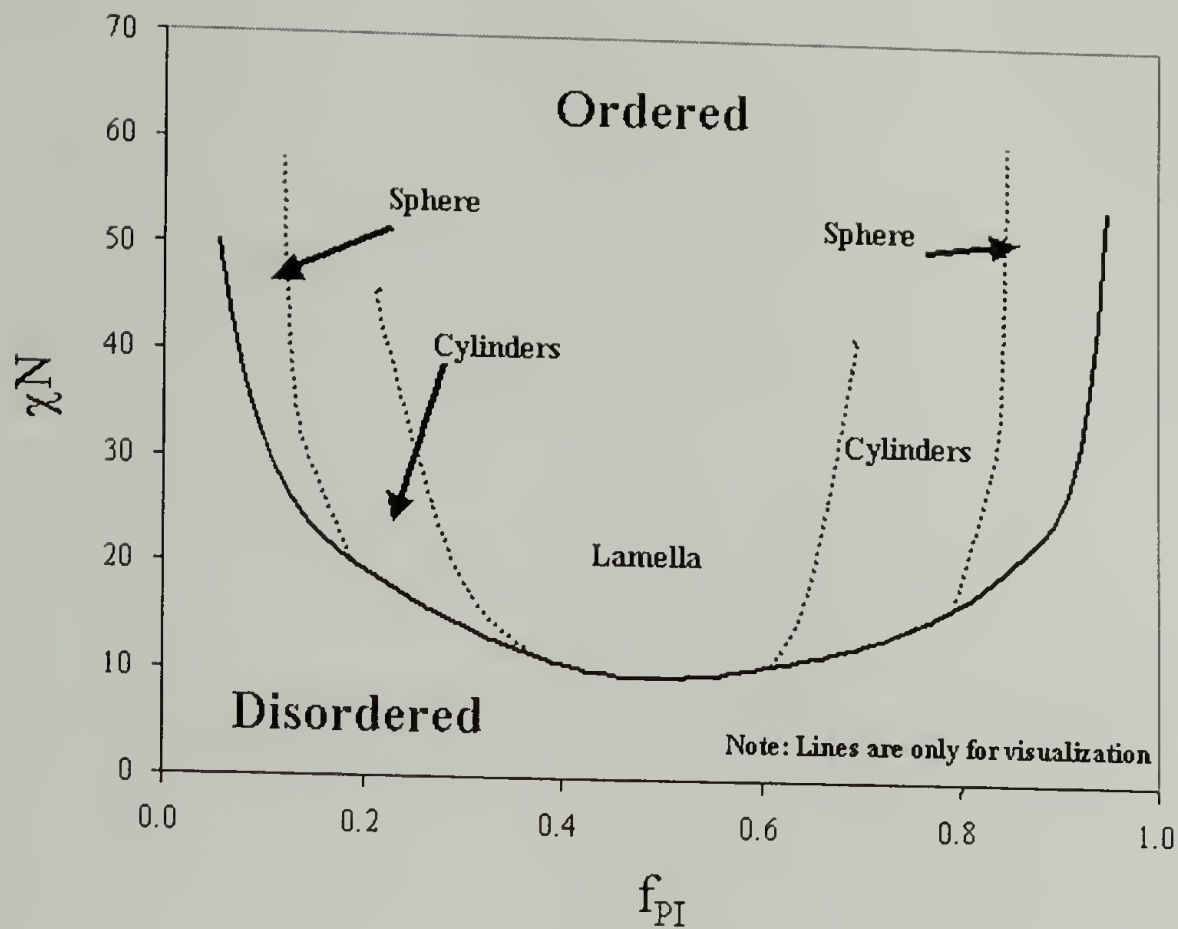


Figure 1.10 Phase diagram of a poly(isoprene-b-styrene) copolymers^{132, 134}

Another advantage of block copolymers is their robust nature in comparison to other self-assembled structures, such as surfactants and liquid crystals. The ideal nanocomposite template should be chemically robust to survive chemical modification, have mechanical integrity for manipulation upon fabrication, and have the ability to be ordered over large length scales relative to the size of the cluster being templated. Introducing macroscopic order in block copolymers (BCP) has been shown by using shear, thermal gradients, roll casting, electric fields, and annealing in supercritical carbon dioxide.^{72, 135-138} These requirements are possible with block copolymers and are a key advantage to their use. With all of the advantages of BCP's, their use as bulk templates has been limited by the mass transport and efficient delivery of materials into the copolymers.

One of the earliest examples of a block copolymer nanocomposite was the fabrication of metallic silver within a thin copolymer film of polystyrene-*block*-poly(2-vinyl pyridine)

(PS-*b*-P2VP).¹⁰⁹ The polystyrene phase was first lightly cross-linked by UV light, to preserve the initial morphology and soaked in a solution containing silver iodide. The silver was bound to the pyridine and thermally reduced in place forming templated silver clusters. A similar preparation was repeated for gold clusters in PS-*b*-P2VP, introducing the nanoreactor concept of metallic particles in copolymers.¹⁰⁹

Solutions of copolymers have been used to prepare templated nanocomposites of metal and metal sulfides.^{2, 38, 40, 41, 45-49} For example, gold nanoparticles were prepared within a PS-*b*-P2VP copolymer in three steps. The copolymer was first dissolved in toluene with a gold salt, forming thermodynamically stable spherical micelles of P2VP, which bound the gold precursor.⁴⁸ Upon reduction with hydrazine, gold clusters were produced within the P2VP phase. Gold clusters remain within the P2VP phase, which acts as a protective shell when films are cast from solution onto a TEM grid. Microcellular wires have similarly been made using PS-*b*-P2VP dissolved in toluene with the same gold precursor.⁴⁸ The volume fraction of P2VP in the copolymer and the concentration of solvent were controlled, establishing a cylindrical phase in solution. The cylindrical phase became the template for binding the gold precursor, which upon evaporation of the solvent and reduction of the metal produced gold wires. Thin films nanocomposites on silicon wafers have been prepared in the same manner. By dipping a wafer into a solution of copolymer and metal precursor, nanoclusters were produced by the reduction of the dry film.⁴⁵

The precipitation method has also been used to make nanocomposites from other copolymer polymers and solvents.³⁵ In one example, a polystyrene-*block*-poly(ethylene oxide) (PS-*b*-PEO) copolymer was dissolved into a mixture of tetrahydrofuran and ethanol. The PEO blocks aggregated into spherical micelles in solution and bound dissolved

palladium acetate, which was subsequently reduced thermally. Catalytic properties of the palladium dispersions were studied by the hydrogenation of cyclohexene and TEM analysis was performed by solvent evaporation onto a copper grid.³⁵ Other work has investigated precipitation from aqueous solutions³⁵ and catalytic properties of nanoparticles prepared in different copolymers.^{33, 36}

The preparation of metal-copolymer nanocomposites by precipitation of benzyl alcohol, polyisoprene-*block*-poly(2-vinylpyridine) (PI-*b*-P2VP), and palladium bis-acetylacetonate in chloroform has been reported.³² This solution produced a cylindrical structure of P2VP, which was able to bind palladium precursor. PI-*b*-P2VP acted as the template and the nanostructure remained after the evaporation of chloroform. Upon heating to 140 °C, benzyl alcohol reduced the palladium and was driven from the film.³²

Commercially available polystyrene-*block*-polyisoprene (PS-*b*-PI) has been used as the starting material for nanocomposites.^{18, 119} The PI phase was chemically modified by epoxidation, allowing it to be converted into a number of different functional groups. A range of different metal and metal sulfide precursors were added to the different functionalized copolymers. Differences in the reduction of metals and semiconductors within the modified copolymer were discussed in relation to hard-soft acid-base theory.¹⁸

The direct preparation of nanocomposites of metal and semiconductor nanoclusters within block copolymers has been demonstrated by Cohen and coworkers.^{4, 20-23, 25-30, 42-44, 99,}

¹⁰⁴ In their first reaction schemes, norbornene-derived monomers were prepared with various pendant organometallic groups. Using Schrock catalysts, these monomers were copolymerized with other norbornene-derived monomers producing a phase separated block copolymer of desired morphology. The copolymers were solution cast followed by reduction

with hydrogen to yield clusters of platinum, palladium, gold and silver, or with hydrogen sulfide, producing zinc sulfide, lead sulfide, and cadmium sulfide nanoclusters.^{44, 99, 104}

To prevent the synthesis of a new monomer each time a different nanocluster was desired, a "universal" technique was introduced.^{27, 28, 99} In this scheme, norbornene-derived monomers were prepared with pendent trimethylsilyl esters and copolymerized with other norbornene-derived monomers. By controlling the monomer ratio, desired lamellae, cylindrical, spherical morphologies of reactive copolymers were achieved.^{27, 28, 99} The ester groups were hydrolyzed to pendent acid groups that can bind metals in an aqueous solution (such as Zn^{2+} , Cd^{2+} , Pb^{2+} , Cu^{2+} , Co^{2+} , Fe^{2+}) when the thin sections of copolymer are placed in contact with the solutions. Metal precursors, such as ZnEt_2 and CdMe_2 , were also infused directly into thin copolymer films from the vapor phase.⁹⁹ Upon reduction with hydrogen or hydrogen sulfide, metal or metal sulfide nanoclusters were formed. Templating of the clusters was verified by characterization with transmission electron microscopy (TEM). Additional templating evidence has been obtained by an X-ray fluorescence map of the nanocomposite containing ZnS. Mapping the X-ray fluorescence results directly onto TEM image, showing that the clusters were only formed within the reactive phase of the copolymer.⁹⁹

Further studies of this 'universal' method have allowed for the effect of the reduction potentials of the metal ions and complexes to be investigated and for the measurement of the diffusion of metal precursors into the copolymers. Diffusivities of approximately 3×10^{-12} cm^2/s were obtained.²⁷ Those low diffusivities essentially preclude the formation of nanocomposites over bulk dimensions. In another example, the universal method was used to produce lamellar copolymer systems loaded with platinum nanoclusters. The platinum

nanoclusters were subsequently used as seed layers for electroless copper deposition within the copolymer domains.²⁰

Diblock and triblock copolymers have been used as templates to fabricate ordered polymer/ceramic nanocomposites.²⁴ Copolymers have been used as templates with one phase containing pendent side-groups capable of undergoing sol-gel chemistry alone or with added ceramic precursors such as TEOS.²⁴ Most commonly, the block copolymers contain a hydrophilic block that is able to absorb water and a ceramic precursor.

An example of this is the fabrication of an ordered nanocomposite from tri-block copolymers of polyethylene oxide-*block*-polypropylene oxide (PPO-*b*-PEO-*b*-PPO) and TEOS.^{139, 140} The PEO phase absorbs the water acting as the template where the sol-gel chemistry occurs depositing an ordered silicon dioxide network.¹³⁹ Other block copolymers and inorganic networks have been prepared using poly(isoprene-*block*-ethylene oxide) (PI-*b*-PEO).¹⁶ In this study, the PEO phase acted as a template, which was selectively swollen by a solution containing an aluminum alkoxide ($\text{Al}(\text{OC}_4\text{H}_9)_3$), TEOS, and GLYMOS (Figure 1.4). A ceramic network structure was fabricated and shown to contain aluminum and silicon dioxide bound to the PEO chains. The morphology was dictated by the block copolymer template structure.¹⁶

1.2.4 Nanoparticle Size and Aggregation

A key consideration for nanocomposites containing metal and metal sulfide particles is the initial particle size and potential aggregation of particles used to produce larger clusters. The particle sizes within a polymer will be determined by the reaction conditions used to synthesize the materials and potentially nanoparticle diffusion and coalescence.

Variations in nanoparticle sizes from different reduction conditions have been investigated^{53, 54, 141-143} or mentioned^{21, 29, 31} in a few sources. Nanoparticle diffusion has been studied within polymer films containing metal sulfides^{143, 144} and metals.^{88, 145-149}

Understanding the growth processes of particle size is essential for developing a rational synthesis mechanism to produce monodisperse nanoclusters within polymeric materials. The growth of semiconductor nanoparticles within block copolymer microdomains reduced by hydrogen sulfide has been investigated and modeled.¹⁴³ The growth of the nanoparticle was found to be influenced by diffusion, aggregation and growth. Other methods of particle growth, such as Ostwald ripening, were ruled out by the large energy penalty required for these mechanisms. Two growth models were proposed: 1) reaction-diffusion and 2) equilibrium.¹⁴³ The reaction-diffusion model assumes that the growth of nanoparticles is governed by the competition between diffusion time for particles to aggregate (τ_d) and reaction time (τ_r) for the production of the nanoclusters. When τ_d becomes much greater than τ_r , the growth of particles will stop and new sites will be nucleated, giving rise to more particles. The equilibrium model assumes an equilibrium number of metal-ligand bonds at any given temperature. Formulas were developed for these two models and were used as a guide to determine the dominant mechanism within a system.¹⁴³

The influence of reduction conditions on nanoparticle size was examined using a platinum precursor/polymer substrate solid solutions.¹⁴² Poly(4-methyl-1-pentene) films were loaded with Pt(COD)Me₂, then the film was cut into pieces, and reduced with hydrogen under conditions of various degrees of plasticization by SC-CO₂. Scherer analysis of the platinum (111) peak measured in WAXS indicated larger clusters were produced with

increasing pressures of SC-CO₂. Increase in CO₂ pressure lead to increasing sorption of CO₂ and thus a large increase in the precursor diffusion to previously formed reduction sites.¹⁴²

The effect of reduction conditions on the properties gold clusters prepared within polystyrene-*block*-poly(4-vinyl pyridine) [PS-*b*-P4VP] has been noted.³¹ The copolymer was dissolved in toluene with a gold precursor, tetrachloroauric acid (HAuCl₄), which yielded gold precursor bound to a P4VP sphere surrounded by a PS corona. Upon solvent casting onto a TEM grid, gold was templated within a spherical P4VP phase and subjected to two different reducing agents. The fast (strong) reducing agent, lithium aluminum hydride (LiAlH₄), produced numerous small nanoparticles within each domain. The slow (weak) reducing agent, trimethyl silane (Me₃SiH), produced a single nanoparticle within each domain, that was larger than with the fast reducing agent and also located at the interface.³¹ The authors attributed differences between the particles to the strength of the reducing agents, but did not comment on the location of the nanoparticles at the copolymer interface or any unreduced precursor which appeared to be visible in the TEM images.

In another study, the photo-reduction of gold salts within a PS-*b*-P4VP copolymer was carried out using an ArF laser.⁵⁴ Again the copolymer with the gold precursor was solvent cast onto TEM grids. Upon reduction with 20 laser pulses at low power (10 mJ/cm²) at 25 °C, numerous small nanoparticles were produced within each copolymer domain. With 10 laser pulses at high power (20 mJ/cm²) at 25 °C, few larger nanoparticles were produced, with a loss of templating. A sample was reduced at low power and at 90 °C, which resulted in a structure similar to that obtained at low temperature and high laser power with larger nanoparticles and a loss of templating. These results suggest that the energy density per laser pulse was the decisive parameter controlling the coalescence of smaller nanoparticles

into larger ones accompanied by a loss of the original template order.⁵⁴ To test the theory that the variation in nanoparticle size was due to only local temperature increases that provided increased mobility for nanocluster diffusion and aggregation, a sample was reduced with the low power and 25 °C followed by heating at 135 °C for 10 seconds, which corresponds to the typical laser-irradiation time. This short heating time did not alter the structure, which showed that the formation of larger clusters by low energy irradiation at elevated temperatures is not simply due to a coalescence of already existing smaller dots, but occurs during of nucleation and growth.⁵⁴

The mobility of gold nanoparticles deposited by evaporation¹⁴⁹ and from an aqueous colloidal suspension¹⁴⁷ on polymer surfaces and sandwiched between polymer films has been studied by TEM microscopy. Four nanometer gold nanoparticles were evaporated onto a polystyrene film followed by annealing for various times at 179 °C, well above the individual glass transition temperatures (T_g) of the homopolymers.¹⁴⁹ The gold nanoparticles were able to diffuse and coalesce to form larger particles at a temperature hundreds of degree below the bulk melting point of gold (1064 °C).¹⁴⁹

Polymer sandwiches of PS-PS, PS-P2VP and P2VP-P2VP were prepared by placing a polymer film onto a second polymer film coated with evaporated gold nanoparticles. Within the PS-PS sandwich, the gold nanoparticles were able to diffuse away from the interface and coalesced together to produce larger particles similar to the results on the polystyrene film.¹⁴⁹ Within the P2VP-P2VP sandwich, the gold nanoparticles were able to migrate away from the interface, but were prevented from aggregation due to strong metal-polymer interaction.¹⁵⁰ Coalescence of the nanoparticles would require rearrangement of the polymer chains bound

to the metal, which is energetically unfavored. Nanoparticles in PS-P2VP interface were pinned at the interface unable to move and also prevented from aggregation.¹⁴⁹

In a second set of experiments, movement of twenty nanometer gold nanoparticles deposited from aqueous colloids was investigated on surface films of PS and P2VP and within polymer sandwiches of P2VP-P2VP, PS-PS, and PS-P2VP during annealing at 179 °C.¹⁴⁷ Gold nanoparticles on the surface of polystyrene were able to diffuse and coalesce at 179 °C. Atomic force microscopy (AFM) of the films revealed that the nanoparticles remained on the top of the film and did not penetrate into the film.¹⁴⁷ However, results for the annealed P2VP films were different; the gold particles were not able to coalesce due to strong metal-polymer binding. AFM revealed another difference. The 20 nm nanoparticles penetrated the film to a depth of only 15 nm as detected by 5 nm spots on the surface. The authors related this difference in PS and P2VP to the use of an aqueous colloid, which would be able to plasticize P2VP more than PS allowing for an initially deeper penetration.¹⁴⁷ However, the addition of a PS film onto the P2VP allowed for deep penetration into the P2VP. The authors related this to the change in the contact angle of P2VP on gold from 9° to essentially zero with PS.¹⁴⁷ Upon annealing a P2VP-P2VP sandwich, gold nanoparticles were prevented from agglomeration, but were able to diffuse into each of the films.

Measurement of nanoparticle penetration depth into polymers has been studied for gold nanoparticles deposited from thermal evaporation or from aqueous colloidal suspensions into poly(*tert*-butyl acrylate),^{88, 145} polystyrene,¹⁴⁶⁻¹⁴⁹ and poly(2-vinyl pyridine).¹⁴⁷⁻¹⁴⁹ Rutherford backscattering spectroscopy was used to measure the penetration depth as this method is ideally suited for determining the location of atomically heavy gold nanoparticles within a light atom polymer matrix. From measurements of penetration depth vs. time,

diffusion of the nanoparticles was calculated within different polymers, at several temperatures and molecular weights. Examples of the diffusion rates are 3×10^{-14} cm²/sec for gold nanoparticles in poly(tert-butyl acrylate) with Mw = 21,000 g/mol at 80 °C¹⁴⁵ and 5×10^{-15} cm²/sec for gold nanoparticles in P2VP with Mw = 82,000 g/mol at 160 °C.¹⁴⁸ Under these conditions, a nanoparticle could diffuse 30 nm in 2.5 and 15 minutes, respectively. Figure 1.11 shows the diffusion of 20 nm gold nanoparticles for two different molecular weights of poly(2-vinyl pyridine).¹⁴⁸ The solid line is the calculated diffusion for a 7.5 nm gold particle using the zero shear rate viscosity for the (Mwt = 82,000) polymer. The results indicated that the diffusion was an order of magnitude slower than predicted, which was explained by a strong binding of P2VP to the gold. This strong binding required the gold nanoparticle to drag along P2VP chains, which essentially increases the size of the particle.

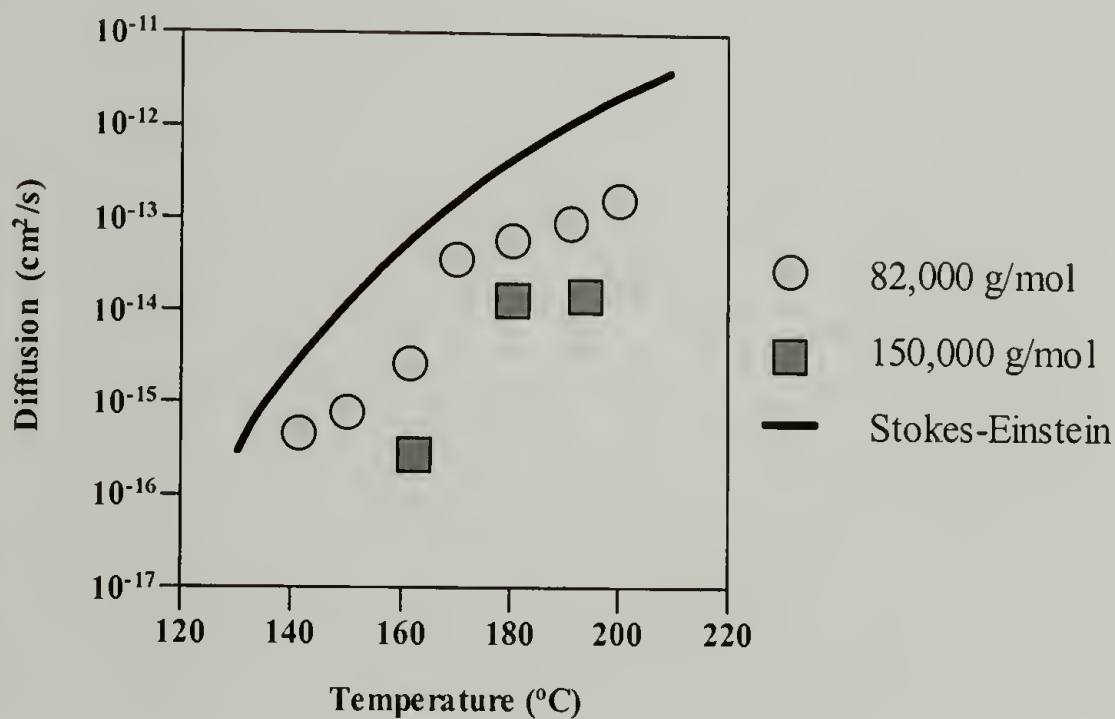


Figure 1.11 Diffusion of 20 nm gold nanoparticles in poly(2-vinyl pyridine)¹⁴⁸

1.3 Background on Supercritical Fluids

A supercritical fluid (SCF) is a substance above its critical temperature and pressure. SCF's have been used as solvents in numerous applications such as the polymerization of ethylene,¹⁵¹ decaffeination of coffee,¹⁵² for organic chemical reactions,^{135, 152-156} and nanocomposite synthesis.^{96, 142, 157, 158} The applications of SCF's arise due to several of its characteristics, such as a wide range of solvent strengths and densities that can be adjusted by tuning the pressure and/or temperature. A number of different small molecules and reactants can be dissolved into SCF's and infused into polymeric systems. This approach also will be used in this research project.

Carbon dioxide is the most widely used SCF. It has a readily accessible critical temperature and pressure ($T_c = 31.06\text{ }^\circ\text{C}$ and $P_c = 73.83\text{ bar}$).¹⁵⁹ The properties of SCF's are coupled to density and controlled by variations in temperature and pressure. Several isotherms of CO_2 are shown in Figure 1.12.¹⁵⁹ Densities approaching or exceeding those of liquid organic solvents ($\sim 0.7\text{-}0.9\text{ g/mL}$) can be obtained with SC- CO_2 while retaining desirable properties of gases, such as high diffusion rates and zero surface tension. Key physical properties of fluids are summarized in Table 1.3. SC- CO_2 is an attractive medium for use with polymers as the solvent is inexpensive, nontoxic, nonflammable and environmentally benign.

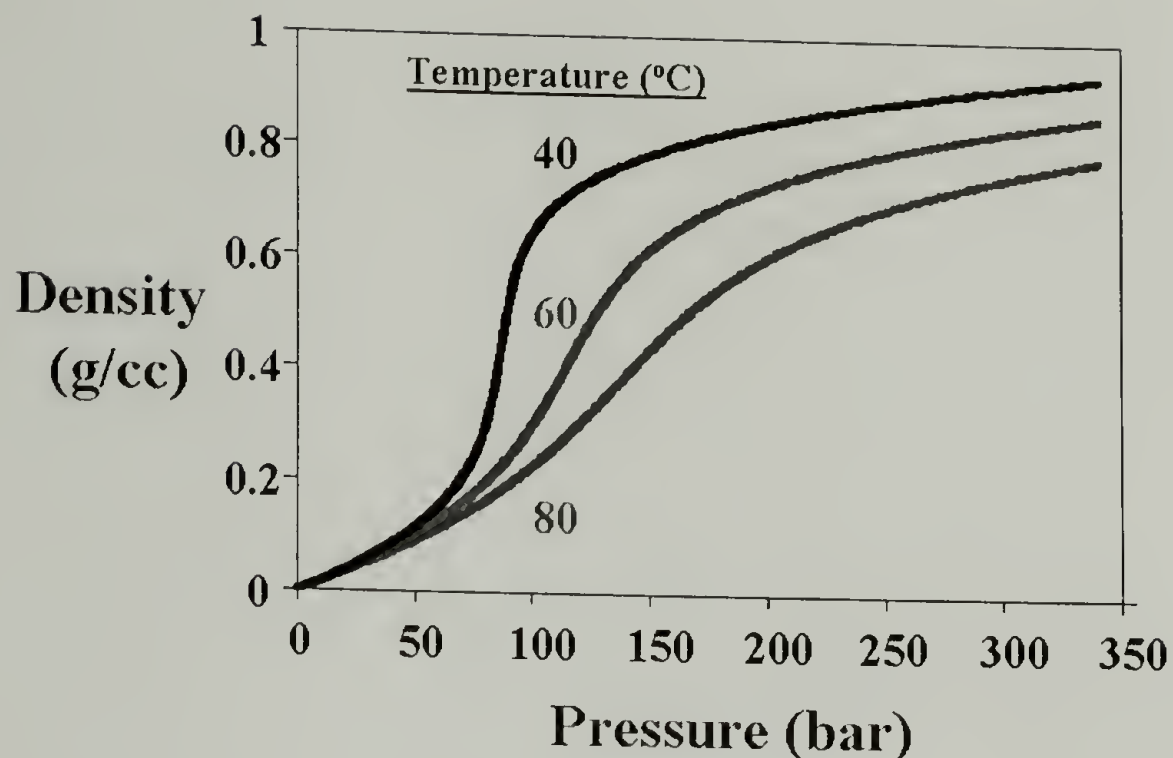


Figure 1.12 SC-CO₂ density isotherms¹⁵⁹

Table 1.3 Physical Properties of Liquids, Gases and SCF's

	Liquids	Gas	SCF's
Density (g/cc)	1.0	0.001	0.1-1.0
Viscosity (Pa*s)	10 ⁻³	10 ⁻⁵	10 ⁻⁴ -10 ⁻³
Diffusion (cm ² /s)	10 ⁻⁵	10 ⁻¹	10 ⁻²

1.3.1 Use of SCF's in Polymers

For polymer applications, supercritical fluids were initially used for high-pressure polymerizations such polyethylene, where ethylene is both the solvent and monomer ($T_c = 9.22$ °C and $P_c = 50.32$ bar).^{151, 160} More recently, supercritical fluids have been used as an aid in polymer processing, and as a solvent for polymer fractionation, polymer synthesis, polymer foaming and for extraction or impregnation of small molecules.^{152, 161-163}

Almost all polymers absorb CO₂ appreciably without being dissolved, allowing for the modification of polymers, by SCF assisted infusion of reactants. However SC-CO₂ is

able to dissolve some polymers such as some polysiloxanes and perfluoralkylpolyether.¹⁵² and fluorinated surfactants for emulsion and dispersion polymerization.¹⁶⁴⁻¹⁶⁷ An example is the dispersion polymerization of acrylonitrile in SC-CO₂ using a fluorinated copolymer, polystyrene-*block*-poly(1,1-dihydroperfluorooctyl acrylate), as a stabilizer.¹⁶⁴

CO₂ sorption in polymers causes a depression in the T_g, an increase in polymer diffusivity and a decrease in viscosity.¹⁶⁸⁻¹⁷⁶ The T_g of polystyrene and poly(methylmethacrylate) (PMMA) is reduced by CO₂ sorption from 100 and 105 °C to 35 °C at 72 bar and 58.8 °C at 101 bar, respectively.^{170, 176} At these conditions, gas sorption within PS was found to be about 10 weight percent and 12 volume percent. For PMMA, the gas sorption was more than 18 weight percent and 28 volume percent swelling.^{170, 176} In some cases, the solubility of SC-CO₂ can be as high as that of typical organic liquid swelling agents.¹⁶⁸

CO₂ sorption in polymers increases free volume and hence decreases viscosity.¹⁷⁵ The viscosity of a CO₂ - PS melt at 150 °C can be reduced by two orders of magnitude with just 4.5 weight percent of dissolved CO₂. The greatest reduction in viscosity is found near the T_g of the polymer. This can be explained by the Williams-Landel-Ferry equation, which relates viscosity at different temperatures to the viscosity at T_g.^{162, 173}

The large decreases in the T_g upon sorption of CO₂ has been used to improve ordering kinetics of block copolymers.⁷² For applications as optical devices, the dimensions of a structure must be on the order of wavelength of light, and high molecular weight block copolymers have this desired length scale ($M_{wt} > \sim 300,00$ g/mole). Thin films of low molecular weight copolymers, such as PS-*b*-PMMA, are able to form well ordered structures upon annealing, but high molecular weight films are kinetically trapped and unable to form

highly ordered structures.¹⁷⁷ The large increase in chain mobility by the large decrease in T_g from CO_2 sorption allows for the ordering of high molecular weight copolymer films.⁷²

1.3.2 Small Molecules in SCF-Swollen Polymers

SC-CO_2 can be used for the impregnation or extraction of small molecules from polymer matrixes. Equilibrium is determined by the partition coefficient of the molecule between pure CO_2 and the swollen polymer. A major effect of CO_2 is to accelerate the kinetics of additive absorption.¹⁶⁸

The diffusion of small molecules within polymers is greatly enhanced by the sorption of CO_2 . In one example, the extraction of ethylbenzene in PS was performed with CO_2 .¹⁷⁸ It was found that at a CO_2 density of 0.22 g/cm^3 , the estimated diffusivity increased by more than six orders of magnitude when compared to the PS matrix.¹⁷⁸ Enhanced diffusion has also been demonstrated by the measurement of tracer diffusion coefficients of azobenzene in polystyrene at $35 \text{ }^\circ\text{C}$ and various CO_2 pressures using Forced Rayleigh Scattering.¹⁷⁹

Small molecule diffusion has been measured in CO_2 -swollen polymer films *in-situ* by fluorescence nonradiative energy transfer techniques.¹⁸⁰ Two polymer films were sandwiched together with one film having a donor molecule (pyrene) chained to PS and the other film having an acceptor (decacyclene) that is free to move. Upon plasticization of CO_2 , the doped acceptors diffuse towards the bound donor to quench the fluorescence. From measurement of the continuous decrease in the donor emission intensity over time, diffusion rates of the acceptor can be determined. It was shown that at a constant temperature of $65 \text{ }^\circ\text{C}$, CO_2 sorption enhances the diffusivity of decacyclene by as much as five orders of magnitude relative to the PS glass at ambient pressure and identical temperature.¹⁸⁰

1.3.3 SCF – Polymer Phase Behavior

Similar to partially miscible polymer blends, block copolymers can phase separate upon cooling through an upper order-disorder transition (UODT) analogous to an upper critical solution transition (UCST) in polymer blends.¹³³ However, due to the tethered nature of the block copolymers, phase separation can only occur on the length scale of the macromolecules, resulting in periodic ordered structures. Although, UODT-type behavior is the norm for block copolymers, a number of block copolymers have recently been found to microphase separate upon heating through a lower disorder-order transition (LDOT), which is analogous to lower critical solution transition (LCST) behavior in polymer blends.¹⁸¹

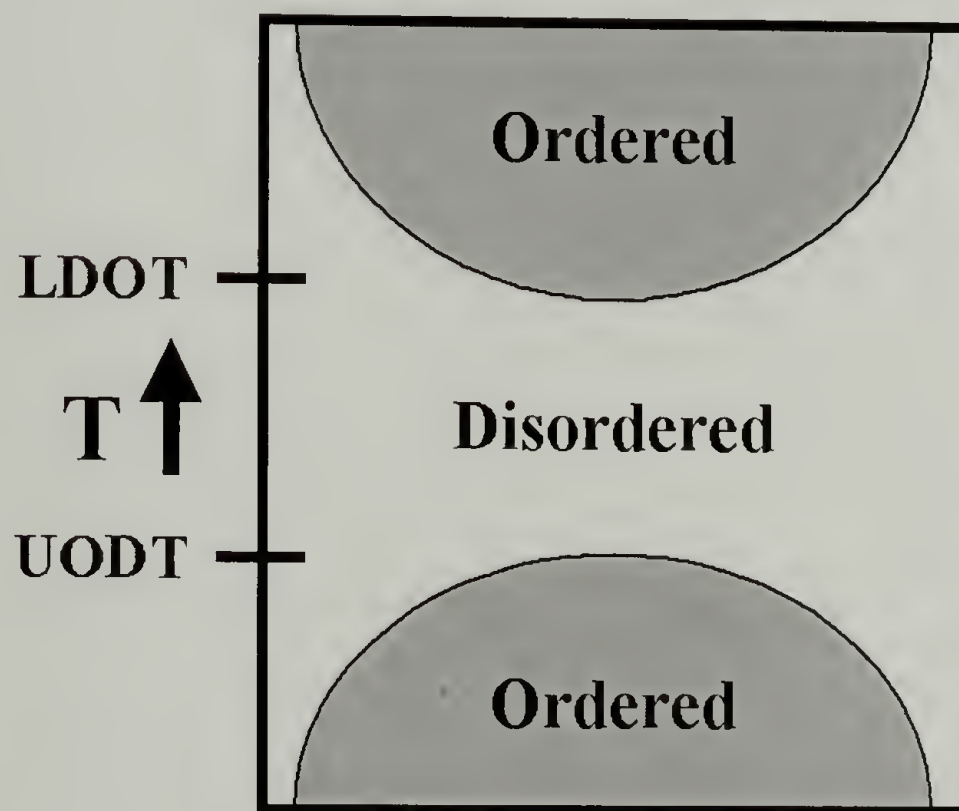


Figure 1.13 Block copolymer phase diagram

By solvating the block copolymer, the location of these transitions can shift, but more importantly, changes in the copolymer morphology can occur depending on solvent selectively.¹⁸²⁻¹⁸⁴ Thus understanding the effect of compressed carbon dioxide on the phase behavior of block copolymer is an important factor in the use of SC-CO₂ swollen copolymers as templates.¹⁸⁵⁻¹⁹⁰ In general it was found that CO₂ sorption can induce phase segregation for systems that exhibit LCST and LCOT behavior, but CO₂ sorption promotes compatibility for systems that exhibit UCST and UCOT behavior.

1.3.4 Supercritical Fluids and Nanoparticles

A number of SCF's have been used as solvents and co-solvents for the production of nanoparticles and for micron-sized particles.^{152, 157, 191-193} Particle design is becoming a very important application, especially in the pharmaceutical industry.¹⁹³

Rapid expansion of supercritical solutions is a process in which the material of interest is dissolved in a SCF and rapidly depressurized through a nozzle, causing an extremely rapid nucleation of the product.¹⁹³ Another common method for the production of micron-sized particles is the formation of particles from gas-saturated solutions.¹⁹³ This process consists of dissolving a supercritical fluid into a liquid material or a solution of the material. The mixture is then passed through a nozzle causing the formation of liquid droplets and the growth of particles. These methods can allow for control of the crystal structure and size of the particle, which is important as the crystal structure can have a large impact on biological functionality.^{191, 193} These methods for precipitation particles within SCF's has been extended into polymers. In one example, micrometer sized particles and fibers of nylon

6/6 were produced by expanding polymer solutions into SC-CO₂, forming micron sized particles.¹⁹²

In the production of several nanoparticles, a supercritical fluid (water or ammonia) was also used as the reducing agent.^{157, 194} However, the corrosive nature of both water ($T_c = 374\text{ }^\circ\text{C}$ & $P_c = 220.6\text{ bar}$)¹⁵⁹ and ammonia ($T_c = 132\text{ }^\circ\text{C}$ & $P_c = 113.3\text{ bar}$)¹⁵⁹ are serious drawback for these processes. A much less corrosive supercritical fluid is carbon dioxide which also has been used as a solvent for making nanoparticles.¹⁵⁷ However in all of these cases, the agglomeration of these nanoparticles is problematic as is the collection of the nanoparticles. One solution to these shortcomings is the encapsulate the nanoparticles with some protective shell, such as a alkanethiol capping ligand.¹⁹⁵

One such synthesis involved the production of nanoparticles directly in a polymer matrix to produce a metal-homopolymer nanocomposites.⁹⁶ A platinum precursor, [Pt(COD)Me₂], was infused into a bulk sample of poly(4-methyl-1-pentene) by SC-CO₂. Upon reducing with hydrogen, platinum nanoclusters were produced. The semi-crystalline homopolymer did not provide for control of cluster sizes or for the overall three dimensional morphology, but prevented cluster aggregation.⁹⁶

CHAPTER 2

POLYMER / CERAMIC NANOCOMPOSITES

2.1 Introduction

The use of disordered and ordered polymer/ceramic nanocomposites is of interest for numerous applications, primarily for improved mechanical properties of polymers.^{1, 16, 196, 197} Ordered polymer/ceramic nanocomposites have been prepared using a variety of self-assembled systems, such as ionic and neutral surfactants,^{6, 101, 121, 122, 198} ionomers,^{8-14, 77, 110, 128, 199} and block copolymers.^{16, 24, 139, 140} The fabrication of both disordered and ordered polymer/ceramic nanocomposites is discussed in detail in the introductory chapter.

In this part of the study, the fabrication of nanocomposites of Nafion and silicon dioxide was explored, as illustrated in Figure 1.1. The ionic domains of a Nafion film were exposed to humidified SC-CO₂ solution, and then infused with a tetraethoxysilane (TEOS) SC-CO₂ solution. Sol-gel chemistry was selectively performed within the ionic domains to produce the quasi-ordered polymer/ceramic nanocomposite. As a preliminary step, the solubility of TEOS in SC-CO₂ was investigated. Nafion/ceramic nanocomposites were also prepared from *n*-propanol solutions. The nanocomposites were characterized by electron microscopy and x-ray scattering.

2.2 Experimental Section

The goal of this part of the research project was the fabrication of ordered polymer/ceramic nanocomposites. The polymeric template was provided by an acidic polymer, Nafion, and the ceramic phase was silicon dioxide produced by TEOS sol-gel

chemistry. SC-CO₂ was used to impregnate the polymer with water and to deliver TEOS into the Nafion to enable the fabrication of bulk ordered polymer/ceramic nanocomposites.^{82, 83} Heat treatment facilitate the TEOS condensation reaction to proceed, which produced the ceramic silicon dioxide network structure. Samples were characterized by various methods including electron microscopy and x-ray scattering.

2.2.1 Materials

Tetrachoxysilane (TEOS) was the ceramic precursor and was used as received (Aldrich Chemical). *p*-Toluenesulfonic acid (*p*-TSA) was an additional acidic catalyst for sol-gel chemistry and used as received (Aldrich Chemical). The solvents for the sol-gel chemistry were Coleman-grade CO₂ (Merriam-Graves) and *n*-propanol (Aldrich Chemical), and were used as received. Nafion-117 films were purchased from DuPont. The clear Nafion films had a thickness of 0.184. Water treated by reverse osmosis was used for the sol-gel reactions and rinsing of Nafion films.

2.2.2 TEOS/CO₂ Phase Behavior

Before exploring the TEOS infusion into the polymers by SC-CO₂, the phase behavior and stability of TEOS/CO₂ mixtures was studied. Initial studies indicated that TEOS solutions with a small amount of water were stable for more than 24 hours in CO₂. The phase behavior determinations were carried out using a high-pressure variable volume view cell shown in Figure 2.1.¹⁵²

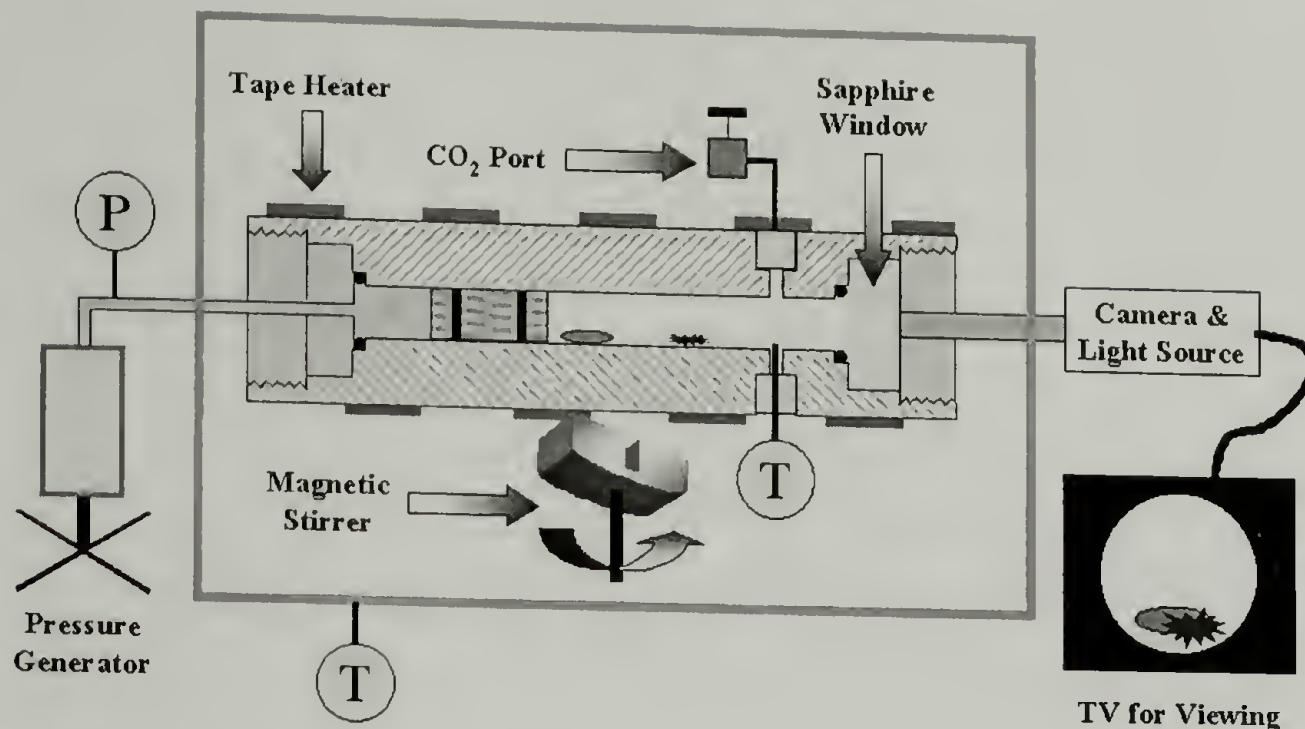


Figure 2.1 Schematic of variable volume view cell used to determine solubility

The view cell allows for direct observation of either reactions or phase behavior under a range of different pressures and temperatures. Internal pressure control of the view cell was provided by a water-filled pressure generator connected to the back of the cell. Water moved an internal piston, which increased or decreased the volume (a maximum of ~10 mL) and hence adjusted the pressure of the fluid phase. The internal pressure of the cell was determined by measuring the water pressure with a digital pressure gauge, assuming no loss of pressure by drag on the piston o-ring seals.¹⁵² Temperature control was provided by two PID temperature controllers attached to two different heating elements. The primary heater was a heating tape directly wrapped around the view cell and controlled to the desired temperature by a thermocouple measuring the fluid temperature directly inside the view cell. The second heater controlled an oven encasing the view cell to maintain a constant temperature of the external components, such as the CO₂ filling port. Constant temperature of the view cell is essential for visualization as temperature gradients will produce refractory

waves within the view cell. Direct visualization of the cell contents was made through a sapphire window and a boroscope attached to a light source and a video camera.

Solubility experiments were conducted by first loading the desired amount of TEOS and a magnetic stir bar into the view cell. The front of the cell was sealed by an o-ring against the sapphire window. Liquid CO₂ was loaded into the view cell from a blind vessel. The amount of CO₂ added was measured by weight difference of the vessel before and after transfer, and the weight percent of TEOS in CO₂ was calculated. The view cell and box were heated to the desired temperature and allowed to fully equilibrate. Under constant agitation provided by the internal magnetic stir bar, the piston was moved forward increasing the pressure until a single TEOS/SC-CO₂ phase was obtained. Pressure was lowered in a stepwise manner until a bubble was observed, indicating the presence of a second phase. The bubble point pressure was recorded and the pressure was increased until a single phase was obtained. The pressure was again lowered in a stepwise fashion with decreasing step-size until a reproducibility was obtained of +/-0.34 bar (+/-5 psi). Once the bubble point was determined at the desired temperature for at a given weight percent TEOS in SC-CO₂, the temperature was changed and the process was repeated. The phase diagram for mixtures of TEOS and SC-CO₂ is shown in Figure 2.2. Lines in Figure 2.2 are shown as a guide. The data show that TEOS is quite soluble.

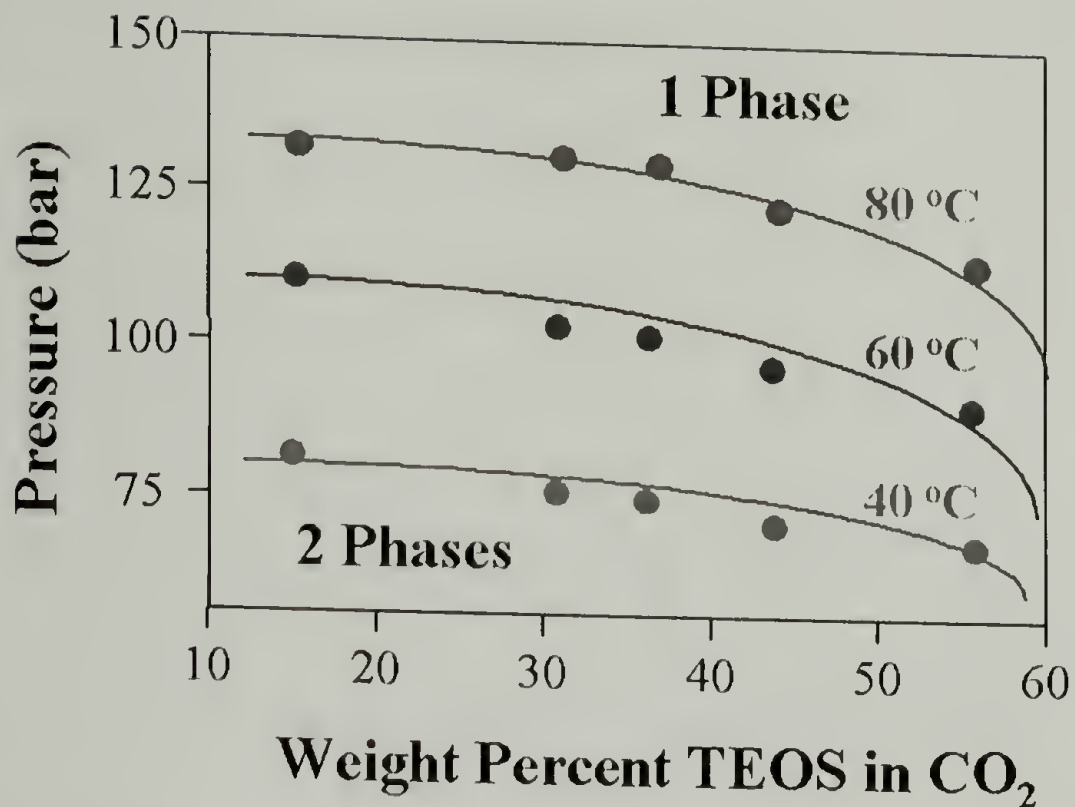


Figure 2.2 Phase behavior of TEOS in SC-CO₂

2.2.3 Silicon Dioxide Deposition

Deposition of SiO₂ on silicon wafers was performed using TEOS to determine if TEOS condensation chemistry can be conducted in CO₂. Reactions were run in 25 mL high-pressure stainless steel reactors (*Thar Designs*) equipped with a high-pressure needle valve. Each vessel was loaded with a silicon wafer (1 cm x 3 cm), *p*-TSA, and a small glass tube (i.d. = 1 cm) containing the TEOS and water separated from the catalyst to prevent reaction before CO₂ dissolved the components. Then the vessel was filled with SC-CO₂ at 120 °C and 260 bar ($\rho=0.28$ g/cc)¹⁵⁹ using a high-pressure computer controlled syringe pump (Isco Inc.). The final concentrations of the reactants are given in Table 2.1.

Table 2.1 Reaction Condition of Deposited Silicon Dioxide Films

Sample	A	B
TEOS (wt %)	4.0	4.0
Water (wt %)	6.0	0.4
<i>p</i> -TSA (wt %)	0.4	0.4
% Weight Gain	10.9	4.4

After a two hour soaking time, the reactors were slowly drained, opened, and the samples were removed for analysis. Weight gains of the silicon wafers are shown in Table 2.1.

The Silicon wafers were coated with a white powder and a white cracked film that was apparent to the eye. Closer observation of the samples obtained at the two reaction conditions was possible using scanning electron microscopy (SEM) Figure 2.3. Prior to SEM analyses, samples were coated with a light coating of gold to dissipate charging of the nonconductive sample.

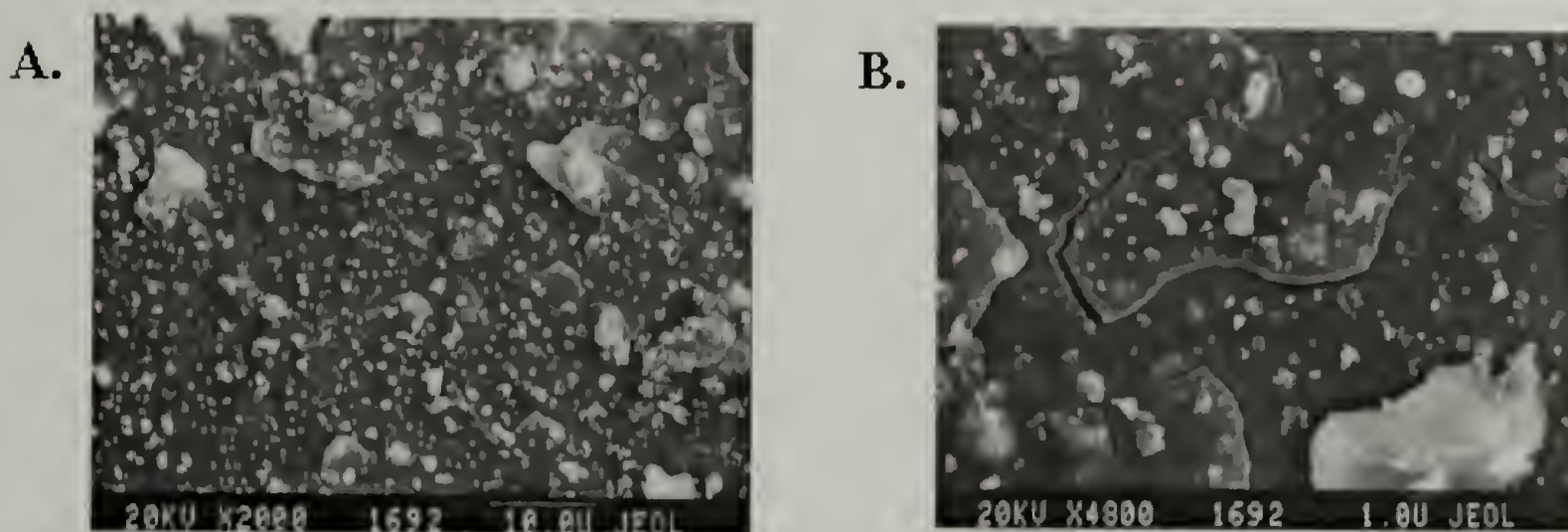


Figure 2.3 Deposition of silicon dioxide films on silicon wafers

Figure 2.3 shows the SEM pictures of the deposited silicon dioxide films. Both of the images showed cracked films of poor quality along with small particles. The particles

observed are a result of gas phase nucleation. There are not significant differences in the morphology of the films. Figure 2.3 B presents a higher magnification. This work showed that neat silicon dioxide could be produced by TEOS condensation in SC-CO₂. These experiments set the stage for subsequent reactions within acidic polymer films.

2.2.4 Nafion/Ceramic Nanocomposites

In this section, the preparation of Nafion/ceramic nanocomposites is discussed. The first step was the quantification of water uptake into Nafion films. Films used for reactions underwent a pretreatment and were subsequently infused with water and TEOS from both alcohol solution and SC-CO₂ solutions. The sol-gel reactions of TEOS with water requires an acid or base catalyst as discussed in the Introduction. The Nafion film has an acid group and could act itself as the catalyst. The resulting nanocomposites were then characterized by various methods such as electron microscopy and x-ray scattering.

2.2.4.1 Water Uptake into Nafion

The water uptake of Nafion was measured on (~2 cm x ~2 cm) squares Nafion pieces used as received. Three different conditions were studied: neat water at 25 °C, 100 °C, and exposure to humidified SC-CO₂ at 70 °C and 152 bar. For water uptake at 25 °C, films of known weight were placed into a covered glass beaker containing a magnetic stir bar and water. The films were removed at different intervals for weighing and returned to soak in the beaker. A similar procedure was used for water uptake at 100 °C, except that the water was refluxed in an Erlenmeyer flask connected to a water-cooled condenser. For three

representative samples, a higher uptake of water was observed at 100 °C than at 25 °C. Weigh percent gains of the Nafion films versus time at the different conditions are shown in Figure 2.4, where samples at 25 °C and 100 °C are represented by open and closed symbols, respectively.

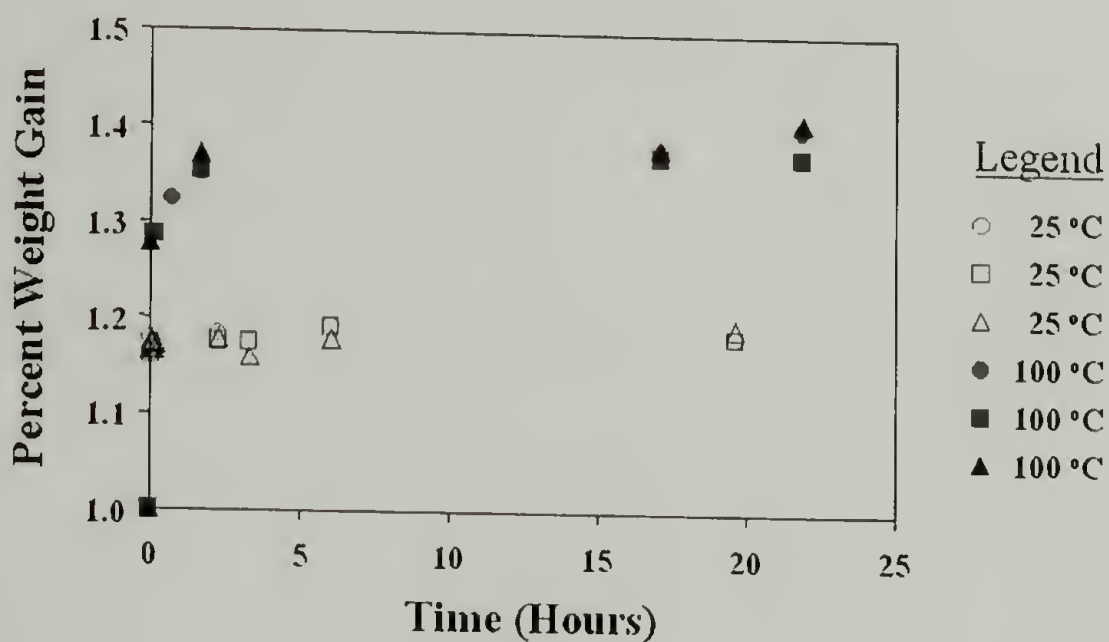


Figure 2.4 Uptake of neat water into Nafion

The uptake of water from SC-CO₂ solutions into Nafion films was also studied. Experiments were carried out in 6 mL high-pressure stainless steel reactors. Nafion film of known weight was placed into the reactor along with 1.0 mL of water held in a small glass support at the bottom of the reactor which prevented direct contact of the films with water. Then the reactor was placed in a thermostatic bath at 70 °C and filled with SC-CO₂ at the same temperature to 152 bar ($\rho=0.51$ g/cc)¹⁵⁹ using a high-pressure computer controlled syringe pump (Isco Inc.). After different intervals, the reactor was vented, the films were weighed. Two of the films were returned to the reactors and the infusion of water in SC-

CO₂ into the Nafion was repeated. The mass uptakes for six different samples are shown in Figure 2.5 with different symbols.

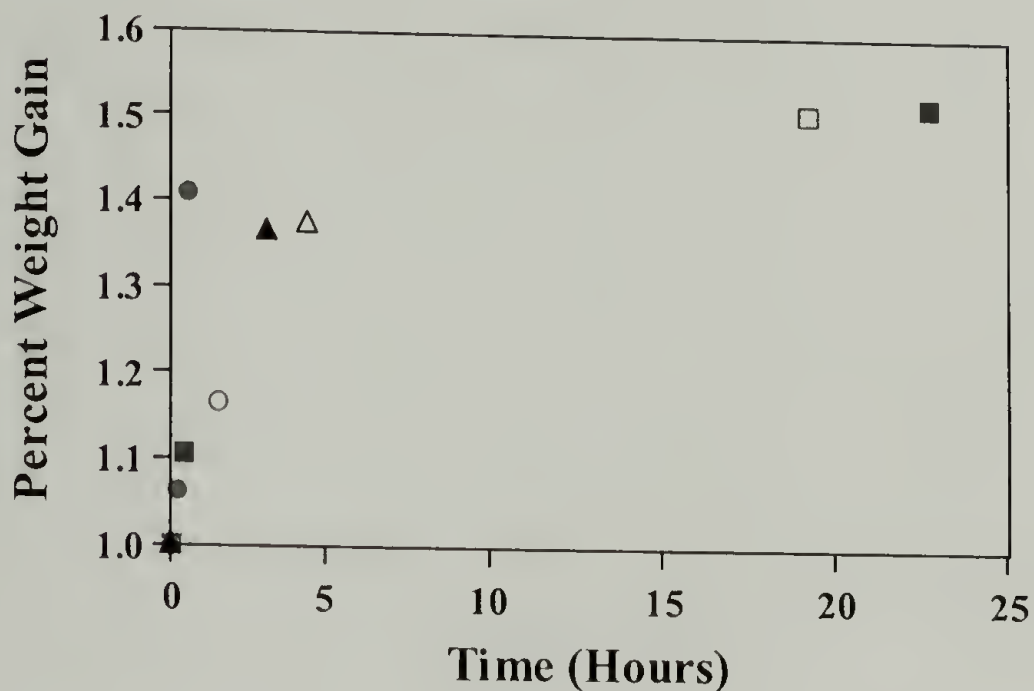


Figure 2.5 Nafion uptake of water from humidified SC-CO₂

In these experiments CO₂ is fully saturated with water as the solubility of water in CO₂ at these conditions is about 0.3 weight percent²⁰⁰⁻²⁰² well below the loading conditions. Comparison of Figure 2.4 and Figure 2.5 shows that the water uptake for the water SC-CO₂ conditions was slightly larger than for the water at 100 °C.

2.2.4.2 Nafion Pretreatment

Before TEOS infusion, the Nafion films were pretreated following a procedure described in the literature¹³⁰ to initialize the films to a common protonated state and to remove contaminants from commercial possessing. Nafion films were cut into squares (~2 cm x ~2 cm) and were soaked in concentrated hydrochloric acid for 12 hours. This was

followed by soaking twice in refluxing water for 12 hours. Afterwards, the films were soaked in concentrated nitric acid for 24 hours to fully oxidize the films. In the end, the films were soaked in stirred water until a neutral pH between 6.5 and 7.0 was measured.¹³⁰ The protonated films were stored in a vacuum oven at room temperature for drying until use.

2.2.4.3 TEOS Reactions in Nafion

Nafion/ceramic nanocomposites have been previously made using TEOS/alcohol solutions.⁸⁻¹² In order to compare with the reactions from TEOS/CO₂ solutions, Nafion/ceramic nanocomposites were made from TEOS/*n*-propanol solutions.⁸⁻¹² Nafion films were pretreated as previously described. After pretreatment, the weighed Nafion films were soaked in a 2:1 (v:v) *n*-propanol/water solution for 4 hours at room temperature, allowing water to be adsorbed into the acidic ionic domains of Nafion. The films were then transferred from the propanol/water solution to a 3:2 (v:v) of *n*-propanol/TEOS solution. Samples were removed at different intervals ranging from 14 to 120 minutes. Upon removal from the TEOS solution, the films were placed in a vacuum oven at 40 °C for 12 hours and then in a second vacuum oven at 120 °C for 12 hours to remove solvent and to further facilitate the sol-gel reaction. The amount of SiO₂ in the nanocomposite was determined by mass uptakes and is shown in Figure 2.6. Samples showed a steady uptake of the inorganic phase in Nafion with increasing soaking time.

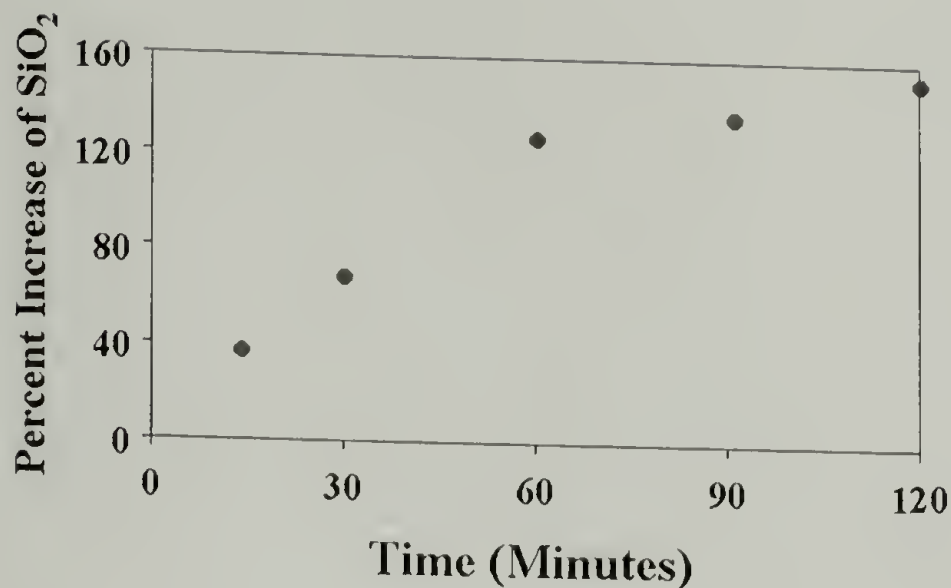


Figure 2.6 Weight percent increase of SiO₂ in Nafion nanocomposites upon reaction in a TEOS/*n*-propanol solution

SC-CO₂ was also used as a solvent instead of *n*-propanol to prepare Nafion/ceramic nanocomposites. Humidified SC-CO₂ was infused into pretreated Nafion and films were soaked in a TEOS/SC-CO₂ solution. Pretreated Nafion films of known weight were loaded into 6 mL high-pressure stainless steel reactors along with 0.25 ml of water. The reactors were sealed and immersed into a thermostatic bath maintained at 40 °C. SC-CO₂ was transferred to the reactors using a high-pressure computer controlled syringe pump (Iseo Inc.) at 40 °C to a pressure of 96 bar ($\rho=0.60$ g/cc),¹⁵⁹ resulting in approximately a 0.12 weight percent solution of water in CO₂.²⁰⁰⁻²⁰² After a four hour soak in humidified SC-CO₂, the reactors were vented through a back-pressure regulator and opened.

The reactors were quickly dried and the Nafion films were placed back into the reactors. TEOS (1.0 mL) was then added to the reactors, which were sealed, immersed into a thermostatic bath at 40 °C, and pressurized with CO₂ to 96 bar. The samples were removed from the reactors in different intervals ranging from 10 to 120 minutes. Upon removal from the reactors, films were placed in a vacuum oven at 40 °C for 12 hours followed by a treatment at 120 °C for 12 hours in another vacuum oven to remove solvent and further

facilitate the sol-gel reaction. The amount of SiO_2 in the nanocomposite was determined by mass uptakes and it is shown in Figure 2.7. The mass uptakes from SC-CO_2 showed more scatter in the data and also reached a lower percentage of SiO_2 than in the Nafion reactions in *n*-propanol (Figure 2.6). The total uptake of SiO_2 was lower due to the low concentrations of water and TEOS used. In several experiment, much higher mass uptakes of SiO_2 were achieved using slightly different reaction conditions. In one experiment, a Nafion sample was soaked in humidified SC-CO_2 followed by a soak in a TEOS/ SC-CO_2 solution at 40°C for 24 hours. After drying in the vacuum oven, this sample resulted in a 53 weight percent SiO_2 Nafion/ceramic nanocomposite.

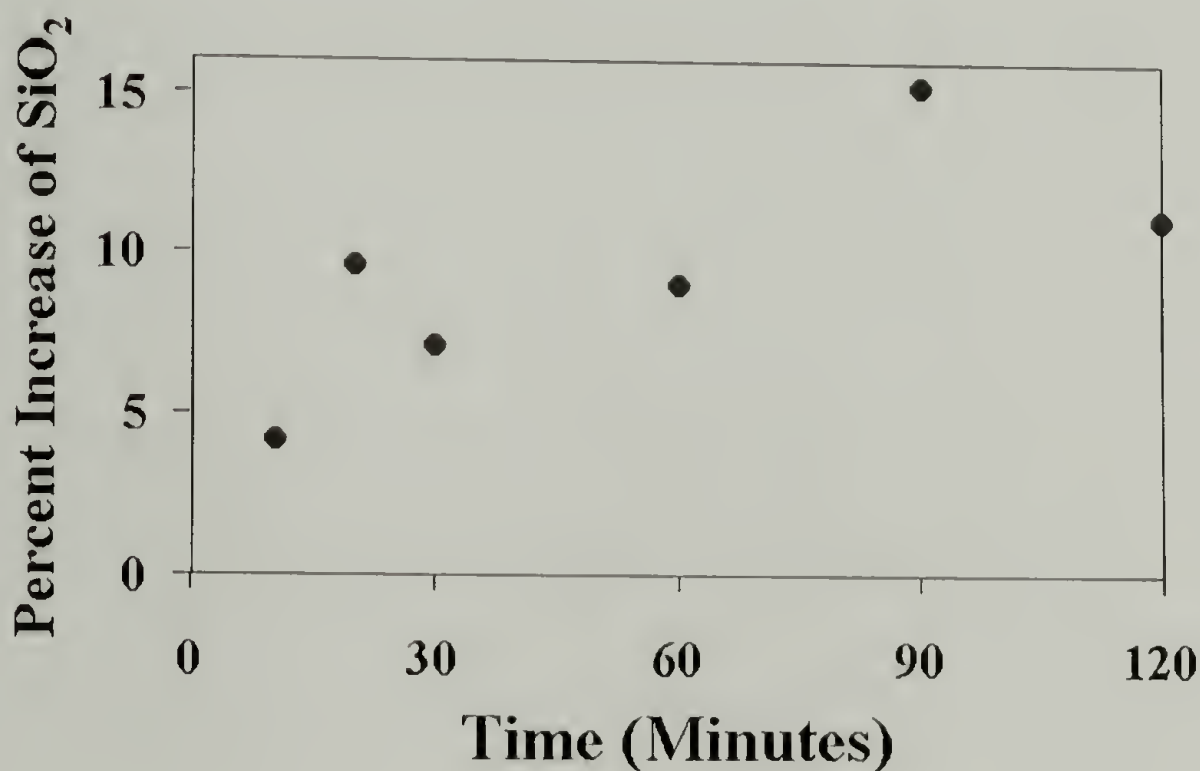


Figure 2.7 Weight percent increase of SiO_2 in Nafion nanocomposites upon reaction of TEOS/ SC-CO_2

Nafion/ceramic nanocomposites were characterized by transmission electron microscopy (TEM) and wide and small angle X-ray scattering (WAXS & SAXS). TEM was conducted using a JEOL 100CX operating at 100 kV. Sections for analysis (~50 nm thick)

were obtained via microtoming at room temperature on a Reichert-Jung microtome using a freshly prepared glass knife. The ceramic nanoparticles provided sufficient contrast for TEM; hence, additional enhancement via staining was not required. WAXS measurements were performed using a Siemens D-500 diffractometer equipped with a copper anode and utilizing the copper $K\alpha$ radiation ($\lambda=1.54 \text{ \AA}$). SAXS measurements were performed on a Rigaku RU-H3R rotating copper anode X-ray diffractometer equipped with an Osmic multilayer focusing optics. The incident copper $K\alpha$ radiation ($\lambda=1.54 \text{ \AA}$) was passed through the sample and scattering patterns were collected with Fuji ST-VA image plates in an evacuated Statton-type scattering camera. Scattering patterns were acquired with a Fuji BAS-2500 image plate scanner and intensity profiles were obtained from radial averages of the scattering pattern intensities. The TEM images of untreated Nafion and a Nafion/SiO₂ nanocomposite are shown in Figure 2.8 and Figure 2.9 respectively. WAXS and SAXS patterns for three different examples are shown in Figure 2.11 and Figure 2.10, respectively.

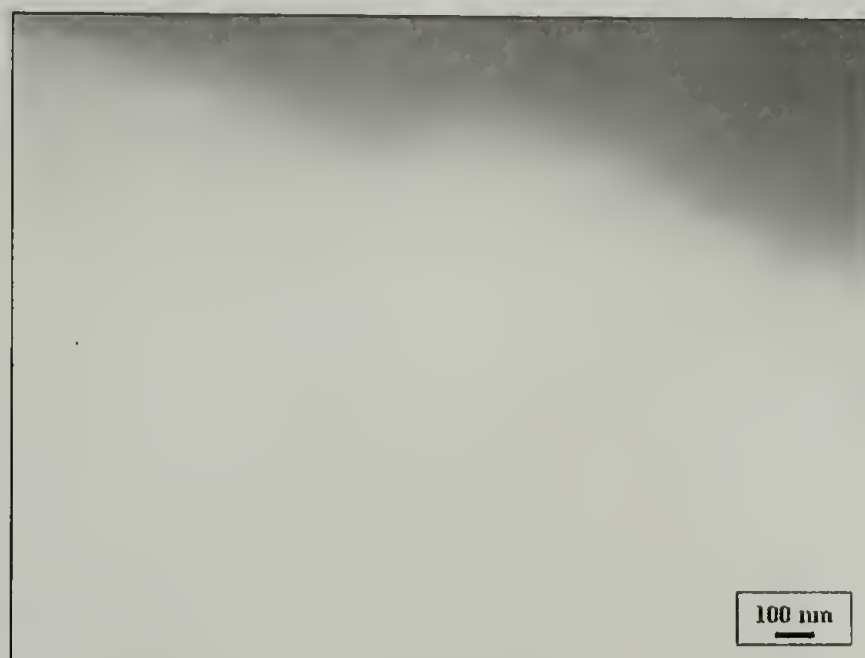


Figure 2.8 TEM micrograph of unmodified Nafion



Figure 2.9 TEM micrograph of 7 weight percent SiO₂ Nafion/ceramic nanocomposite

It was important to note that Nafion did not have any visible structure upon TEM imaging before modification, hence any new morphology would be due to the SiO₂ phase in Nafion. Nafion film was microtomed and collected on a copper grid. Figure 2.8 shows the featureless TEM image of untreated Nafion, where the black line bar at the top of the figure part is of the copper grid. Nafion/ceramic nanocomposites were microtomed and investigated by TEM. Figure 2.9 shows an example of a TEM image of a Nafion/ceramic nanocomposites containing 7 weight percent of SiO₂. SiO₂ nanoparticles (~4 nm) were observed evenly distributed through the Nafion film.

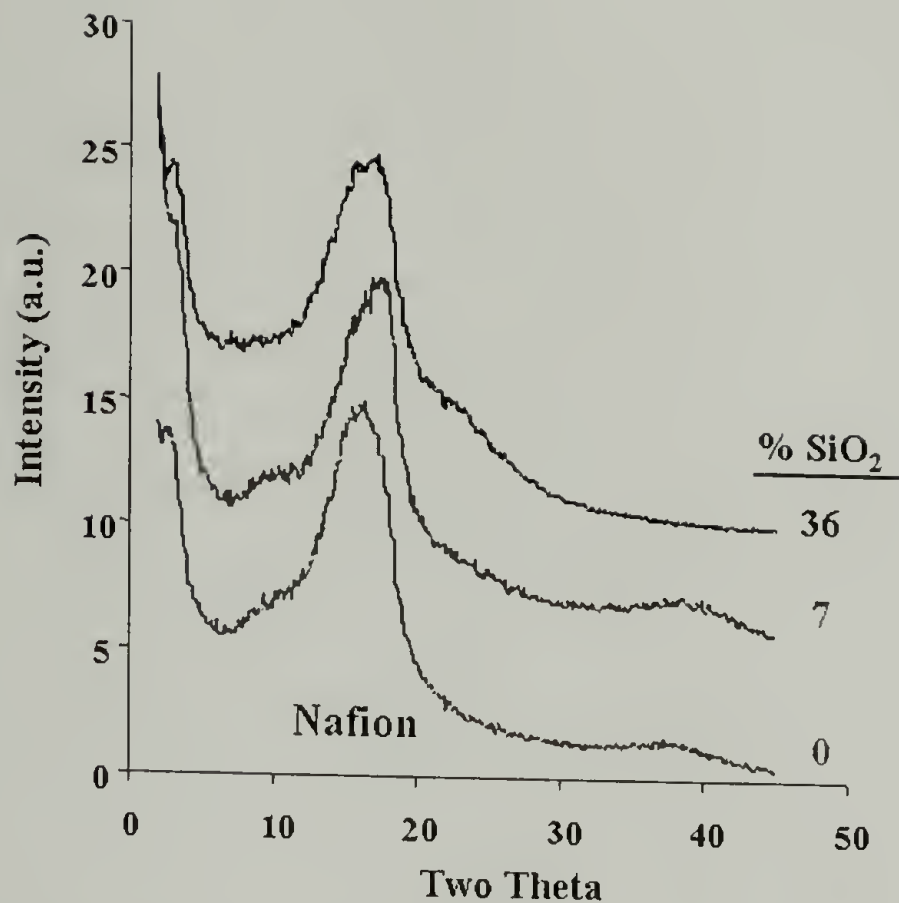


Figure 2.10 WAXS of Nafion and Nafion/silica nanocomposites

Figure 2.10 shows the WAXS pattern of a Nafion film and the Nafion/SiO₂ nanocomposites with 7 and 36 weight percents of SiO₂. This scattering patterns show several peaks, such as a small shoulder located at 3 degrees two theta which corresponds to a size of about 3 nm, the rough spacing of the ionic clusters. A second broad peak centered around 18 degrees two theta corresponding to the crystalline peak of Nafion.^{10-12, 127} This peak survives infusion of the ceramic phase which shows that the crystallinity of the Nafion is not affected by the formation of the ceramic network.¹⁰⁻¹² Another small peak at about 38 degrees two theta is also observed. This peak is inherent to Nafion and most likely a secondary reflection of the crystalline peak.¹⁰⁻¹² Sol-gel chemistry of TEOS will typically produce amorphous SiO₂^{78, 79} and the SiO₂ fabricated with Nafion is also amorphous. This is supported by the small shoulder at about 23 degrees two theta in the sample with the highest weight percent

SiO₂ and the absence of peaks characteristic of a crystalline SiO₂ phase occurring at 43 degrees two theta.²⁰³

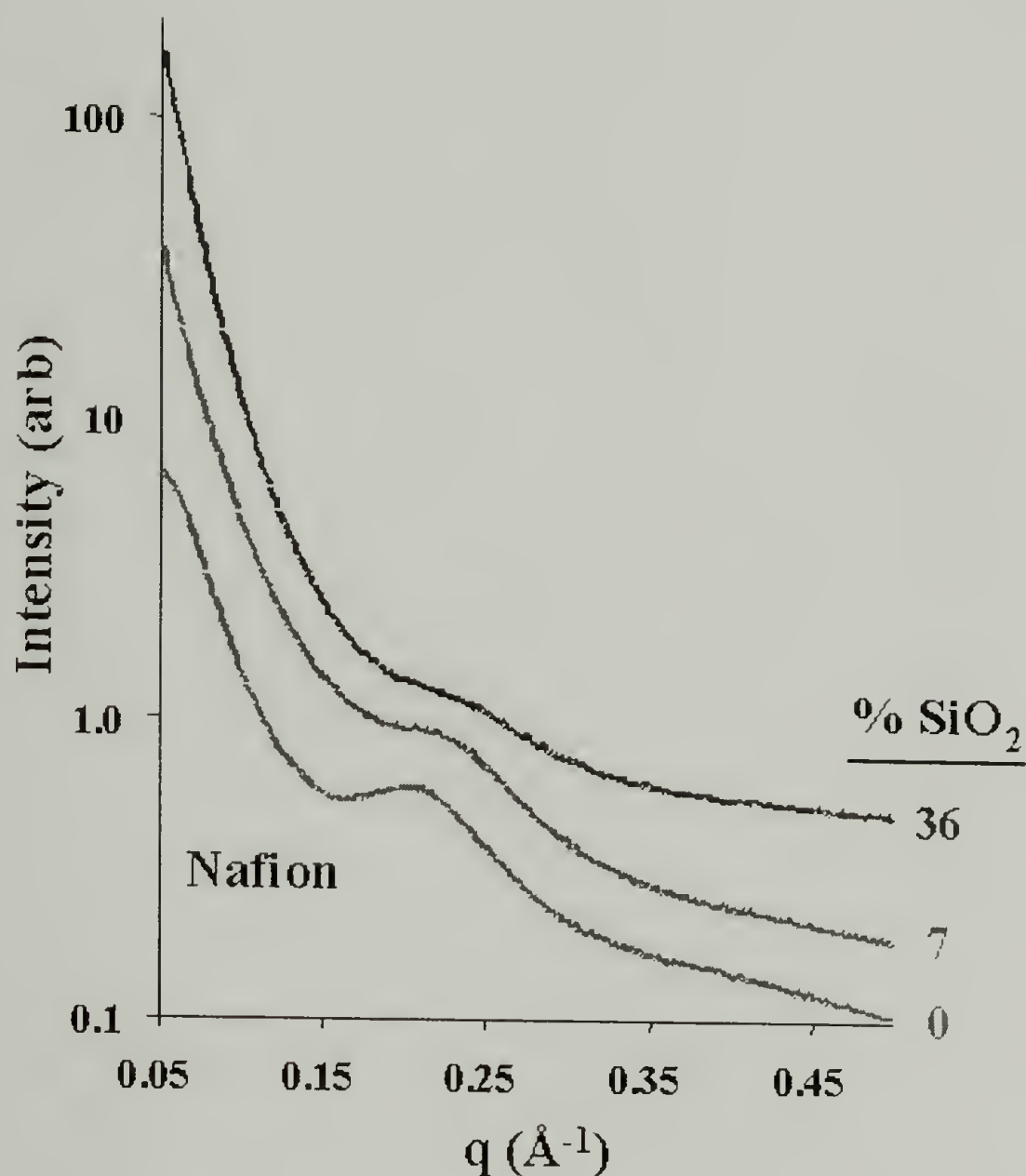


Figure 2.11 SAXS of Nafion/ceramic nanocomposites

Figure 2.11 shows the SAXS patterns for the same three sets of samples as shown in Figure 2.11. Nafion shows a broad peak centered at a scattering vector of $q = 0.21 \text{ \AA}^{-1}$, correlating to a size of about 3 nm. After TEOS infusion and condensation, this peak remains in approximately the same location suggesting the structure of the Nafion template is

preserved. This directly matches with the literature for Nafion/ceramic nanocomposites, including the loss decrease in the SAXS peak due to a decreasing contrast factor.¹⁰⁻¹²

CHAPTER 3

POLY(STYRENE)-*BLOCK*-POLY(ACRYLIC ACID) NANOCOMPOSITES

3.1 Introduction

Ordered polymer/metal nanocomposites have previously been prepared within both diblock and random copolymers containing acidic groups such as poly(acrylic acid) (PAA) as reviewed in the Introduction.^{27-29, 102, 103, 113, 204} Polystyrene (PS) and PAA random copolymers have been used to produce disordered polymer/metal sulfide nanocomposites upon loading thin films with aqueous metal sulfide precursors. Upon subjecting the films to hydrogen sulfide, metal sulfide nanoparticles were produced.^{102, 103, 113, 204} Ordered polymer/metal and polymer/metal sulfide nanocomposites have been fabricated from diblock copolymers with one domain containing carboxylic acid functionality. The acidic groups bound aqueous or volatile precursors, which were subsequently reduced or subjected to hydrogen sulfide to produce metal or metal sulfide nanoparticles.²⁷⁻²⁹ This previous work demonstrates the feasibility of using a PS-*b*-PAA block copolymer to produce ordered nanocomposites.

In this section, the fabrication of ordered nanocomposites using supercritical carbon dioxide (SC-CO₂) as a solvent to infuse metallic precursors into a polymeric template is described, as outlined in Figure 1.1. The first sets of experiments consisted of the infusion of a platinum precursor into PS to investigate the effect of the reduction conditions on the nanoparticle size. Infusion of organometallics by SC-CO₂ solutions was then carried out in a polystyrene-*block*-poly(acrylic acid) (PS-*b*-PAA) copolymer which resulted in the

organometallics selectively binding to the poly(acrylic acid) domain. Reduction, yielded the metal nanocomposites, where were then characterized.

3.2 Experimental Section

Nanocomposites were produced within polystyrene and polystyrene-*block*-poly(acrylic acid) copolymer. The nanocomposites were fabricated by the infusion of organometallic/CO₂ solutions into the polymeric systems followed by treatment with either hydrogen or hydrogen sulfide yielding the corresponding polymer/metal or polymer/metal sulfide nanocomposites. Characterization of the materials was carried out by TEM and WAXS.

3.2.1 Materials

Polystyrene ($M_{wt} = 280,000$ g/mole) was used as received from Aldrich Chemical. Polystyrene-*block*-poly(acrylic acid) (PS-*b*-PAA) was used as received from Dr. Steve Smith at Procter & Gamble. The copolymer had a total molecular weight of 107,000 g/mol (100,000 g/mole PS and 7,000 g/mole PAA) with a 6.5 volume percent of PAA to give a spherical nature of PAA surrounded by PS, with the chemical structure shown in Figure 3.1. The metal precursors were (1,5-cyclooctadiene) silver (hexafluoroacetylacetonate) [Ag(COD)hfac] (Aldrich Chemical), (1,5-cyclooctadiene) dimethylplatinum (II) [Pt(COD)Me₂] (Strem Chemical), and Iridium (II) (Acetylacetonate) (1,5-Cyclooctadiene) [Ir(COD)acac] (Strem Chemical) and were all used as received. Palladium (II) cyclopentadiene methylallyl [PdCp(C₃H₅)] was synthesized by Dr. David Long in our group

and sublimed prior to use.⁹³ The structures of the different metal precursors are shown in Figure 3.2. Reduction of Pt(COD)Me₂ with hydrogen is autocatalytic as shown in Figure 1.5 and discussed in the Introduction.^{90-92, 96, 98} These organometallics dissolve in SC-CO₂ and are easily reduced with hydrogen to yield metal films.^{93-95, 97} For the fabrication of metal sulfide nanoparticles, lead bis-hexafluoroacetylacetonate [Pb(hfac)₂] was used as received from Strem Chemical. This precursor reacts with hydrogen sulfide to produce lead sulfide (PbS). N,N-Dimethylformamide (DMF) was used as received from Aldrich Chemical. Coleman grade carbon dioxide, ultra-high purity hydrogen (H₂), and hydrogen sulfide (H₂S) were used as received from Merriam Graves.

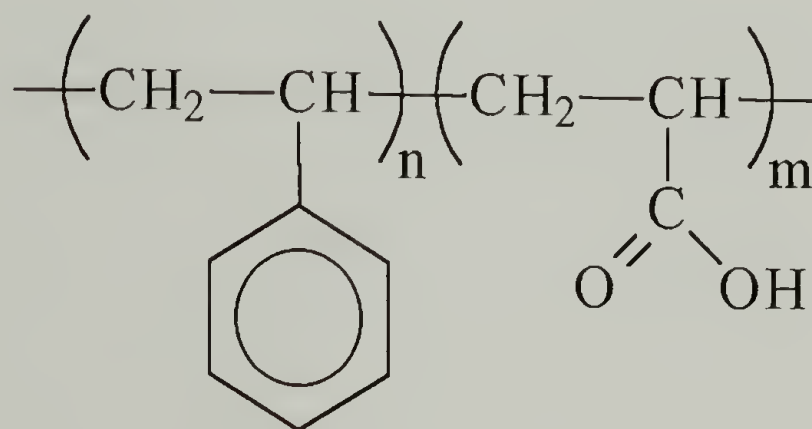


Figure 3.1 Polystyrene-*block*-poly(acrylic acid) copolymer

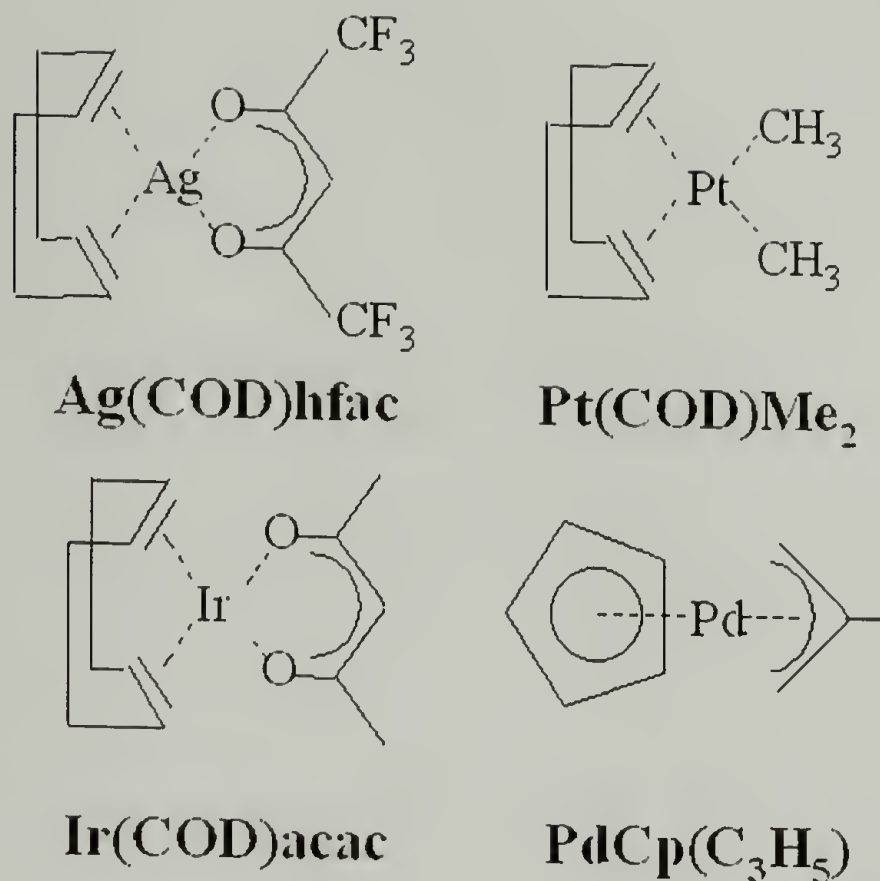


Figure 3.2 Metal precursors for nanoparticle formation

3.2.2 Polystyrene/Platinum Metal Nanocomposites

The effect of the reduction conditions for a platinum precursor within bulk polystyrene was studied. A polystyrene plaque was prepared by melt pressing at 160 °C and loaded with 117 mg of Pt(COD)Me₂ into a high-pressure stainless-steel reactor equipped with a high-pressure needle valve. The reactor was heated to 60 °C in a thermostatic bath and filled with SC-CO₂ at the same temperature to 135 bar using a high-pressure, computer-controlled syringe pump (Isco Inc.). After a 30 hour soak to allow the precursor diffusion through the PS, the reactor was cooled to 0 °C, and slowly vented through a back-pressure regulator. The drop in temperature will allow for system to drop below the glass transition temperature (T_g) of the polymer, which is 105 °C at atmospheric pressure, 65 °C at a pressure of 36 bar, 50 °C at a pressure of 48 bar, and 35 °C at a pressure of 60 bar of CO₂.¹⁷⁶ The

reactor was opened and the sample was cut in half. Each part was subjected to different hydrogen reduction conditions: neat H₂ and a plasticizing SC-CO₂/H₂ mixture, as show in Table 3.1. Neat H₂ was added to the reactor at 60 °C from a high-pressure manifold via a pressure drop to 102 bar. After a two hour soak, the reactor was slowly vented. The reduction with the SC-CO₂/H₂ mixture was carried out by first plasticizing the infused PS for 2 hours with SC-CO₂ at 60 °C & 135 bar and then adding H₂ to a final pressure of 170 bar from a high-pressure manifold via a pressure drop. After an additional 2 hour soak, the reactor was cooled to 0 °C, slowly vented, and the sample removed for analysis.

Transmission electron microscopy (TEM) was conducted using a JEOL 100CX operating at 100kV. Sections for analysis (40 nm thick) were obtained via microtoming at room temperature on a Reichert-Jung microtome using a freshly cut glass knife. Wide angle X-ray scattering (WAXS) was performed using a Siemens D-500 diffractometer with a copper anode ($\lambda=1.54 \text{ \AA}$).

Different nanoparticles sizes were observed for Pt(COD)Me₂ reduction under the different reaction conditions (Table 3.1). Neat H₂ reduction produced approximately 10 nm clusters (Figure 3.3) while the SC-CO₂/H₂ reduction produced approximately 30 nm clusters (Figure 3.4). The WAXS images (Figure 3.5) also reflected the difference in the size of the platinum nanoparticles and the width of the platinum (111) peak centered at 40 degrees two theta.²⁰³ According to the Scherrer equation (Equation 3.1), the apparent crystallite size is inversely proportional to the width of the peak at half maximum height.

$$Size(\text{\AA}) = \frac{C\lambda}{B \cos \theta_B} \quad \text{(Equation 3.1)}$$

In Equation 3.1, λ is the X-ray wavelength (1.54 Å for Cu K $_{\alpha}$), C is a constant that accounts for numerous factors such as wavelength broadening of the instrument (C = 0.9,

determined by running a inorganic crystalline standard), B is the width of the peak at half the maximum peak, and θ_B is the peak location.

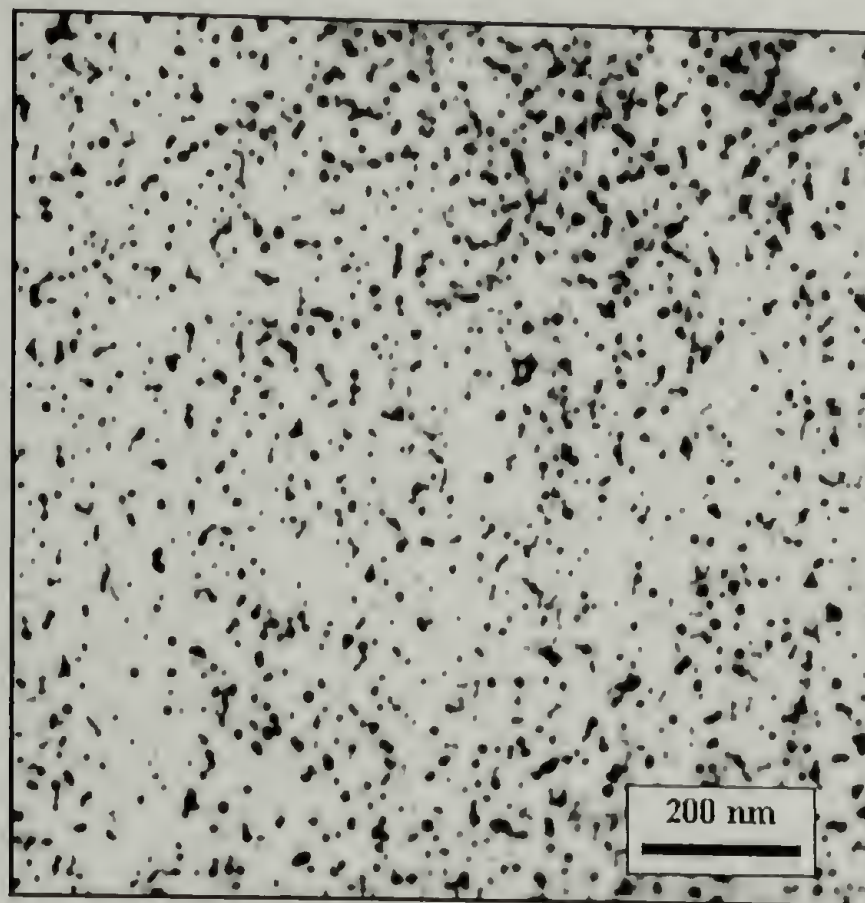


Figure 3.3 H_2 reduction to produce ~ 10 nm Pt nanoclusters in PS

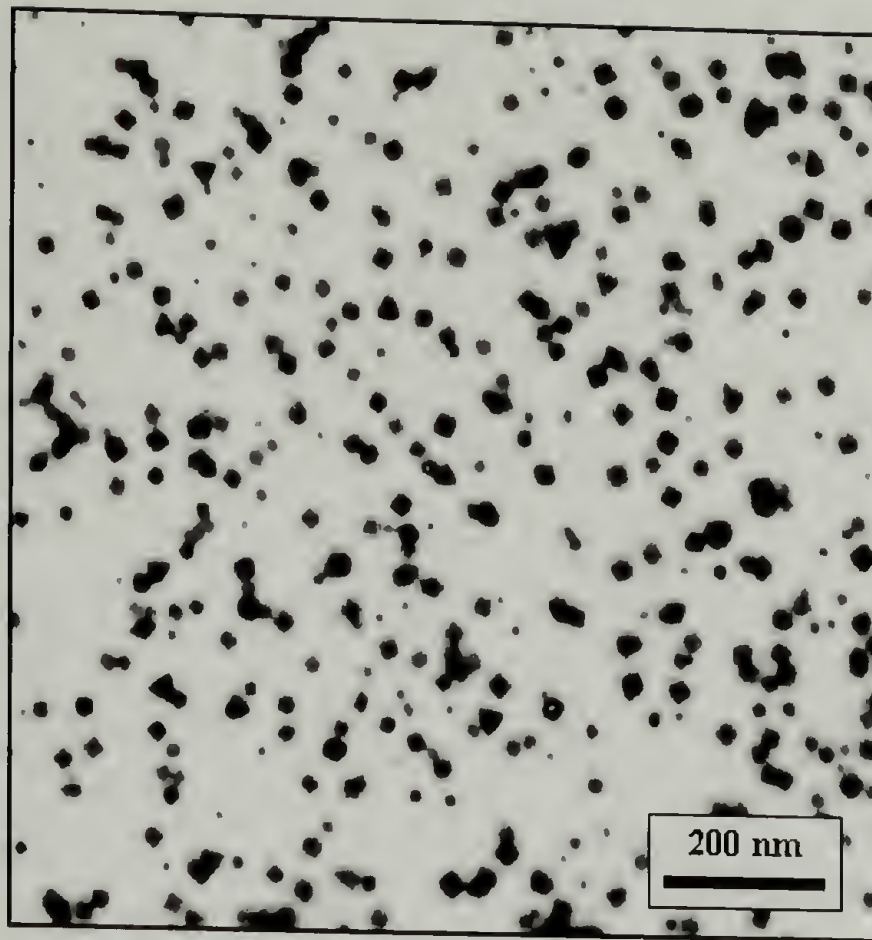


Figure 3.4 CO_2/H_2 reduction to produce ~ 30 nm Pt nanoclusters in PS

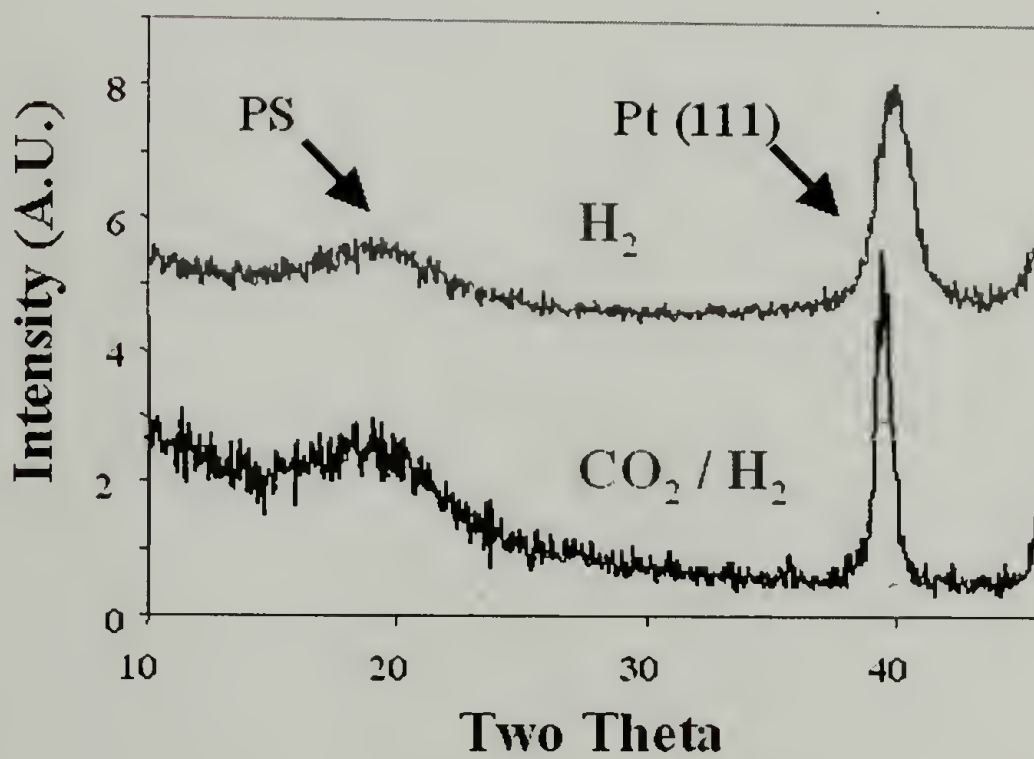


Figure 3.5 WAXS of platinum nanoparticles in polystyrene

Table 3.1 Preparation of Platinum Nanoparticles in Polystyrene

SC-CO ₂ (bar)	H ₂ (bar)	TEM size (nm)	TEM Picture	Apparent Scherrer Analysis Size (nm)
-	102	~10	Figure 3.3	6
135	170	~30	Figure 3.4	11

Scherrer analysis of the platinum peak gave apparent sizes of 6 nm for the sample reduced with neat H₂ reduction 13 nm for the sample reduced with the SC-CO₂/H₂ mixture (Table 3.1). The crystallite sized determined by the Scherrer equation does not always agree with the actual size, as nanoparticles could be made up of a large number of crystallites.^{21, 205}

The size of the platinum nanoparticles is determined by a competition between the rate of nucleation and the diffusion of the platinum precursor to a nucleation site within the polystyrene. In the unplasticized system with neat H₂, the diffusion of the organometallic is slow and reduction of the precursor will occur in place giving rise to smaller particles, as nucleation dominates vs. diffusion and growth. In the polystyrene plasticized with the CO₂/H₂ mixture, the organometallic has much higher mobility and could diffuse to previously reduced platinum clusters producing larger particles.

3.2.3 PS-*b*-PAA / Metal Nanocomposites

PS-*b*-PAA diblock copolymer were used as templates for the formation of ordered nanocomposites, containing platinum and silver nanoclusters. This templating scheme is illustrated in Figure 3.6. Additional nanocomposites of palladium and iridium were also fabricated.

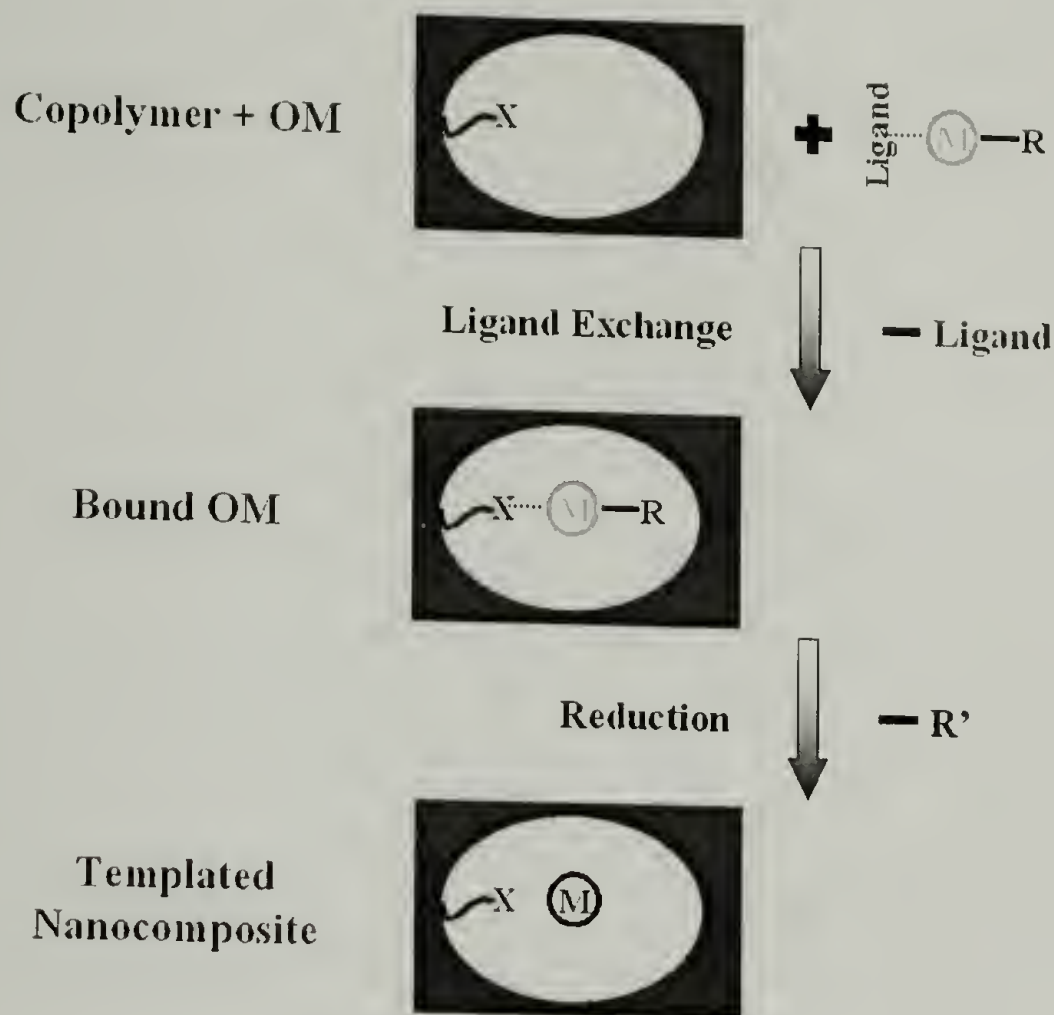


Figure 3.6 Copolymer templating process

Figure 3.6 illustrates the templating process used within PS-*b*-PAA diblock copolymer for the formation of ordered nanocomposites. One block of the copolymer has an active phase, represented by the white domain and the functional group X (in this example PAA), and an inactive phase show as the darker region (PS). A suitable organometallic is dissolved in SC-CO₂ and impregnated inside the block copolymer where the organometallic undergoes ligand exchange with the functional group X (acrylic acid) within the active phase (PAA). This selective binding of the precursor prior to reduction is the key to the templating process. Upon the proper reduction conditions, the organometallic is reduced to produce a templated nanocomposite.

3.2.3.1 PS-*b*-PAA / Platinum Nanocomposites

Platinum/PS-*b*-PAA nanocomposites were fabricated following the scheme shown in Figure 1.1 and Figure 3.6. The platinum precursor was first infused into PS-*b*-PAA using a SC-CO₂ solution. These samples were then subjected to different reduction conditions to study their effect on platinum particles size. Different reductions are expected to yield different results, as the nanoparticle size is determined from the competition between nucleation and crystal growth.

PS-*b*-PAA films were prepared by solvent casting the copolymer from DMF solutions onto glass slides. The films were dried under vacuum for 24 hours at 125 °C to remove any remaining solvent. A sample of the film was cut, weighed and placed into a glass test tube (i.d. = 1 cm). Pt(COD)Me₂ (30 mg) was added into a high-pressure stainless steel reactor equipped with a high-pressure needle valve within a nitrogen glove box. The test tube simplified sample handling and was placed within the reactor to initially separate the copolymer from the organometallic, while not interfering with the precursor diffusion into the polymer from SC-CO₂ solution. The reactor was sealed, heated to 60 °C in a thermostatic bath, and filled with SC-CO₂ at the same temperature to a pressure of 135 bar. This resulted in a 0.8 weight percent solution of Pt(COD)Me₂ in CO₂. At these conditions, the organometallic compound completely dissolved in CO₂.²⁰⁶ After a 12 hour soaking period, the reactor was cooled to 0 °C, and slowly vented through a backpressure regulator to suppress polymer foaming. The excess unbound precursor was removed by repeating the soaking process three times. After the final extraction, the sample was cut into four pieces, one was saved for analysis and three were subjected to different reduction conditions, as shown in Table 3.2.

Table 3.2 Various Reduction Conditions of Platinum precursor in PS-*b*-PAA

Reduction	Temperature (°C)	SC-CO ₂ (bar)	H ₂ (bar)	TEM Picture
A	60	135	170	Figure 3.8
B	60	-	135	Figure 3.9
C	25	-	14	Figure 3.10

Reduction A was carried out on a section of the platinum infused copolymer in a high-pressure reactor. The reactor was filled with SC-CO₂ at 60 °C and 135 bar. After a two hour soaking time, additional hydrogen was added via pressure drop from a high pressure manifold to a final pressure of 170 bar. These conditions were maintained for an additional 2 hours, after which time the reactor was cooled to 0 °C and slowly vented. Reductions B and C were carried out with neat H₂ at two different conditions. Reduction B was carried out on a section of the platinum-infused copolymer into a high-pressure reactor with hydrogen at 60 °C and 135 bar for 2 hours. Reduction C was carried out on a section of the platinum infused copolymer into a high-pressure reactor with hydrogen at 25 °C and 14 bar for 48 hours.

Each of the samples was analyzed by TEM. Figure 3.7 shows the platinum infused PS-*b*-PAA sample prior to reduction. The TEM micrograph of the sample subjected to the plasticizing CO₂/H₂ mixture, Reduction A is shown in Figure 3.8. The reductions with neat hydrogen at different pressures and temperatures, Reduction B and Reduction C, are shown in Figure 3.9 and Figure 3.10, respectively.

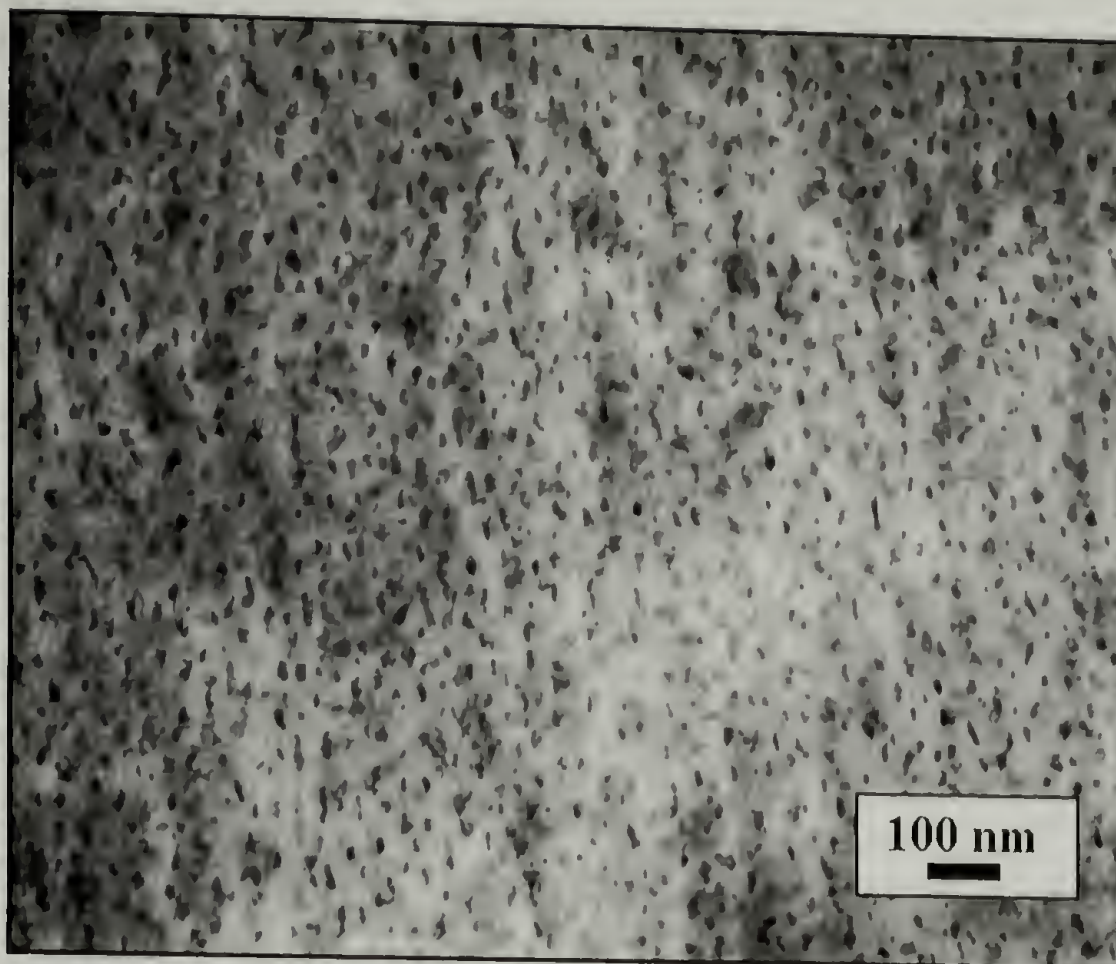


Figure 3.7 Platinum precursor in PS-*b*-PAA before reduction

Figure 3.7 demonstrates the templating ability and spherical nature of the PAA. The observed contrast arise directly from the platinum precursor and is not enhanced by additional staining agents common for studying block copolymer morphology. The aggregates are just under 20 nm in size and some are slightly elongated, which is an artifact of microtoming.

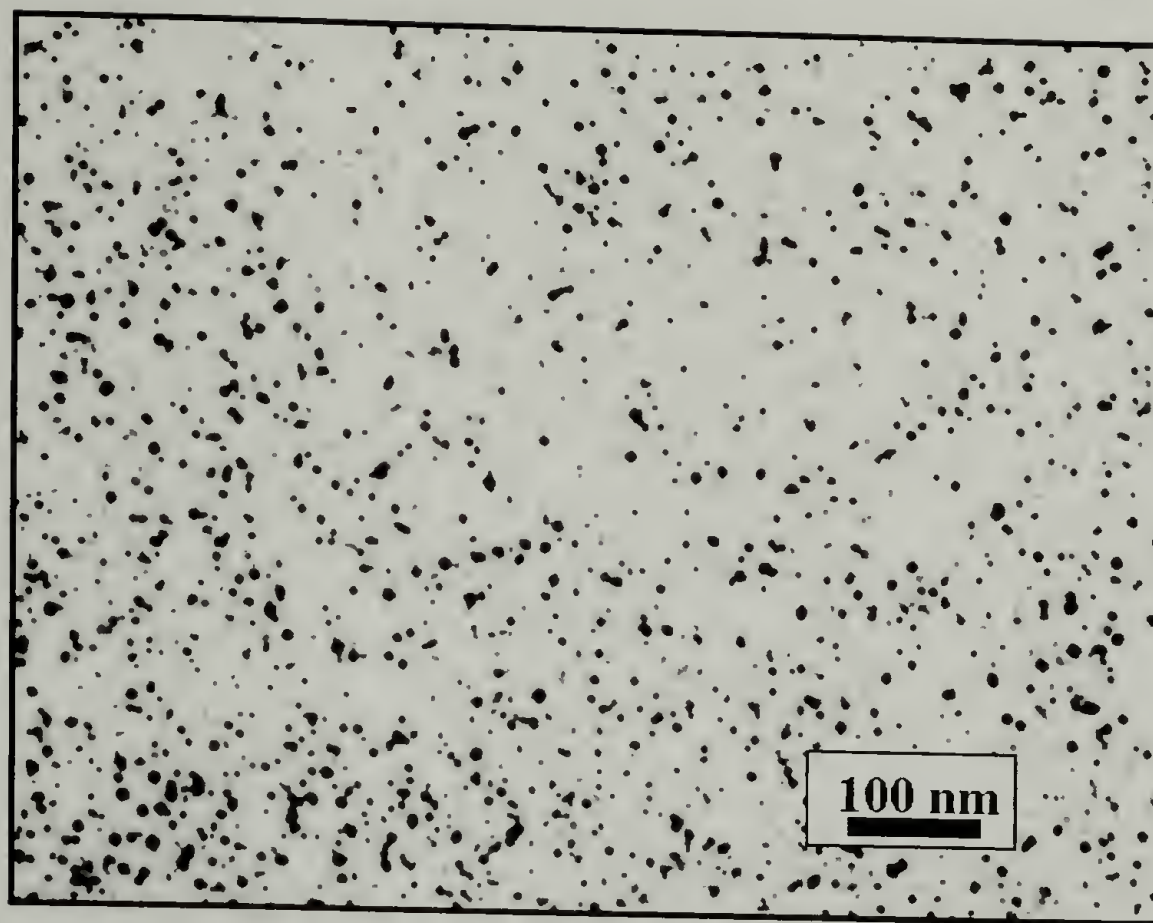


Figure 3.8 Platinum/PS-*b*-PAA nanocomposite subjected to Reduction A

The sample reduced using the plasticizing CO₂/H₂ mixture (Reduction A) gave the largest nanoparticles and an apparent loss of template structure with nanoparticles ranging from 5-20 nm (Figure 3.8). This is a consequence of the large mobility of the precursor during reduction under these conditions which allows the diffusion of precursor to other pre-formed platinum catalytic sites. The plasticizing system also provides for an increasing mobility of the nanoparticles which could lead to nanoparticle aggregation or coalescence, as these particles are larger than in the other samples (Reduction B and C).

The effect of the CO₂ plasticization on the growth of platinum nanoclusters has also been observed within poly(4-methyl-1-pentene) (PMP) films.¹⁴² PMP films were loaded with Pt(COD)Me₂ cut into pieces and reduced with hydrogen in the presence of different amounts of plasticization by SC-CO₂. Upon analysis by WAXS, larger clusters were produced with increasing pressures of SC-CO₂.¹⁴²

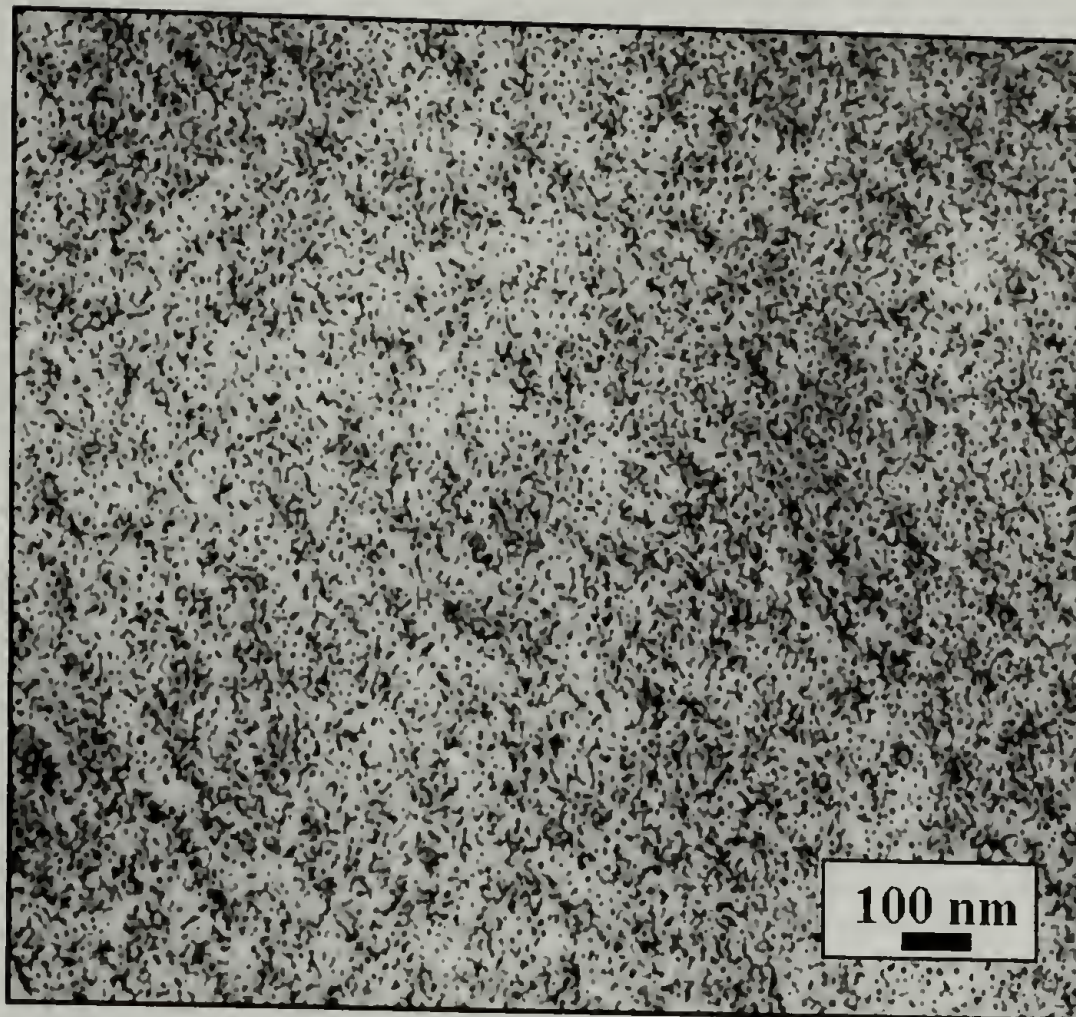


Figure 3.9 Platinum/PS-*b*-PAA nanocomposite subjected to Reduction B

The material produced from the neat hydrogen reduction of Pt(COD)Me₂ in PS-*b*-PAA at 60 °C and 135 bar, (Reduction B) showed loss of template structure as with the CO₂/H₂ mixture (Reduction A). In this case, however, smaller platinum nanoparticles (~5 nm) than in the plasticizing reduction scheme were observed suggesting the lower mobility of the precursor in neat H₂.

The cases for imperfect templating of nanoparticles within copolymers has been investigated for other systems. In the synthesis of nanocomposites made by static casting from solution with the precursor followed by reduction with H₂ (100 °C and 5 bar) or UV radiation by Cohen and coworkers problems arose where the morphology of the palladium and platinum nanoclusters within microphase separated diblock copolymers did not match

perfectly with either the starting copolymer or the sample before reduction.²¹ Some of the clusters are found outside the microdomains suggesting that the precursor can travel through the copolymer matrix before reducing or small cluster could move following reduction.²¹⁻²³ This could be due to exothermic reduction process, which raise the local temperature above the T_g of the blocks.²¹ At conditions above the T_g of the polymer matrix, the movement of the nanoparticles would increase and could result in the disruption of the morphology.

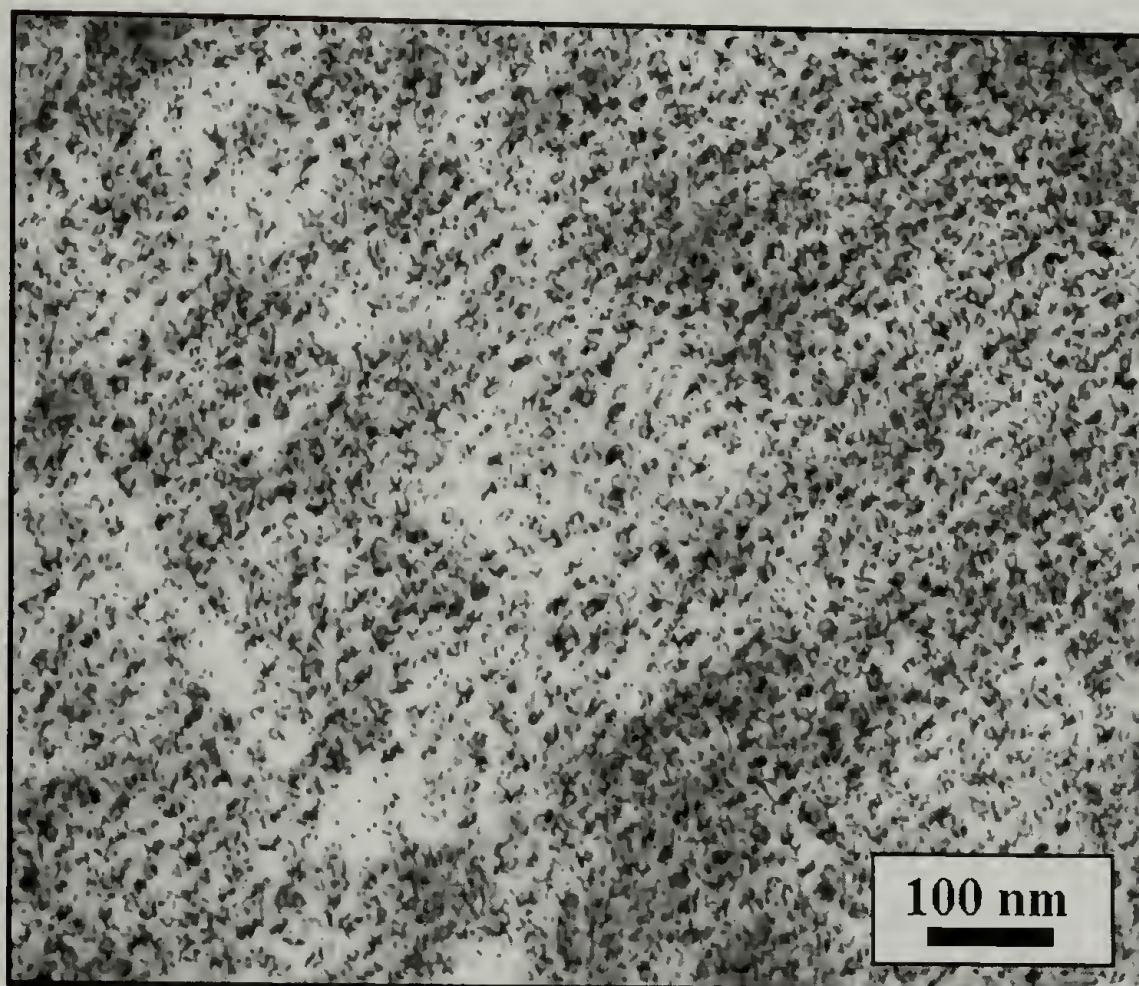


Figure 3.10 Platinum/PS-*b*-PAA nanocomposite subjected to Reduction C

In our experiments, neat hydrogen reduction of Pt(COD)Me₂ infused PS-*b*-PAA copolymer at 25 °C and 14 bar (Reduction C) gave the smallest platinum nanoparticles, ~2 nm, and the best templating (Figure 3.10). The nanoparticles grouped in spherical domain under 20 nm in size. This aggregates have a similar size to the PAA domains shown in the as infused sample Figure 3.7 Proving that reduction at these conditions preserves the structure

of the template. Diffusion of the precursor or the small platinum nanoparticles at this lower temperature is less likely to occur. The reduction conditions for this sample were the least aggressive with the lowest temperature and pressure.

3.2.3.2 PS-*b*-PAA / Silver Nanocomposites

PS-*b*-PAA/Silver nanocomposites were prepared in the same manner as shown in Figure 1.1 and Figure 3.6. PS-*b*-PAA films were first prepared by solvent casting the copolymer from DMF as previously described. Within a nitrogen glove box, 25 mg of a silver precursor [Ag(COD)hfac] and the polymer sample were added into a high-pressure stainless steel reactor equipped with a high-pressure needle valve. The vessel was sealed, heated to 40 °C in a thermostatic bath and filled with SC-CO₂ at the same temperature and 135 bar, resulting in approximately a 0.5 weight percent solution of Ag(COD)hfac in CO₂.

After a three hour soak, the reactor was cooled to 0 °C, and slowly vented through a back-pressure regulator to suppress polymer foaming. The sample underwent SC-CO₂ extraction to remove excess unbound precursor by repeating the filling and venting conditions three times. The reactor was opened and part of the unreduced sample was sectioned away for analysis. The remaining sample was placed back into a high-pressure reactor and reduced with neat hydrogen at 40 °C and 100 bar for one hour. Then, the reactor was cooled to 0 °C and slowly vented, opened, and the sample was removed for TEM analysis.

The TEM micrograph of the sample before hydrogen reduction is shown in Figure 3.11. The TEM micrograph of the sample after hydrogen reduction is shown in Figure 3.12.

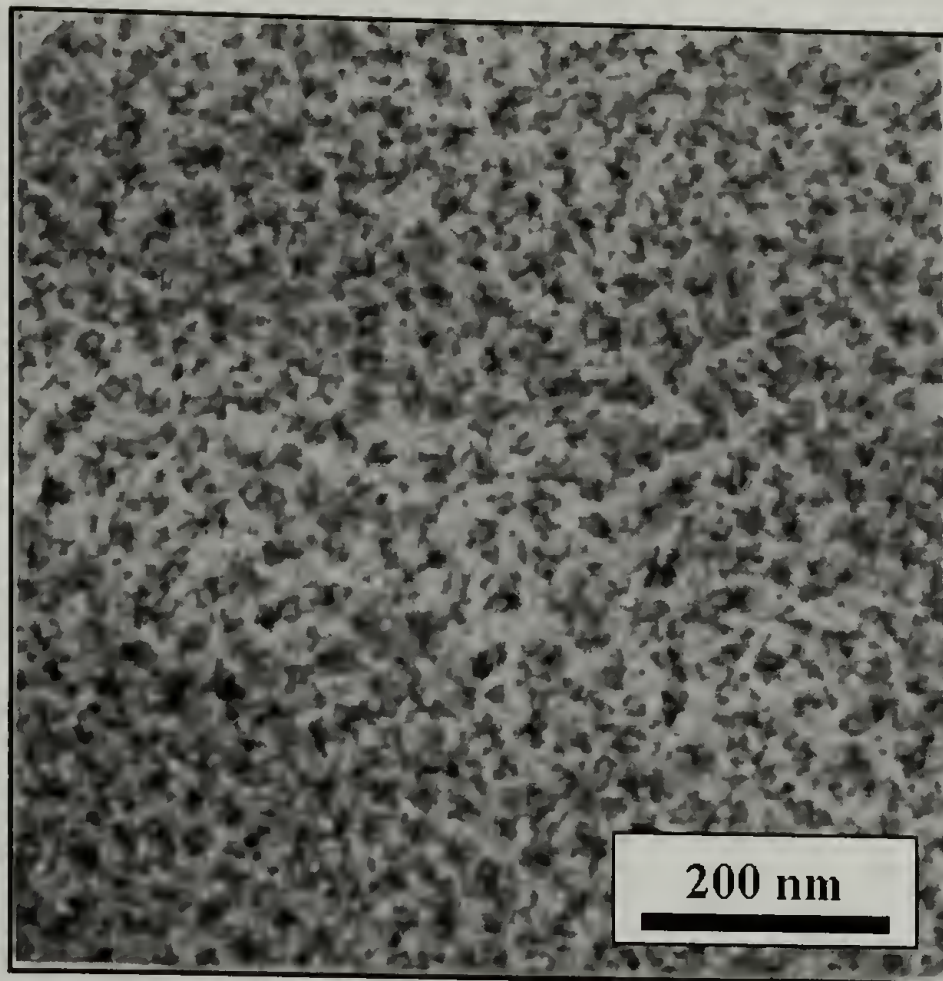


Figure 3.11 Silver precursor in PS-*b*-PAA before reduction

Spherical aggregates were observed that are just under 20 nm in size in Figure 3.11 in the unreduced sample. The image could be distorted by the large thickness of the sample, which leads to imaging of spheres in several planes. This result is similar to the platinum infusion prior to reduction within PS-*b*-PAA shown in Figure 3.7 as the same size PAA domains are observed.

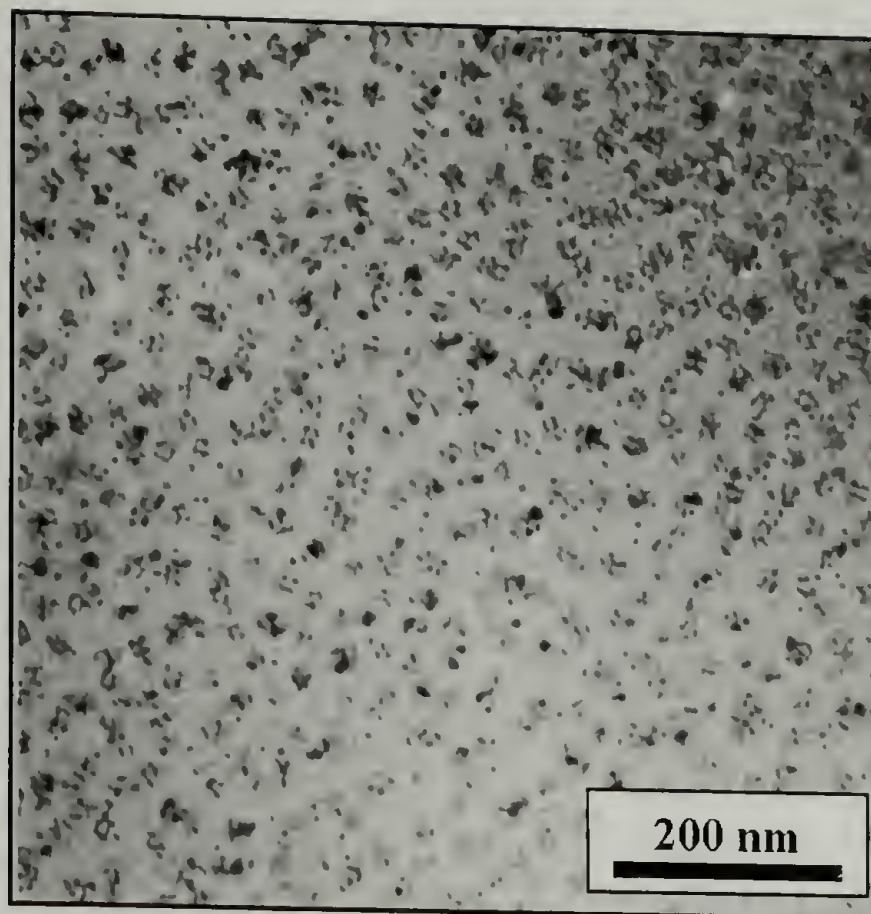


Figure 3.12 Silver/PS-*b*-PAA nanocomposite after reduction

The TEM micrograph of the sample after hydrogen reduction showed the formation of an ordered silver/PS-*b*-PAA nanocomposite, which preserved the structure of the template (Figure 3.12). Small silver nanoparticles (~5 nm) are observed within a larger spherical aggregates that were ~20 nm in size. This example demonstrates that our method can be a viable means for fabrication of bulk ordered nanocomposites from block copolymers.

3.2.3.3 Other Metals in PS-*b*-PAA

Other organometallics were infused into PS-*b*-PAA films solvent cast from DMF as described earlier. Within a nitrogen glove box, the precursors Pt(COD)Me₂, Ir(COD)acac, and PdCp(C₃H₅) were added to different high-pressure stainless steel reactors. Each reactor

was sealed, heated to 60 °C in a thermostatic bath and filled with SC-CO₂ at 60 °C and 135 bar, resulting in approximately 0.5 weight percent solution of the organometallics in CO₂.

After a three hour soak, the reactors were cooled to 0 °C, and slowly vented through a backpressure regulator to suppress polymer foaming. The reactors were opened, cleaned to remove any precursor precipitated on the reactor walls, and resealed with the samples. Neat hydrogen at 60 °C and 135 bar was added to reduce the precursors. After one hour soak, the reactors were vented, opened, and the samples removed for WAXS analysis (Figure 3.13).

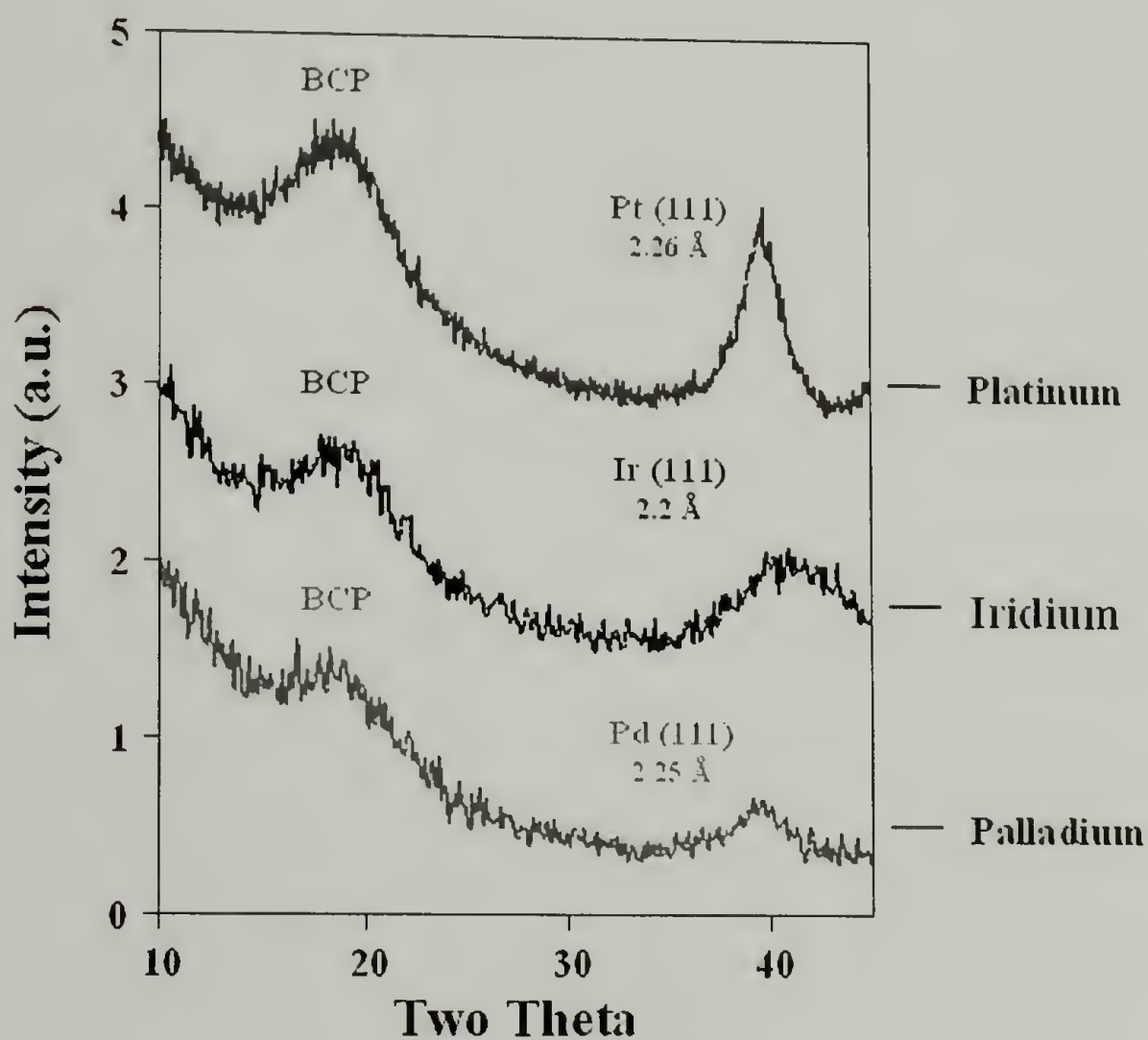


Figure 3.13 Various Metal/PS-*b*-PAA Nanocomposites

Figure 3.13 shows the WAXS patterns of the different organometallics reduced within the PS-*b*-PAA copolymer. In each of the patterns, the broad amorphous peak centered around 18 degrees two theta is characteristic of the block copolymer, labeled by the BCP.

The second peak at higher two theta values observed in each of the patterns corresponds to the (111) plane of the different metals. The spacing of these planes taken from the literature is shown in the same figure.²⁰³ The trends in cluster size can be determined by measuring the apparent size by Scherrer analysis. The calculated apparent sizes for platinum, iridium, and palladium are 4 nm, 1 nm, and 2 nm respectively. Peaks for palladium and iridium are poorly defined so errors in the determination for these metals are larger.

Reduction depends on the nature of the organometallic compound and the balance between nucleation and crystal growth so at the same reduction conditions different sized metal nanoparticles are observed. Previous work in our group has shown the palladium precursor is reduced faster in the presence of hydrogen than the platinum precursor for the production of thin metal films grown from SC-CO₂ solution.²⁰⁷ This suggests that there is a direct relationship between ease of reduction or rate of reduction and particle size. The faster the reduction, the smaller the particle size.

3.2.4 Metal Sulfides into PS-*b*-PAA

Lead sulfide nanoparticles were prepared within PS-*b*-PAA as a demonstration for extension of the infusion method to produce polymer/metal sulfide nanocomposites. PS-*b*-PAA films were prepared as previously described and loaded into high-pressure reactor along with 25 mg of Pb(hfac)₂. The reactor was heated to 60 °C and SC-CO₂ was added to 135 bar, resulting in a 0.7 weight percent solution of Pb(hfac)₂ in SC-CO₂.

After a three hour soak, the reactor was cooled to 0 °C and slowly vented through a backpressure regulator to suppress polymer foaming. The reactor was opened, cleaned,

resealed with the PS-*b*-PAA inside, and heated to 60 °C in a thermostatic bath. Hydrogen sulfide was then added to the vessel to a pressure of 4 bar for 2 hours.

Due to the high toxicity of hydrogen sulfide, a special setup was used to test for leaks and trap the exiting gas from the vessel. Wet lead acetate paper strips were used to test for the presence of H₂S. Upon exposure, the strips would turn black. The reactor was slowly vented through a series of four H₂S scrubbers that consisted of a saturated solution of lead nitrate in water. When the H₂S was vented through the system, insoluble PbS precipitated out of solution.²⁰⁸ After draining, the reactor was pressurized with house compressed air (~4 bar) and then vented again through the H₂S scrubbers. With four purge cycles with air, no further black precipitate was observed upon venting, indicating the absence of H₂S. The removed sample had changed color from the original clear PS-*b*-PAA film to black, suggesting a successful formation of lead sulfide. To remove any remaining hydrogen sulfide, the sample was placed under vacuum overnight and analyzed with WAXS Figure 3.14.

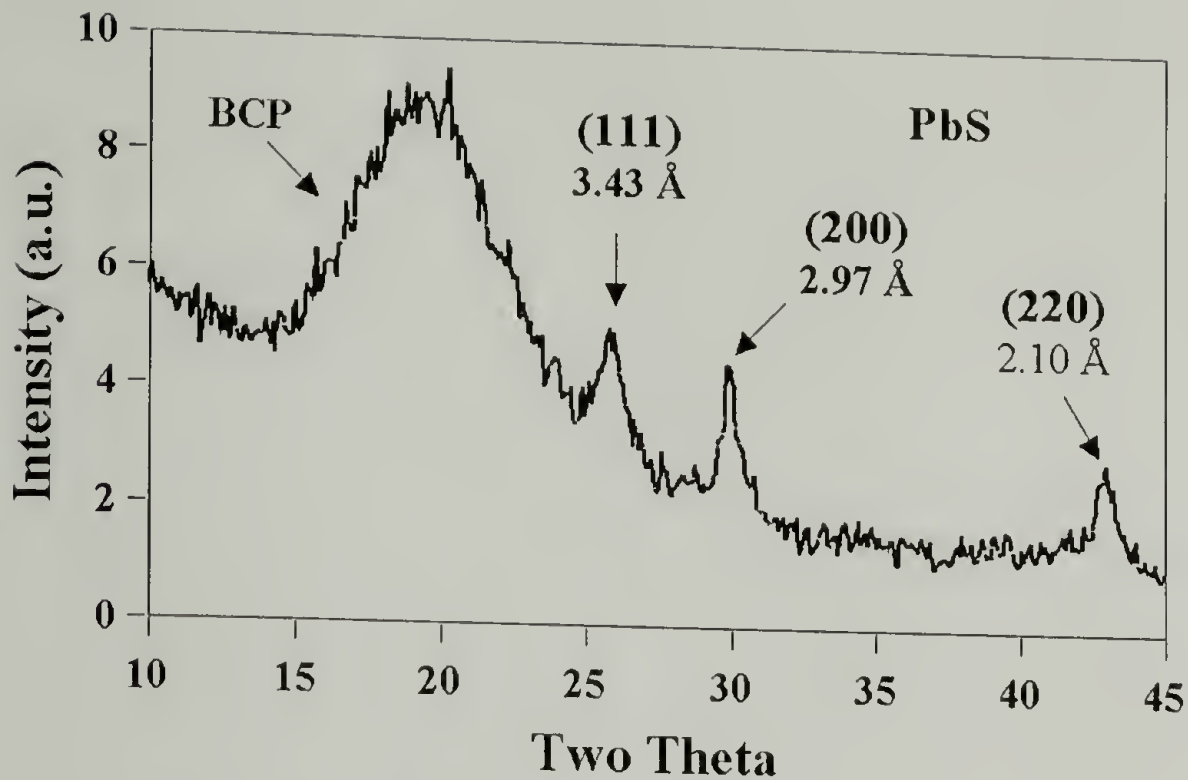


Figure 3.14 Lead Sulfide in polystyrene-*block*-Poly(acrylic Acid)

Figure 3.14 shows the WAXS analysis of the PS-*b*-PAA/PbS sample, which showed several peaks corresponding to the amorphous block copolymer and lead sulfide. Scherrer analysis on the (111) plane of PbS gave an apparent size of 5 nm.²⁰³ Three different peaks of PbS are observed and are indexed along with the scattering of the block copolymer (BCP) in Figure 3.14. This example demonstrates that polymer/metal sulfides can be fabricated with our method.

CHAPTER 4

POLYSTYRENE-*BLOCK*-POLY(VINYL PYRIDINE) NANOCOMPOSITES

4.1 Introduction

Polystyrene-*block*-poly(vinyl pyridine) copolymers (PS-*b*-PVP) have been used to prepare ordered polymer/metal nanocomposites as discussed in the introduction.^{45-52, 54} Typically, PS-*b*-PVP was dissolved in an organic solvent yielding a micellar structure of PVP core and a PS corona. A suitable metal precursor that can bind to the PVP phase was added to the PS-*b*-PVP solution and the solution was solvent cast. The metal precursor remained bound within the spherical PVP domains, surrounded by PS. The films were then reduced to produce metal nanoparticles whose size, shape, and three dimensional morphology was determined by the copolymer template.^{45-52, 54}

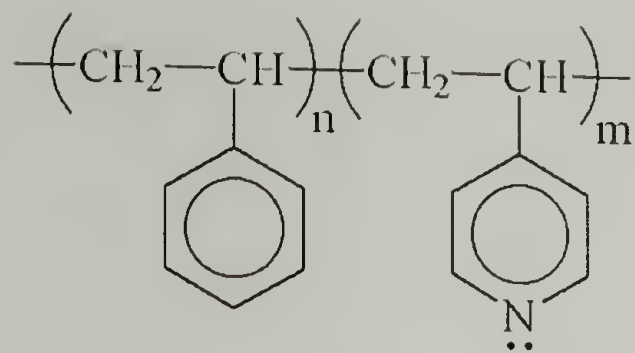
Supercritical carbon dioxide (SC-CO₂) is an ideal solvent to achieve a more direct method for the preparation of ordered polymer/metal nanocomposites, based on the delivery of a metallic precursors into a solvent-dilated polymer (Figure 1.1 and Figure 3.6). In this section its utility for the fabrication of ordered polymer/metal nanocomposites using polystyrene-*block*-poly(vinyl pyridine) copolymers as templates is demonstrated. First the partitioning of the organometallic into homopolymers, polystyrene and poly(2-vinyl pyridine), in the presence of CO₂ was studied. These experiments indicate that the silver organometallic was selective towards P2VP. This work was followed by the preparation of ordered nanocomposites with different polystyrene-*block*-poly(vinyl pyridine) copolymers.

4.2 Experimental Section

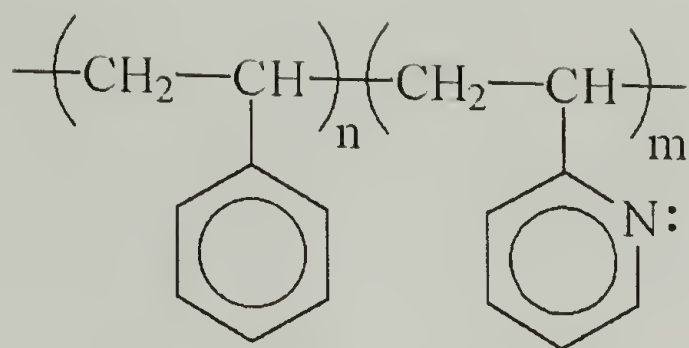
Ordered nanocomposites were fabricated within polystyrene-*block*-poly(vinyl pyridine) copolymers. This was achieved by the infusion of organometallic metal precursors into the copolymers with SC-CO₂ solutions followed by hydrogen reduction. Characterization of the samples was performed by transmission electron microscopy (TEM) and wide angle x-ray scattering (WAXS).

4.2.1 Materials

Polystyrene-*block*-poly(vinyl-pyridine) copolymers were used as received from Polymer Source. Figure 4.1 and Table 4.1 present the different copolymer structures and molecular weight of the copolymers used. The majority of the work was carried out with polystyrene-*block*-poly(2-vinyl-pyridine) [PS-*b*-P2VP], whose molecular weights for styrene and 2-vinyl-pyridine segments were 52,400 and 28,100 respectively. This represents a 33 volume percent for P2VP resulting in a cylindrical morphology of P2VP surrounded by a continuous phase of PS. These copolymers were chosen as previous experiments demonstrated the potential for selective binding. PS did not bind the organometallics whereas P2VP was reactive toward metallic precursors.^{47, 119, 147, 148} The homopolymer analogues to the copolymer segments, polystyrene (Mw = 280,000) and Poly(2-vinyl-pyridine) (Mw = 200,000) were used as received from Aldrich Chemical and Polysciences, respectively.



Polystyrene-*b*-Poly(4-Vinyl Pyridine)



Polystyrene-*b*-Poly(2-Vinyl Pyridine)

Figure 4.1 Polystyrene-*block*-poly(vinyl pyridine) copolymers

Table 4.1 PS-*b*-PVP Copolymers Used as Templates

PS (M_{wt})	PVP (M_{wt})		χ_N (25 °C)	χ_N (60 °C)	% PVP	PVP Structure
35,500	3,680	P4VP	80	68	8	Spheres
52,400	28,100	P2VP	160	140	33	Cylinders
91,500	115,000	P2VP	420	350	54	Lamella

The phase behavior of polystyrene and poly(2-vinyl pyridine) copolymers has been reported previously.^{38, 52, 150, 209, 210} The temperature dependence for the Flory interaction parameter (χ) of PS and P2VP homopolymers can be approximated by equation 4.1.²⁰⁹

$$\chi(T) = \frac{91.6}{T} - 0.095 \quad \text{(Equation 4.1)}$$

For samples at 25 °C, χ is approximately 0.2. At any appreciable molecular weight, a block copolymer of PS and P2VP is phased separated. Approximate χ_N shown in Table 4.1.^{38, 209-211} In the calculations of χ_N , it was assumed that the P4VP-PS values for the polymers used are the same interaction parameter as with P2VP-PS.

(1,5-cyclooctadiene) dimethylplatinum (II) [Pt(COD)Me₂] (Strem Chemical) and (1,5-cyclooctadiene) silver (hexafluoroacetylacetonate) [Ag(COD)hfac] (Aldrich Chemical),

were used as received. The structure of the organometallic compounds are shown in Figure 4.2. These precursors are soluble in SC-CO₂ and can be easily reduced to thin metal films with hydrogen^{95, 206} or by thermal reduction.⁸⁶ Similar metallic precursors have previously been used to bind to acid domains within copolymers.²² Cyclooctadiene has been shown to be a liable ligand that undergoes ligand exchange with pyridine.⁹⁸ This selective binding of the precursors prior to reduction is the key to the templating process (Figure 3.6). Coleman grade carbon dioxide and ultra-high purity hydrogen were used as received from Merriam Graves.

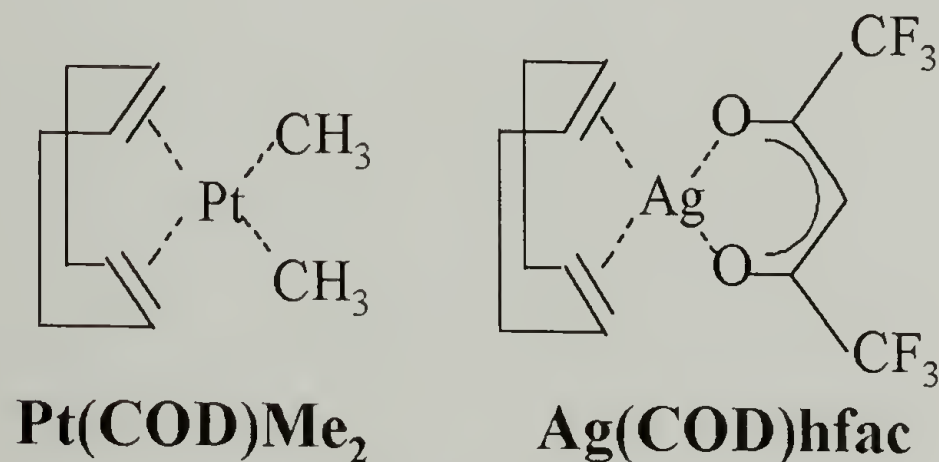


Figure 4.2 Platinum and silver precursors

Transmission electron microscopy (TEM) and electron diffraction were conducted using a JEOL 100CX operating at 100kV. Sections for analysis (~40 nm thick) were obtained via microtoming at room temperature on a Reichert-Jung microtome using a freshly-cut glass knife. The bound metal precursor or the metal nanoclusters provided sufficient contrast for TEM; hence, additional enhancement via staining was not typically required. In some cases, to determine the location of metal nanoparticles relative to the different domains, selective staining of one of the domains of the block copolymer was

carried out. Selective staining was achieved by exposing the sample to iodine vapor for one hour. Iodine selectively stained the poly(vinyl pyridine) domains.³⁸ Scanning electron microscopy (SEM) was conducted on a JEOL 35 CF operating at 20 kV using the secondary electron detector. Polymer samples were prepared by microtoming a smooth block face with a freshly cut glass knife. The block face was then mounted on a sample holder facing up and coated with a light gold sputter coating. This amount of gold sputter was not enough to mask the features, but sufficient to prevent charging on the polymeric material. Wide angle x-ray scattering (WAXS) was performed using a Siemens D-500 diffractometer with a copper anode ($\lambda=1.54 \text{ \AA}$).

4.2.2 Platinum Precursor Partitioning Between Polystyrene and CO₂

To help determine the optimum reaction conditions for the infusion of the organometallics into the copolymer systems, the partitioning of the platinum precursor between polystyrene and CO₂ was investigated. Polystyrene films were melt pressed at 160 °C and trimmed to a constant weight of 500 mg (+/- 0.3 mg). A constant weight of Pt(COD)Me₂, 12.5 mg (+/- 0.1 mg), and the polymer sample were placed into a high-pressure stainless steel reactor equipped with a high-pressure needle valve. The reactor was sealed, heated to 60 °C in a thermostatic bath, and filled with SC-CO₂ at the same temperature to a pressure ranging from 40 to 350 bar using a high-pressure computer controlled syringe pump (Isco Inc.). After a two hour soaking, the vessel was cooled to 0 °C, and slowly vented through a backpressure regulator to suppress polymer foaming. The samples were removed and weighed. CO₂ dissolved slowly from the polymer phase and weight of the samples decreased with time. To thoroughly allow for CO₂ out gassing from the polymer, final

weights of the samples were recorded after two weeks. Weight gains of the samples infused at the different conditions were used to determine the platinum precursor uptake. Mass uptakes of platinum precursor into polystyrene samples at 60 °C and various pressures are shown in Figure 4.3. Figure 4.4 shows the same data plotted against density of the CO₂.

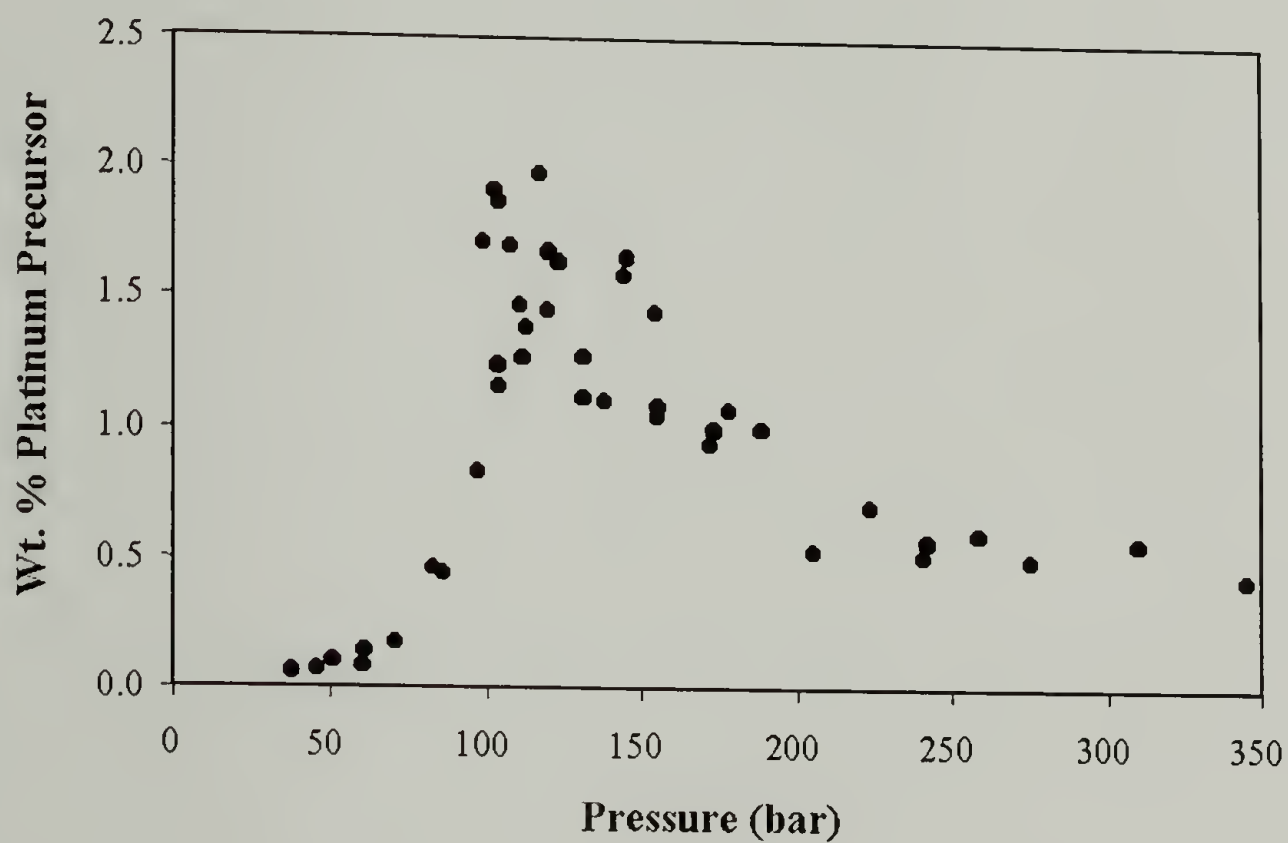


Figure 4.3 Mass uptake of Pt(COD)Me₂ within PS infused with CO₂ at 60 °C and different pressures

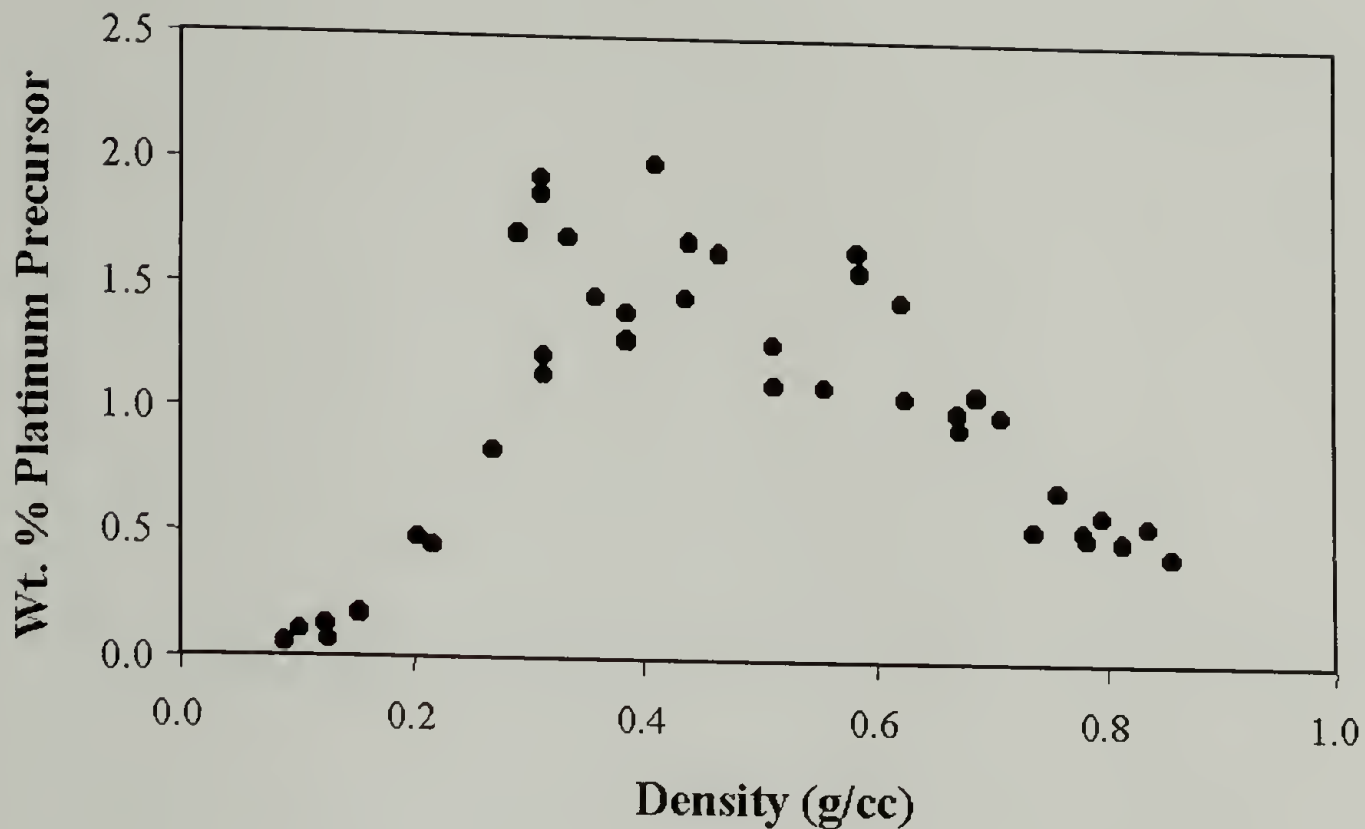


Figure 4.4 Mass uptake of Pt(COD)Me₂ within PS infused with CO₂ at 60 °C and different densities

Figure 4.3 shows the results for the uptake of platinum precursor into polystyrene samples at various pressures. Two different regions can be observed. The region below 120 bar, shows a mass uptake increasing with pressure. At the lower pressures, polymer swelling is low as is the solubility of the precursor in CO₂ and the infusion of the precursor into the polymer is kinetically limited.¹⁴² At higher pressures, the polymer swelling increases as well as the solubility of the precursor and more precursor infuses into the polystyrene. The uptake of platinum precursor into polystyrene reaches a maximum around 120 bar. Above this pressure, the mass uptake becomes equilibrium controlled and decreases with increasing the pressure of CO₂. This occurs because the precursor becomes more soluble in the CO₂ fluid and partitioning of the organometallic into the CO₂ phase is favored. The same data and trends are observed when plotted against density of CO₂ (Figure 4.4).

4.2.3 Phase Selectivity of the Organometallics

The selectivity of the organometallic silver precursor between polystyrene and poly(2-vinyl-pyridine) homopolymers was investigated. Plaques of the homopolymers were melt pressed at 160 °C to a nominal thickness of 0.5 mm and were trimmed to achieve a constant weight of 150 mg. The two homopolymers were loaded into the same 25 mL Thar reactor with 50 mg of Ag(COD)hfac, sealed, heated to 40 °C and filled with SC-CO₂ to a pressure of 95 bar, resulting in approximately a 0.35 weight percent solution. The samples were then subjected to three extractions by repeated fillings, 2-hour soakings, and venting. The samples were then reduced with hydrogen at 40 °C and 100 bar for 2 hours. After opening the vessels, the samples were placed under vacuum at room temperature for 12 hours and weighed. The results are summarized in Table 4.2.

Table 4.2 Distribution of Ag(COD)hfac Between PS and P2VP

	PS	P2VP
Wt. Before (mg)	150.0	150.1
Wt. After (mg)	150.1	171.9
Wt. Gain (mg)	0.1	21.8
% Gain	0.1	14.5

The mass uptake of silver into the P2VP homopolymer was much higher than that of the PS. This suggests that there is a strong associative mechanism through ligand exchange of pyridine for cyclooctadiene which results in the strong binding of the silver precursor to the homopolymer.¹⁵⁰ In the PS phase, however, no such strong binding exists and upon extraction most of the organometallic is removed from the PS phase.

The strong binding of the silver precursor with P2VP is illustrated in a SEM cross-section by the silver band (Figure 4.5). This picture corresponds to a P2VP sample soaked in a 1.0 weight percent solution of silver precursor in CO₂ at 40 °C and 95 bar for 4 hours followed by hydrogen reduction at 135 bar at 25 °C as described previously. The sample was then placed in a vacuum oven for 12 hours at 25 °C.

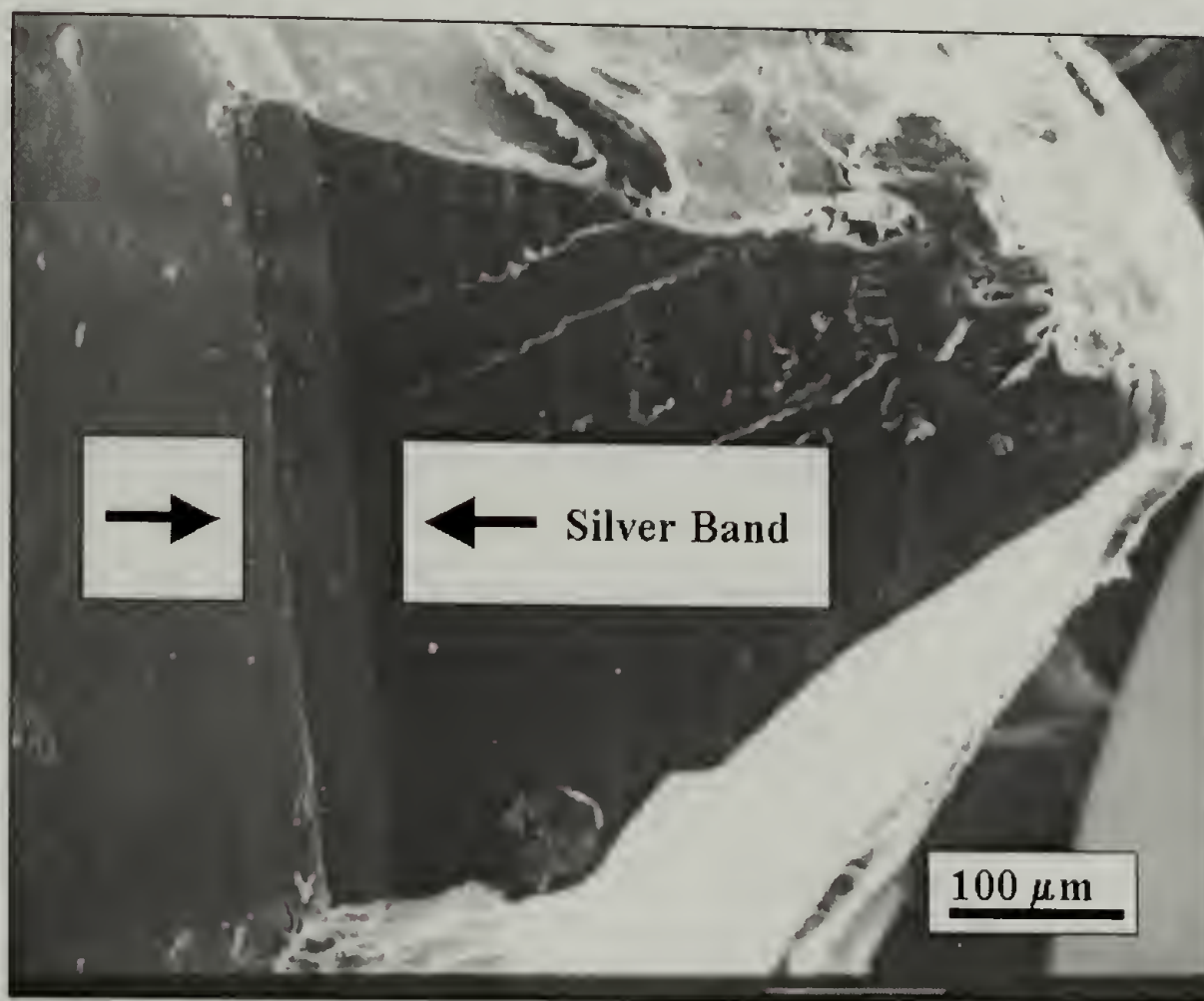


Figure 4.5 SEM image indicating strong silver – P2VP binding

Figure 4.5 was obtained by cutting a part of the sample, which was microtomed to obtain a smooth block face. The nanocomposite was placed on a sample holder with the block face up and then lightly coated with gold via sputter coating. The gold coating was light enough to only to dissipate charging of the polymer sample, and not obscure the silver layer. The silver regions will appear brighter than areas free of silver due to more electrons

being scattered from the electron dense region. At higher magnification (Figure 4.6), a very sharp interface was observed. The width of the silver band was 28 μm in this sample. After infusion and reduction, the sample was found to contain 3 weight percent silver. Using a geometric argument and assuming all the silver was located in the bright band, the local weight percent silver in the band was approximately 30 percent. Due to the strong silver metal binding to the outer layer, it is possible that accumulation of further silver in this region is hindered.

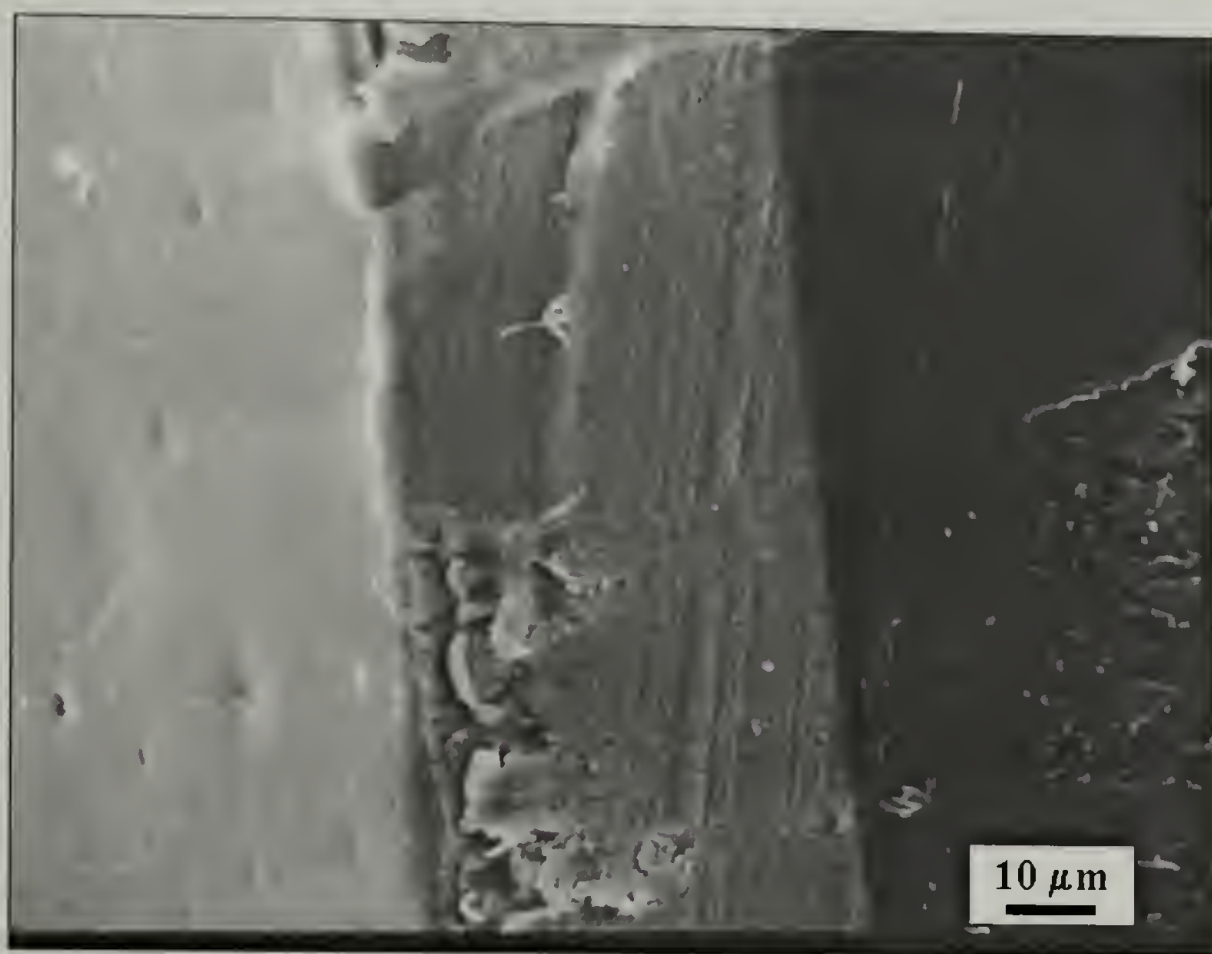


Figure 4.6 Close-up of interface between silver and neat P2VP

The identity of metallic silver upon the reduction of $\text{Ag}(\text{COD})\text{hafc}$ was confirmed by WAXS (Figure 4.7).

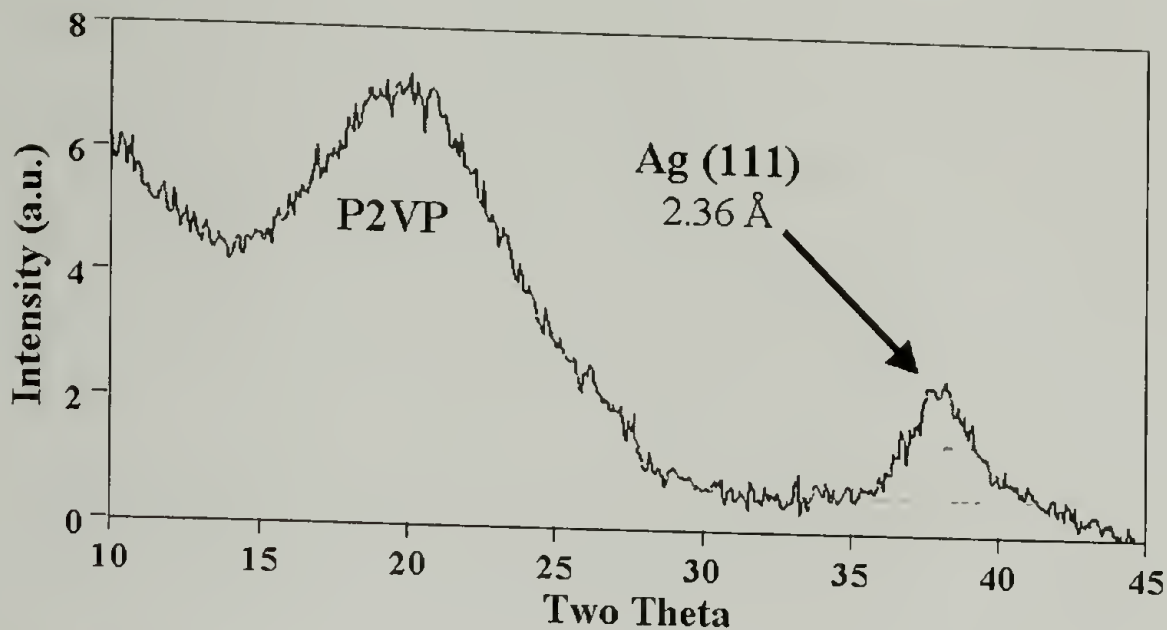


Figure 4.7 WAXS of silver nanoparticles within homopolymer P2VP prepared at 40 °C

Figure 4.7 shows the WAXS spectrum of the silver/polymer nanocomposite. This diffraction pattern is similar to those previously shown for polymer/platinum nanocomposites (Figure 3.5). The peak around 20 degrees two theta is due to the amorphous polymer. The second peak located at 38 degrees two theta, matches the literature value for silver.²⁰³ Scherrer analysis (Equation 3.1) of the silver peak gave an apparent crystallite size of 3 nm.

4.2.4 PS-*b*-PVP / Platinum Nanocomposites

This section presents examples of the infusion of organometallic platinum precursor into polystyrene-*block*-poly(vinyl pyridine) copolymers to produce ordered polymer/metal nanocomposites, as depicted in Figure 1.1. Different copolymers containing both poly(2-vinyl pyridine) and poly(4-vinyl pyridine) domains were used, as shown in Table 4.1. Poly(vinyl pyridine) is a reactive phase that can undergo association with ligands as illustrated in Figure 3.6. Ag(COD)hfac is therefore selective for P2VP over PS (Table 4.2).

4.2.4.1 PS-*b*-P4VP Copolymer

The first polystyrene and poly(vinyl pyridine) copolymer investigated was a PS-*b*-P4VP copolymer with an overall molecular weight of 39,200 g/mole. The molecular weight of the blocks were 35,500 and 3,680 g/mole for the PS and P4VP respectively, which yields spherical domains of P4VP surrounded by PS. Before the infusion of the organometallic into the copolymer, the initial copolymer morphology was investigated by TEM. A melt pressed copolymer film was microtomed with a freshly cut glass knife and samples collected onto copper grids. These samples were stained for one hour with iodine vapor, which selectively bound to the poly(vinyl pyridine) domains.³⁸ Figure 4.8 shows the stained P4VP spheres (~20 nm in size) on the unstained PS matrix. The elongation of the spheres and diagonal banding are artifacts of microtoming



Figure 4.8 PS-*b*-P4VP copolymer stained with iodine

The PS-*b*-P4VP was used as a template to prepare an ordered copolymer/metal nanocomposites as depicted in Figure 1.1 and Figure 3.6. The copolymer was melt-pressed to a nominal thickness of 0.5 mm at 160 °C. A sample of the film (~0.5 cm x ~3 cm) was placed into a glass test tube (i.d. = 1 cm) for ease of sample handling. The platinum precursor, Pt(COD)Me₂, was weighed (12 mg) and added into a high-pressure stainless steel reactor at 40 °C equipped with a high-pressure needle valve. A copolymer sample of known mass was then placed into the reactor which was then sealed and heated to 40 °C in a thermostatic bath. SC-CO₂ was transferred to the reactor to a pressure of 100 bar using a high-pressure computer controlled syringe pump (Isco Inc.). The initial mass of Pt(COD)Me₂ represents approximately a 0.5 weight percent solution in CO₂. The copolymer was allowed to soak in the solution for 12 hours. After soaking, the reactor was cooled to 0 °C and slowly vented through a backpressure regulator to suppress polymer foaming. The sample was removed and placed back into the reactor for SC-CO₂ extraction to remove excess or unbound precursor by repeating the filling and venting conditions three times. The reactor was opened and a part of the unreduced sample was sectioned away for analysis. The remaining sample was placed back into the reactor for reduction with hydrogen. Reduction was carried out with neat hydrogen at 25 °C and 100 bar. After soaking for 2 hours, the reactor was opened and the sample analyzed. TEM imaging was done on the samples both before and after hydrogen reduction, as shown in Figure 4.9 and Figure 4.10, respectively.

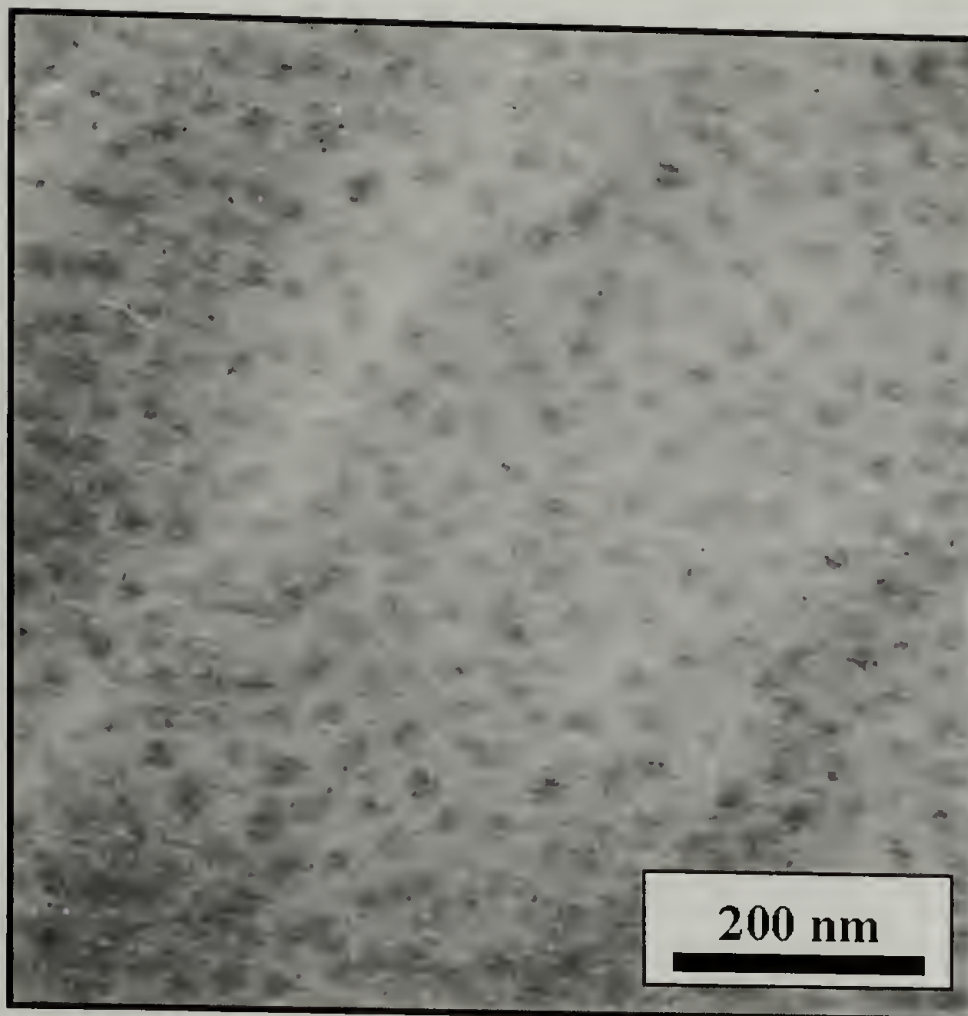


Figure 4.9 Platinum infused PS-*b*-P4VP before H₂ reduction

Figure 4.9 shows the TEM micrograph of the PS-*b*-P4VP copolymer with platinum precursor prior to reduction, where a evenly distributed spheres of approximately 20 nm in size are observed. The contrast in the sample was due to the unreduced platinum precursor within the P4VP domains. These domains have the same size and structure as that of the template showing the templating ability of the PS-*b*-P4VP copolymer.

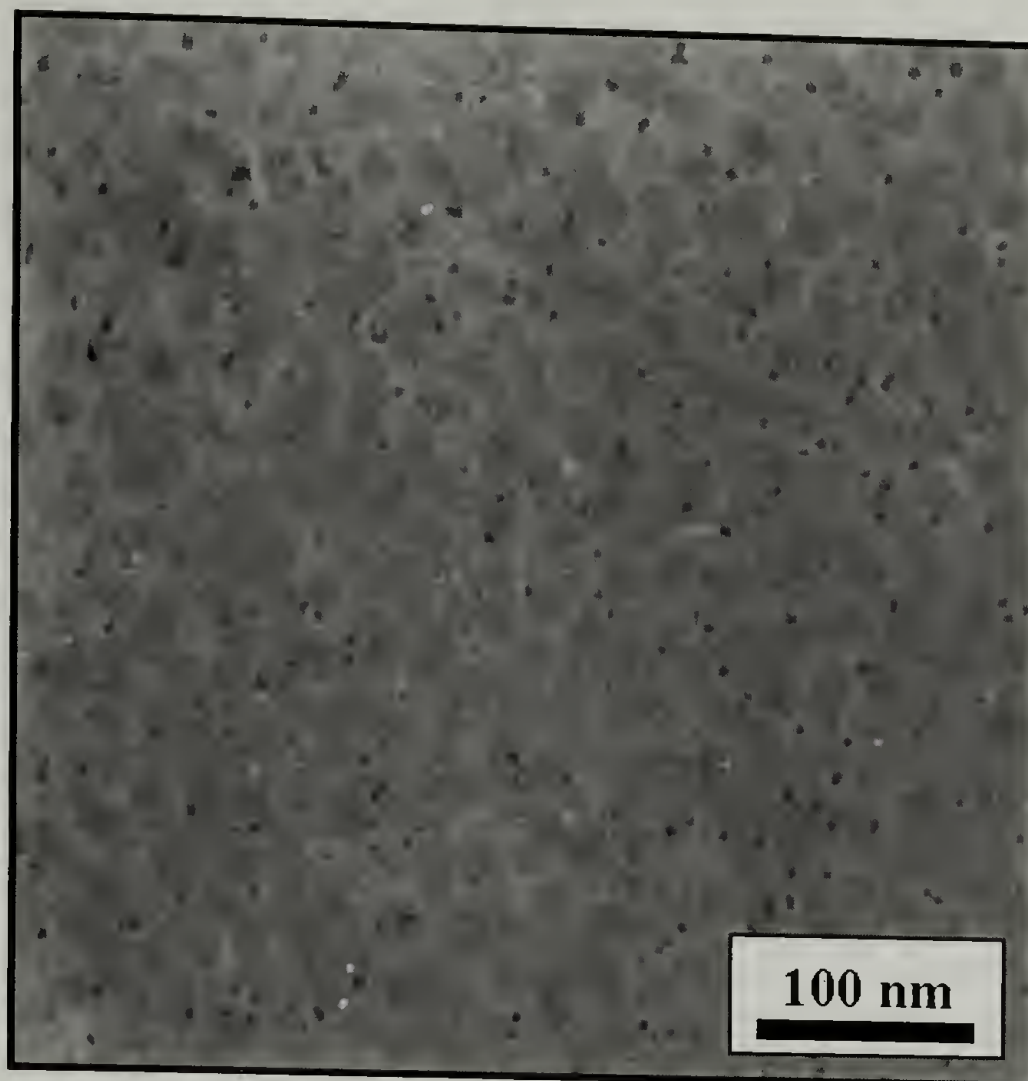


Figure 4.10 Platinum infused PS-*b*-P4VP after H₂ reduction

Figure 4.10 shows the TEM image of the PS-*b*-P4VP/platinum nanocomposite produced after hydrogen reduction. The image shows two main features. The first feature consists of small black dots, which are platinum metal nanoparticles about 5 nm in size. The second feature shows gray spherical regions about 20 nm in size that match the morphology of the sample before reduction, as well as the morphology of the copolymers. This diffuse gray background matching the spherical region could be due to unreduced platinum within the P4VP domain, as upon higher magnification, did not show smaller nanoparticles. Similar images, with small metal nanoparticles surrounded by gray regions can be observed in the literature for some copolymer/metal nanocomposites.³¹ The authors did not comment on the gray regions or any possible unreduced metal precursor.

4.2.4.2 PS-*b*-P2VP Copolymer

The next copolymer/metal system to be investigated was that of polystyrene and poly(2-vinyl pyridine), with a cylindrical morphology of P2VP surrounded by PS. These nanocomposites were prepared following the same procedure used to make the PS-*b*-P4VP nanocomposites previously described. The platinum organometallic was infused within the block copolymer at 60 °C and 135 bar and was reduced with neat hydrogen at 135 bar and 60 °C. A TEM picture of a samples obtained at these conditions is shown in Figure 4.11.

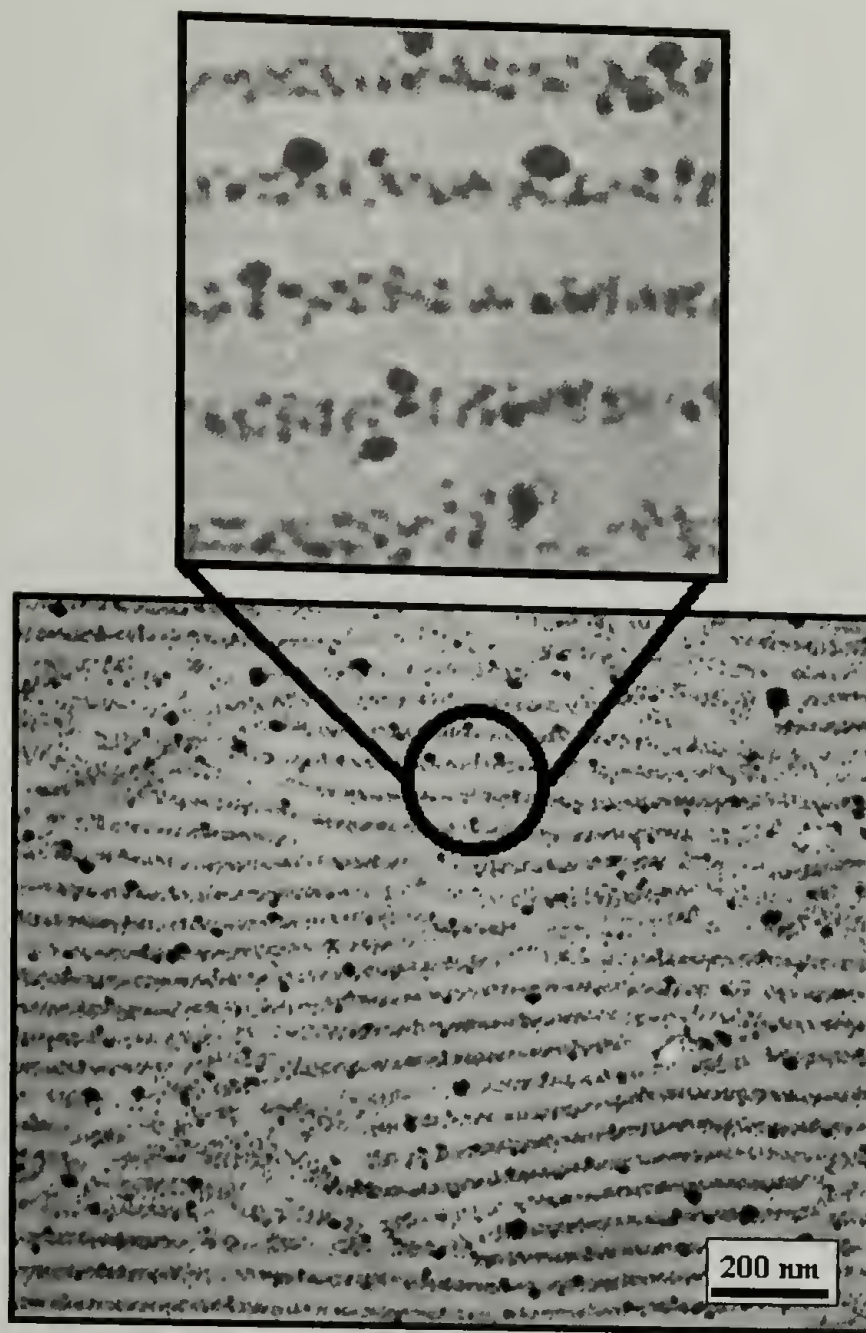


Figure 4.11 Platinum nanoparticles in PS-*b*-P2VP

Figure 4.11 shows an SEM micrographs of one of the ordered polymer/metal nanocomposites. This picture shows that the location of platinum nanoparticles has been controlled by the cylindrical structure of the copolymer template. It is also interesting to note that the defects in the copolymer template structure were carried over to the nanocomposite structure. Small platinum nanoparticles about 5 nm in size were observed within the P2VP domain. At the copolymer interface, larger platinum nanoparticles, up to about 20 nm in size, were observed. These larger nanoparticles may be a result of reduction of platinum precursor from the PS phase on a preformed platinum nanoparticle within the P2VP or from

the trapping of platinum nanoparticles produced in the PS domain at the copolymer interface. Similar trapping of gold nanoparticles has been observed in the literature at the interface of PS and P2VP homopolymers.¹⁴⁷

The PS-*b*-P2VP copolymer appeared to have given a more complete reduction of platinum compound in the P2VP than the P4VP. It is possible that the platinum precursor can bind more strongly to P4VP than to P2VP due to a larger steric hindrance of the nitrogen atom with the polymer backbone in P2VP. Significant differences in the binding of P4VP and P2VP has been observed in Raman spectra of the homopolymers bound to silver surfaces.¹⁵⁰ The data suggest that the P2VP has less steric hindrance and might allow for a more complete reduction of the metal, and the use of the copolymer containing P2VP was explored further.

Formation of metal nanoparticles was demonstrated by the electron diffraction image and wide angle x-ray scattering. Electron diffraction pattern of the platinum metal nanoparticles in a nanocomposite is shown in Figure 4.12. Figure 4.13 shows WAXS of a platinum containing nanocomposite.

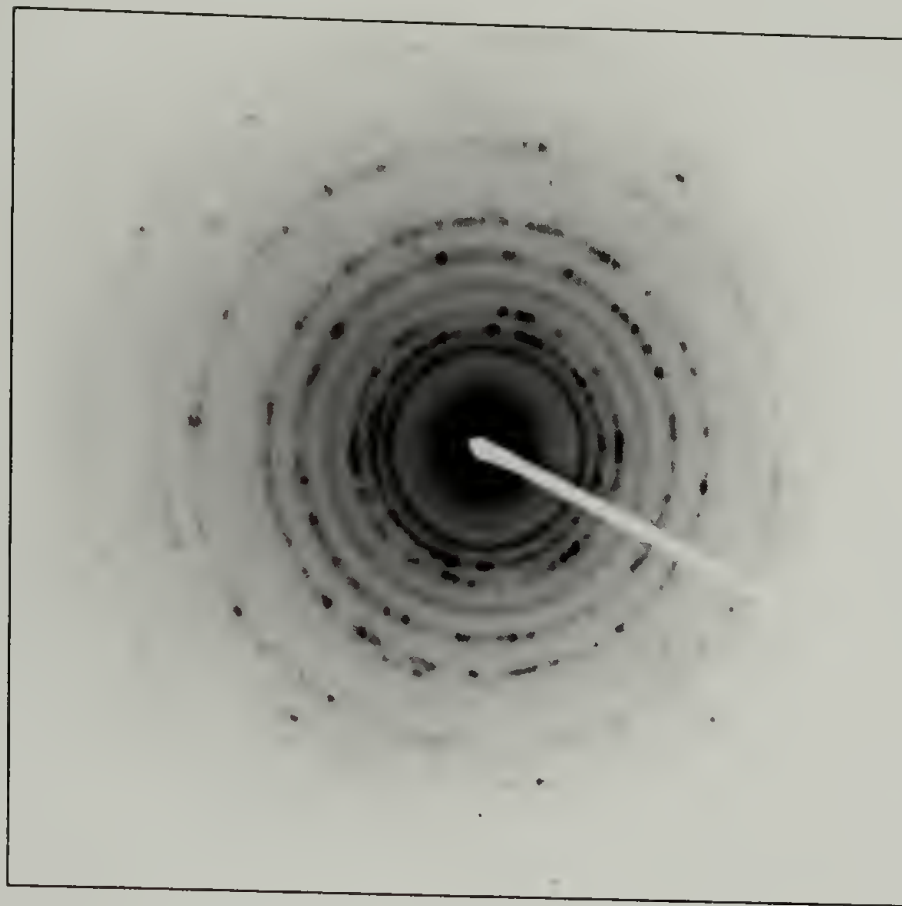


Figure 4.12 Electron diffraction of a PS-*b*-P2VP/platinum nanocomposite

Figure 4.12 shows defined rings due to the platinum metal nanoparticles and a diffuse background, due to the amorphous halo of the copolymer in the electron diffraction pattern. The identity of the platinum nanoparticles was confirmed by comparison with an electron diffraction pattern of a platinum standard. The standard was prepared by platinum evaporation onto a TEM grid followed by diffraction at the same conditions on the electron microscope. The electron diffraction image of the untreated copolymer and unreduced platinum infused in a copolymer only showed an amorphous halo.

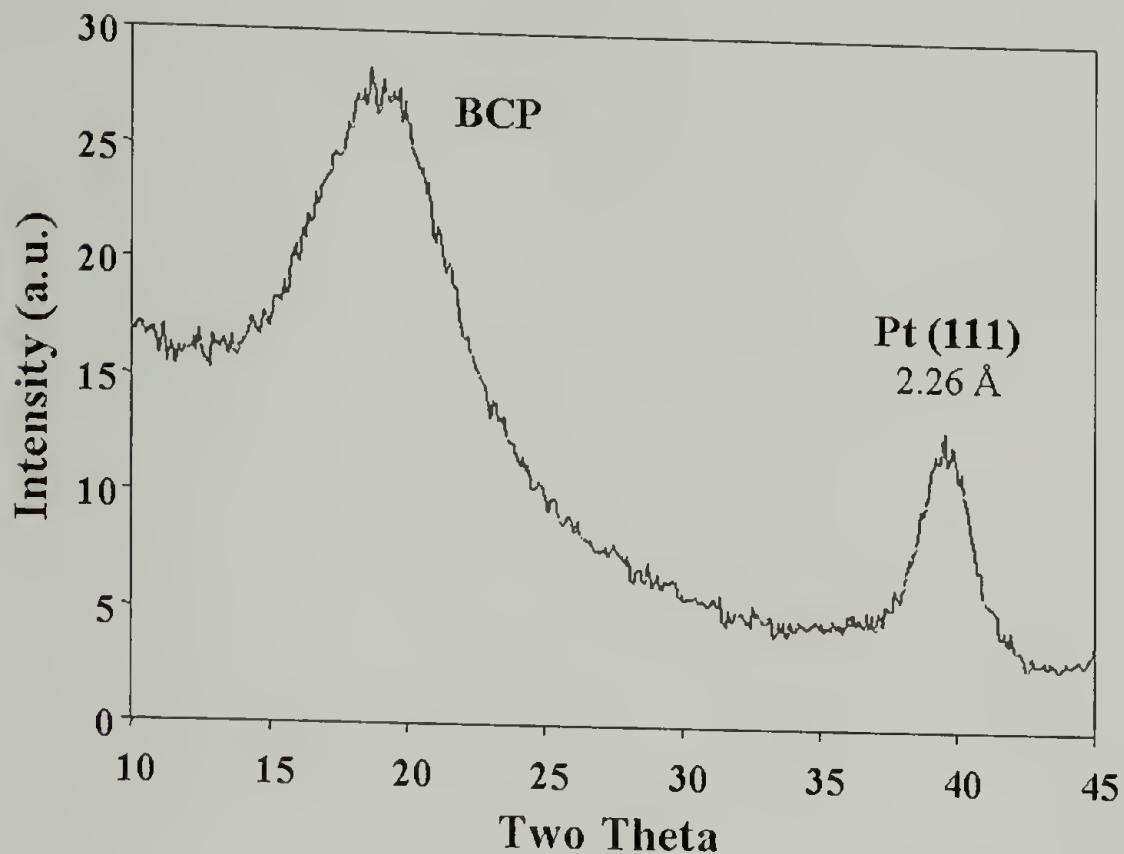


Figure 4.13 WAXS of a PS-*b*-P2VP/platinum nanocomposite

Figure 4.13 shows the WAXS pattern for a PS-*b*-P2VP nanocomposite containing 6 weight percent platinum metal. In this spectrum, two peaks can be observed. One is from the halo from the copolymer located around 18 degrees two theta and the other is the diffraction peak from the platinum (111) plane, which matches the literature value of 39.8 degrees two theta.²⁰³ Scherrer analysis (Equation 3.1) of the platinum peak gave an apparent crystallite size of 4 nm.

The evolution of the platinum peak during nanocomposite fabrication in a PS-*b*-P2VP copolymer is shown Figure 4.14.

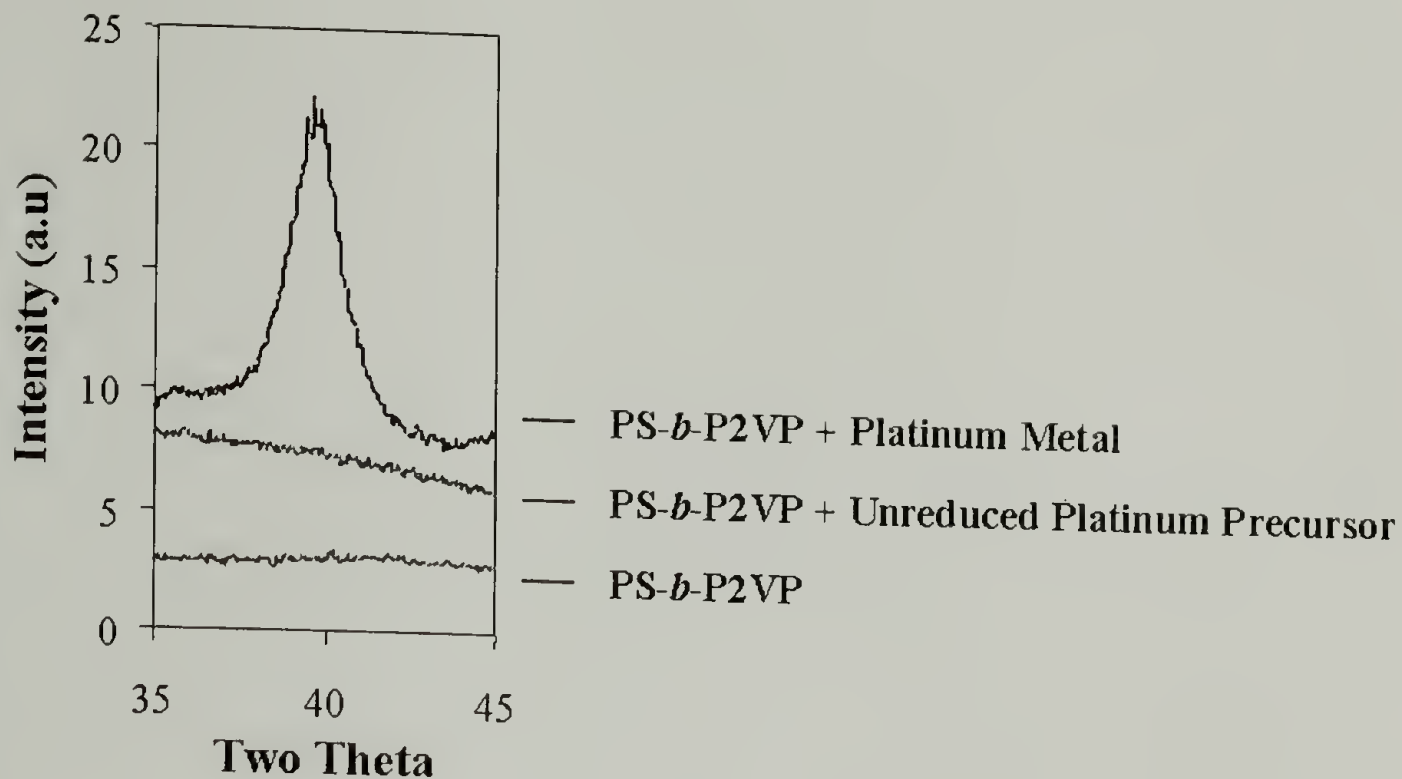


Figure 4.14 Evolution of platinum peak observed in WAXS in a PS-*b*-P2VP copolymer

Figure 4.14 illustrates the evolution of the diffraction peak for platinum with a PS-*b*-P2VP copolymer. The bottom line in the scattering pattern of a different sample in Figure 4.14 shows the WAXS pattern of the copolymer for the area of interest, around 40 degrees two theta. After SC-CO₂ infusion of the platinum metal precursor into the copolymer, the WAXS pattern did not show the presences of platinum metal nanoparticles. With hydrogen reduction, platinum metal nanoparticles were produces as indicated by the sharp peak. Scherrer analysis of the peak (Equation 3.1) gave an apparent size of 5 nm

4.2.5 PS-*b*-P2VP / Silver Nanocomposites

This section discusses the infusion of Ag(COD)hfac into a polystyrene-*block*-poly(2-vinyl pyridine) copolymer for the fabrication of ordered polymer/metal nanocomposites, as depicted in Figure 1.1 and Figure 3.6. The PS-*b*-P2VP had a total molecular weight of

80,500 g/mole with molecular weights for PS and P2VP segments of 52,400 and 28,100 g/mole respectively. P2VP represented a 34 volume percent, resulting in a cylindrical morphology of P2VP surrounded by a continuous phase of PS as shown in Table 4.1.

Ag(COD)hfae was first infused into the PS-*b*-P2VP at identical reaction conditions to those of the platinum infusion. Infusion of the organometallic precursor, Ag(COD)hfae, into the melt pressed copolymer was carried out at 60 °C and 135 from a SC-CO₂ solution (~1 weight percent). After 12 hours soaking, cooling down to 0 °C and slow venting, the infused polymer samples changed in color from a slightly yellow clear copolymer to colored samples ranging from red to deep purple. The color depended on reaction conditions and was a consequence of thermal reduction of the bound organometallic silver during the soaking and infusion steps. This precursor is known to be reduced thermally or photolytically, so the thermal reduction of this organometallic within the copolymers was possible.⁸⁶

The sample was then extracted and reduced with hydrogen at 60 °C and 135 bar in the same manner as before. Reduction of the sample produced a color change in the sample from dark purple to black, indicating further thermal reduction of the organometallic to produce silver nanoparticles. TEM analysis of the sample before and after reduction showed minor differences, as most of the compound was thermally reduced at these conditions. Figure 4.15 shows one of the samples after reduction with hydrogen.

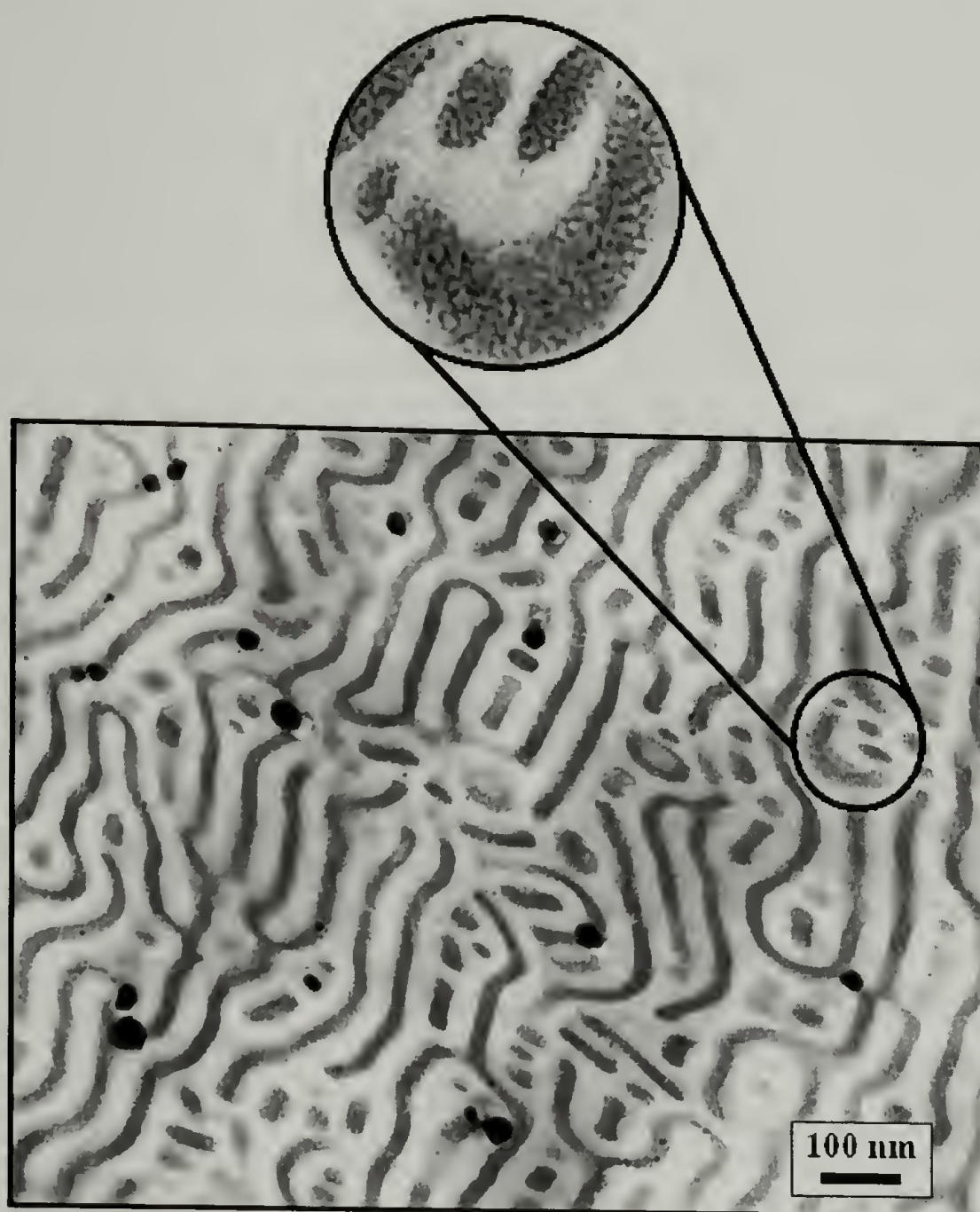


Figure 4.15 Silver nanoparticles within cylindrical P2VP domains of PS-*b*-P2VP prepared using reactions at 60 °C

Figure 4.15 shows small silver nanoclusters (~2 nm) deposited selectively within the P2VP domain, with occasional larger clusters. This is the same copolymer as used to prepare the ordered platinum nanocomposites in Figure 4.11. Differences in the structure of nanocomposites arise from the melt pressing, in which the copolymer template was in different morphologies.

In an attempt to minimize the thermal reduction of Ag(COD)hfac, the reaction temperature was reduced to 40 °C for the infusion and extraction steps. To maintain the same SC-CO₂ density used at 60 °C ($\rho = 0.55$ g/cc),¹⁵⁹ the pressure was reduced from 135 bar

to 95 bar. After the infusion step, the copolymer did not change color, indicating that much less thermal reduction occurred. Sample were reduced with hydrogen at mild reduction conditions at 25 °C and 14 bar for 2 days. Upon reduction the color of the sample changed to deep purple. The sample was analyzed via TEM before and after reduction in Figure 4.16 and Figure 4.17 respectively.

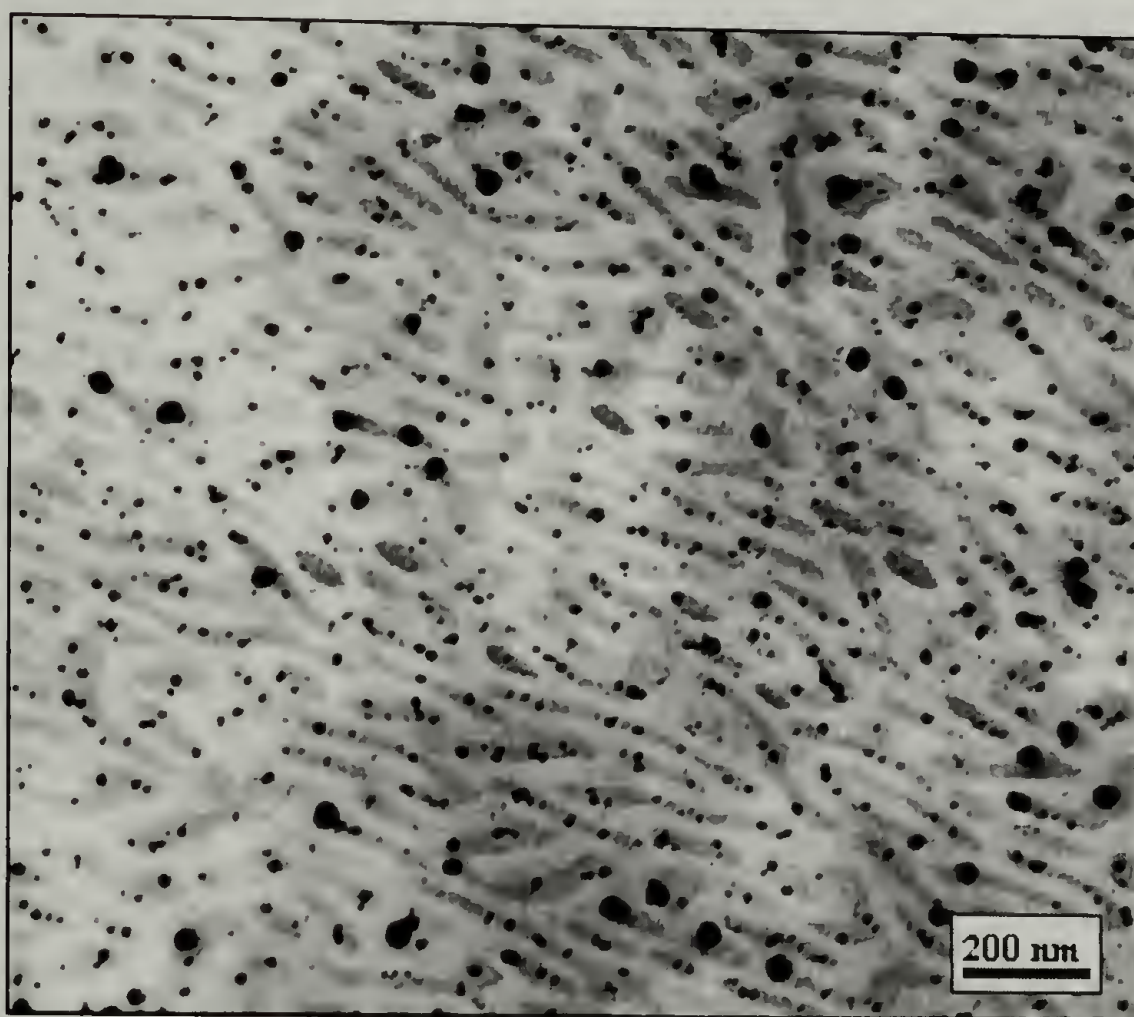


Figure 4.16 Silver precursor within PS-*b*-P2VP prior to the addition of hydrogen prepared using reactions at 40 °C

Figure 4.16 shows some gray banding due to unreduced silver precursor which acted as a stain for the P2VP phase. Some silver nanoparticles can be observed that are possibly a result of thermal reduction at these temperatures. However, the possibility of photolytic reduction of the silver precursor within thin microtomed films due to exposure to normal room light cannot be ruled out.

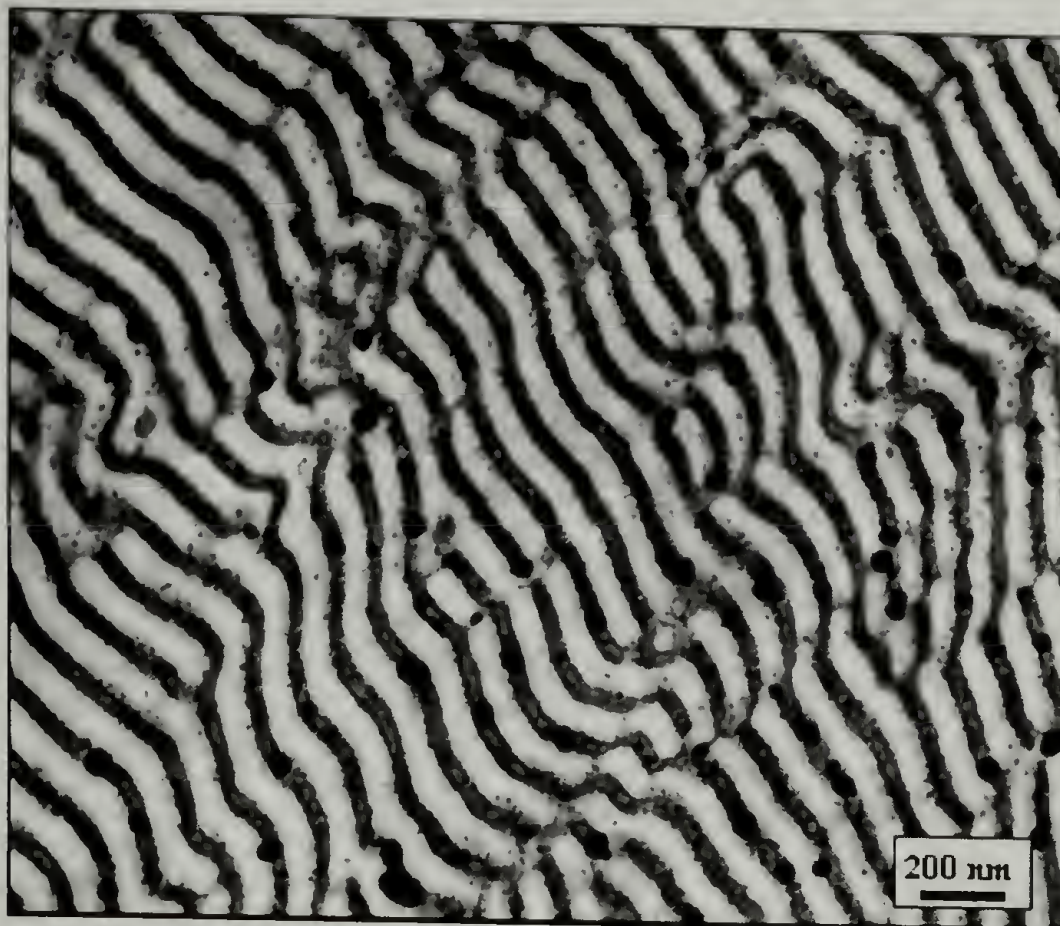


Figure 4.17 Silver nanoparticles within cylindrical P2VP domains of PS-*b*-P2VP prepared using reactions at 40 °C

Figure 4.17 shows the same sample after hydrogen reduction, where silver nanoparticles were produced throughout the sample. Within the P2VP phase, silver nanoparticles were ~2-5 nm in size. The amount of silver within the PS increases at the mild reduction conditions in comparison to Figure 4.15. Growth of small nanocluster of ~5 nm in size within the P2VP domains can also be observed. Large nanoparticles can also be observed similar in size to what was observed in Figure 4.16, indicating that some thermal reduction is still taking place even at the low temperature.

The strong binding between silver and copolymers was studied in thicker samples. Figure 4.18 and Figure 4.19 are TEM images of the same sample and show a sharp line, similar to what was observed within the P2VP homopolymers (Figure 4.5 and Figure 4.6).

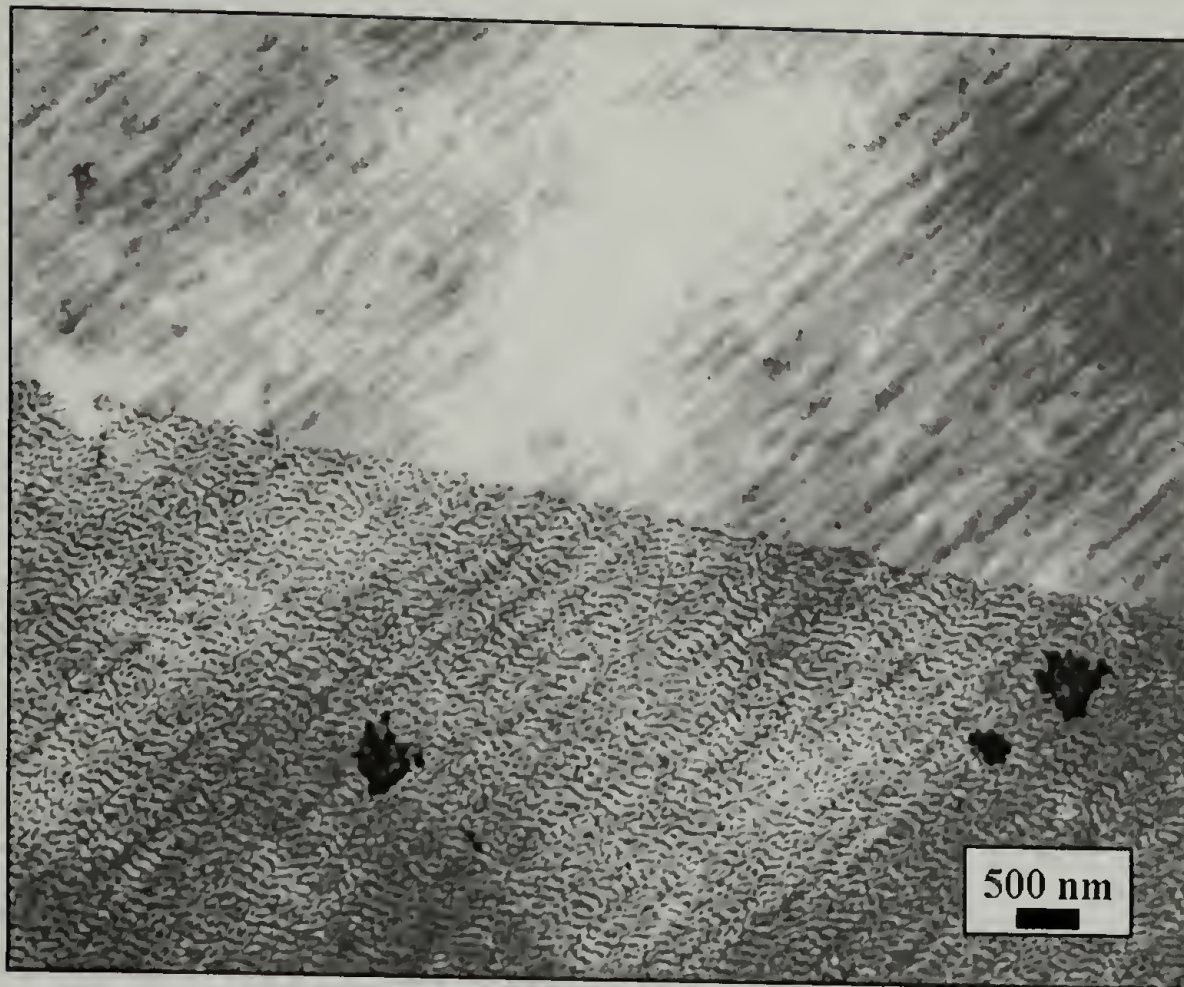


Figure 4.18 TEM of silver interface within PS-*b*-P2VP prepared using reactions at 40 °C

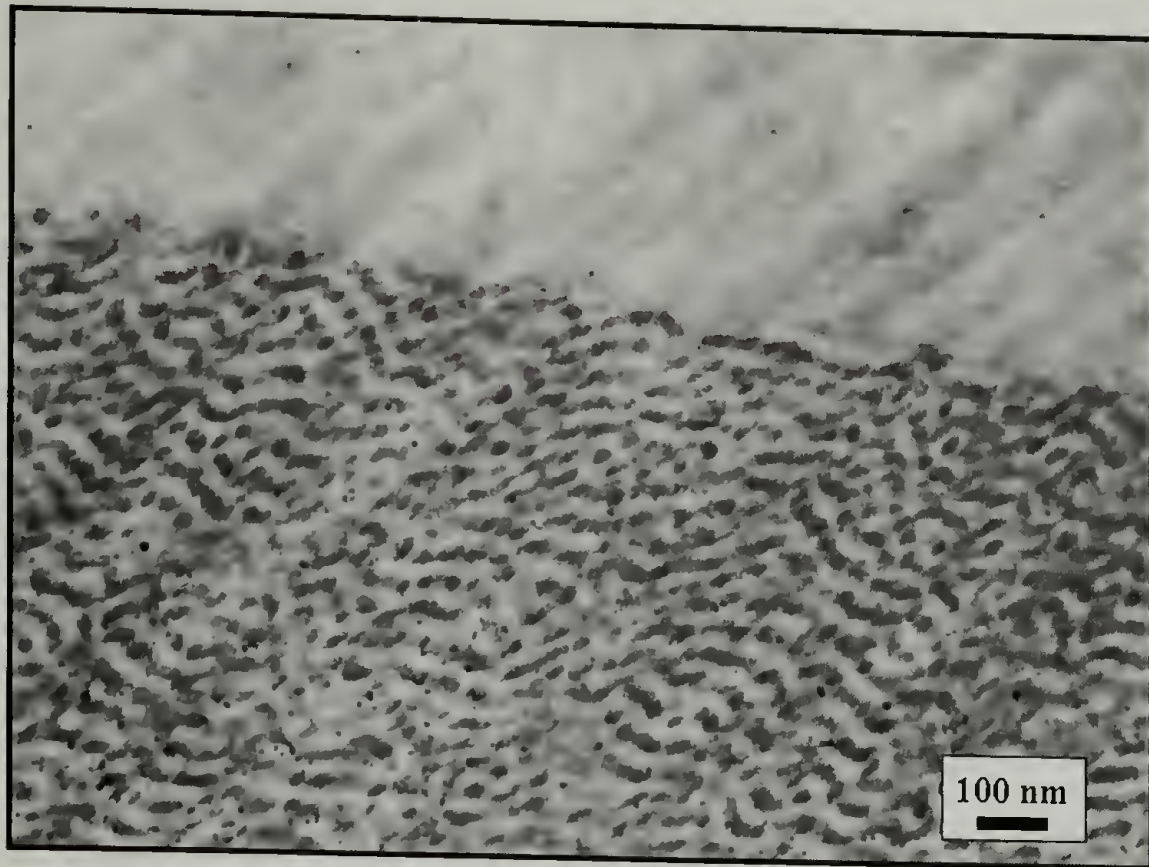


Figure 4.19 Close-up of interface TEM of silver interface within PS-*b*-P2VP from reactions at 40 °C

In Figure 4.18 the copolymer morphology of the P2VP can be observed. The TEM picture also show some artifacts due to the microtoming, such as the light region in the middle of the image where the film is thinner. Black spots from dust on the film and chatter lines which run diagonally in a direction different than the inherent P2VP morphology can also be observed. In Figure 4.19 at the higher magnification, the small silver nanoparticles can be observed within the P2VP phase.

CHAPTER 5

CONCLUSIONS AND FUTURE DIRECTIONS

In this dissertation, ordered polymer/ceramic and polymer/metal nanocomposites were prepared within polymeric templates as outlined in Figure 1.1. Ceramic and metallic precursors were infused and bound or reacted within specific domains within polymeric templates from SC-CO₂ solutions, which is the key to this templating process. The polymer templates were ionomers and block copolymers which can have controllable morphologies. Sorption of SC-CO₂ solution into the polymer matrix mitigates the mass transport limitations for delivering precursors into bulk systems. CO₂ sorption can be controlled and has the added benefit of preserving the long-range order of a block copolymer which is often not the case with traditional solvents. Under proper reaction conditions, ceramics, metals, or metal sulfides nanoparticles are produced and their organization is dictated by the polymeric template.

The polymer templates used were Nafion and reactive block copolymers, PS-*b*-PAA and PS-*b*-PVP. Nafion contains ionic domains that can support sol-gel chemistry to produce templated amorphous SiO₂ nanoparticles. Block copolymers were used as they have a range of controllable morphologies and can direct the structure of nanoparticles synthesized within the domains. Each of these block copolymers has one phase which is able to undergo chemical binding with an organometallic (Figure 3.6). In both cases, SC-CO₂ was used as a solvent to infuse the precursors into the polymeric templates. The use of SC-CO₂ has numerous advantages such as being an environmentally benign solvent, but most importantly it can be used to deliver reactants into polymeric templates without destroying the initial

template morphology. Achieving high diffusion rates of the precursors into the polymeric systems while preserving the morphology of the template is a key use of SC-CO₂ allowing for ordering of nanoparticles over bulk dimensions.

Chapter 2: Polymer/Ceramic Nanocomposites

TEOS was shown to be soluble in SC-CO₂ up to high weight percents and capable of depositing SiO₂ films from CO₂ solutions upon acid catalysis with water.

A Nafion template was then used to prepare ordered polymer/ceramic nanocomposites. Ionic domains within Nafion were exposed to water from a humidified SC-CO₂ followed by a TEOS/SC-CO₂ solution. Sol-gel chemistry, catalyzed by the ionic domains, produced templated amorphous SiO₂ nanoparticles.

*Chapter 3: PS-*b*-PAA Nanocomposites*

Polystyrene/platinum nanocomposites were prepared to investigate the effect of reduction conditions on nanoparticle size. Reductions of Pt(COD)Me₂ within PS were carried out with a mixture of CO₂/H₂ and neat hydrogen. CO₂ has a plasticizing effect in polymer matrixes and increases diffusion of precursor which produced larger nanoparticles than in the case of neat reduction.

PS-*b*-PAA/platinum nanocomposites were prepared by first infusing Pt(COD)Me₂ into the copolymer. The spherical morphology of the PAA domains was observed prior to reduction. Proper reduction conditions were again essential for controlling nanoparticle size. The best templating occurred with the least aggressive reduction conditions. Reduction in a plasticized polymer with a mixture of CO₂/H₂ resulted in a loss of templating.

Ordered polymer/silver nanocomposites were prepared by the infusion of Ag(COD)hfae into PS-*b*-PAA. Reduction of this system produced an excellent example of an ordered nanocomposite.

Other PS-*b*-PAA/metal nanocomposites of platinum, palladium, and iridium were then prepared under identical reaction conditions. These systems showed that different organometallics produced different sized nanoparticles under identical reaction conditions.

*Chapter 4: PS-*b*-PVP Nanocomposites*

Pt(COD)Me₂ partitioning between PS and CO₂ was investigated by varying pressure at constant temperature and loading of precursor and PS. The optimum pressure window for impregnations reactions was identified. Two different regions were observed. The first region was a kinetically-limited regime where the uptake of precursor was limited by mass transfer. The second regime was equilibrium limited; increasing solubility of the platinum precursor in CO₂ upon increasing pressure favors partition of the precursor into the fluid phase.

Next the phase selectivity of Ag(COD)hfae between the homopolymers PS and P2VP was investigated. This work showed that the silver precursor was very selective towards P2VP. SEM analysis of the nanocomposites cross section also demonstrated the strong binding between the P2VP and Ag(COD)hfae.

PS-*b*-PVP/platinum nanocomposites were prepared. These nanocomposites were prepared within a PS-*b*-P4VP copolymer, where P4VP appeared to prevent the full reduction of the platinum precursor. Extension of this into a PS-*b*-P2VP gave a more complete reduction of the platinum precursor for ordered nanocomposites.

PS-*b*-P2VP/silver nanocomposites were also prepared. The silver precursor could be thermally reduced at 60 °C and better nanocomposites were fabricated at 40 °C. The silver precursor could be reduced thermally without the addition of hydrogen, while the platinum precursor could not be reduced without the addition of hydrogen.

Future Directions

This project has demonstrated that block copolymers can be successfully used as templates for the fabrication of bulk ordered nanocomposites. Potential applications that can be pursued from this work are in the area of dielectric materials, photonic devices, and polymer electrolyte modification.

A block copolymer template with one phase selective towards water can be ordered on a surface. Sol-gel chemistry is selectively run within this domain producing an ordered polymer/ceramic nanocomposite. Upon calcination the organic block copolymer is removed, leaving a porous ceramic structure determined by template. Application of these structures could be in the area of dielectric insulators, an application of interest to the microelectronics industry. This ideas is being further studied by other member of the group.

Another key potential application for ordered nanocomposites fabricated by this method are for optical materials. As an example, a high molecular weight lamellar block copolymer could be ordered upon SC-CO₂ annealing into a periodic structure whose spacing are on the order of the wavelength of light. Modification of the refractive index of one phase, such as by the selective deposition of silver metal or metal sulfides nanoparticles could produced nanocomposites with direct optical applications.

Another application could be the modification of poly(ethylene oxide) (PEO) by the deposition of SiO₂ nanoparticles. Lithium doped-PEO are used as polymer batteries as they are intrinsically safe and easily processable into complex geometries. However, crystallization of PEO causes a reduction in ion conductance to unacceptable levels. By using some of the techniques developed for the Nafion work, ceramic nanoparticles can be produced directly within a poly(ethylene oxide) film by sol-gel chemistry. This could lead to a unique method for the direct preparation of the solid polymer membranes for polymer battery applications.

APPENDIX

NANOPARTICLE MOVEMENT

Movement of nanoparticles after reduction of organometallics was investigated to evaluate the possibility of nanoparticle agglomeration following synthesis. Nanoparticle sizes within polymers can be determined by both the reaction condition used to fabricate the nanoparticles and followed by any nanoparticle diffusion and coalescence,¹⁴³ as reviewed in the introduction.

The loss of templating ability by a block copolymer has been postulated to be due to localized heating upon the reduction of the organometallic compounds.²¹ This could then lead to an increase in the diffusion rates of nanoparticles allowing for agglomeration. Nanoparticle movement within block copolymers been tested with gold nanoparticles in a PS-*b*-P4VP copolymer. The metal nanoparticles were produced by photo reduction using an ArF laser after solvent casting the gold precursor with the block copolymer onto a TEM grid.⁵⁴ With mild reduction conditions (20 pulses at 10 mJ/cm² and 25 °C) numerous small nanoparticles were produced within each copolymer domain. Harsher conditions (10 pulses at 20 mJ/cm² and 25 °C) produced larger nanoparticles with a loss of templating. Reduction at a higher temperature (20 pulses at 10 mJ/cm² and 90 °C) gave a structure similar to the mild reduction conditions, illustrating that the decisive parameter was the reduction conditions through the laser power.⁵⁴

To test the theory that nanoparticles agglomerate due only to local temperature increase during reduction, a sample was reduced with the low power at 25 °C followed by heating at 135 °C for 10 seconds, which corresponds to the typical laser-irradiation time.

This heating time did not alter the structure which showed that the formation of larger nanoparticles is dictated by the reduction conditions and is not due to a coalescence of already existing smaller dots, but occurs during the process of nucleation.⁵⁴

The mobility of the nanoparticle was tested on nanocomposites prepared within this dissertation. Samples were imaged within the TEM and then subjected to external heating followed by reexamination of the morphology in the TEM. The heating conditions was done for 4 hours at 120 °C in a thermostatic oven.

An example of the result of this is shown here for a sample of silver nanoparticles within homopolymer P2VP, prepared as described earlier in Chapter 4. The TEM image of the sample before heating is shown in Figure A.1. This sample was heated 4 hours at 120 °C and reexamined in the TEM. The TEM image after heating is shown in Figure A.2.

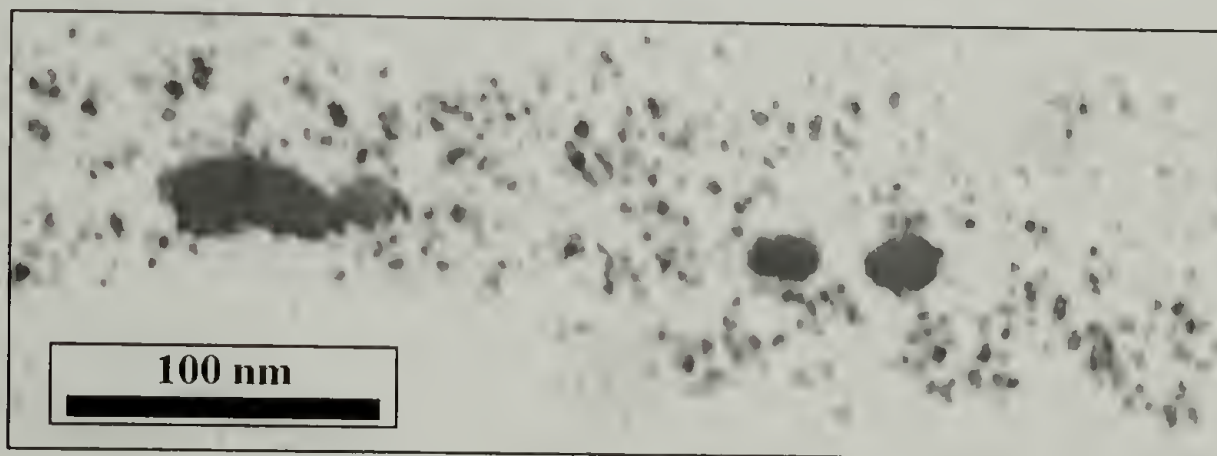


Figure A.1 Silver nanoparticles within P2VP

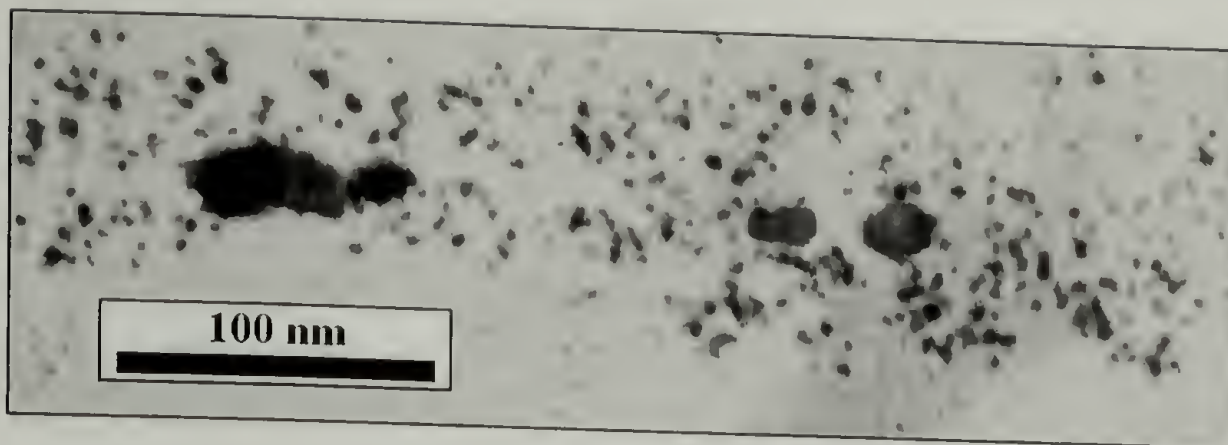


Figure A.2 Silver nanoparticles within P2VP after heating at 120 °C

Within this sample, heating did not have any influence on the nanoparticle movement within the P2VP. This can be seen in the essentially identical TEM images, which show nanoparticles of the same size and location with a difference in the contrast of the background due to development of the prints. This is important as it is in agreement with what has been previously shown for nanoclusters within P2VP homopolymers and also PS-*b*-P2VP copolymers, where nanoparticles do not agglomerate within P2VP. This helps to illustrate that the key to controlling nanoparticle size is the reduction conditions.

BIBLIOGRAPHY

1. Novak, B. M.; "Hybrid Nanocomposite Materials - Between Inorganic Glasses and Organic Polymers;" *Advanced Materials* **1993**, *5*, 422-433.
2. Moller, M.; "Inorganic Nanoclusters in Inorganic Glasses - Novel Materials for Electro-Optical Applications;" *Synthetic Metals* **1991**, *41-43*, 1159-1162.
3. Perrin, J., Despax, B. and Kay, E.; "Optical Properties of Microstructure of Gold-Fluorocarbon Polymer Composite Films;" *Physical Review B* **1985**, *32*, 719-732.
4. Sohn, B. H. and Cohen, R. E.; "Processable Optically Transparent Block Copolymer Films Containing Superparamagnetic Iron Oxide Nanoclusters;" *Chemistry of Materials* **1997**, *9*, 264-269.
5. Tanev, P. T. and Pinnavaia, T. J.; "Biomeimetic Templating of Porous Lamellar Silicas by Vesicular Surfactant Assemblies;" *Science* **1996**, *271*, 1267-1296.
6. Firouzi, A., Kumar, D., Bull, L. M., Besier, T., Sieger, P., Huo, Q., Walker, S. A., Zasadzinski, J. A., Glinka, C., Nicol, J., Margolese, D., Stucky, G. D. and Chmelka, B. F.; "Cooperative Organization of Inorganic-Surfactant and Biomimetic Assemblies;" *Science* **1995**, *267*, 1138-1143.
7. Attard, G. S., Glyde, J. C. and Goltner, C. G.; "Liquid-Crystalline Phases as Templates for the Synthesis of Mesoporous Silica;" *Nature* **1995**, *373*, 366-368.
8. Shao, P. L., Mauritz, K. A. and Moore, R. B.; "[Perfluorosulfonate Ionomer]/[SiO₂-TiO₂] Nanocomposites via polymer-In Situ Sol-Gel Chemistry: Sequential Alkoxide Procedure;" *Journal of Polymer Science: Part B: Polymer Physics* **1996**, *34*, 873-882.
9. Deng, Q., Moore, R. B. and Mauritz, K. A.; "Novel Nafion/ORMOSIL Hybrids via in Situ Sol-Gel Reactions. 1. Probe of ORMOSIL Phase Nanostructures by Infrared Spectroscopy;" *Chemistry of Materials* **1995**, *7*, 2259-2268.
10. Deng, Q., Cable, K. M., Moore, R. B. and Mauritz, K. A.; "Small-Angle X-Ray Scattering Studies of Nafion®/[Silicon Oxide] and Nafion®/ORMOSIL Nanocomposites;" *Journal of Polymer Science: Part B: Polymer Physics* **1996**, *34*, 1917-1923.
11. Deng, Q., Hu, Y., Moore, R. B., McCormick, C. L. and Mauritz, K. A.; "Nafion/ORMOSIL Hybrids via in Situ Sol-Gel Reactions. 3. Pyrene Fluorescence Probe Investigations of Nanoscale Environment;" *Chemistry of Materials* **1997**, *9*, 69-44.
12. Deng, Q., Moore, R. B. and Mauritz, K. A.; "Nafion/ (SiO₂, ORMOSIL, and Dimethylsiloxane) Hybrids Via In situ Sol-Gel Reactions: Characterization of Fundamental Properties;" *Journal of Applied Polymer Science* **1997**, *68*, 747-763.

13. Harmer, M. A., Farneth, W. E. and Sun, Q.; "High Surface Area Nafion Resin/Silica Nanocomposites: A New Class of Solid Acid Catalyst;" *Journal of the American Chemical Society* **1996**, *118*, 7708-7715.
14. Heidekum, A., Harmer, M. and Holderich, W. F.; "Dimerization of α -Methylstyrene over Nafion/Silica Composite Catalysts;" *Catalysis Letters* **1997**, *47*, 243-246.
15. Sakai, T., Takenaka, H. and Torikai, E.; "Oxygen/Nitrogen Separation by a Nafion - Ag Microcomposite Membrane;" *Journal of Membrane Science* **1987**, *31*, 227-234.
16. Simon, P. F. W., Ulrich, R., Spiess, H. W. and Wiesner, U.; "Block Copolymer-Ceramic Hybrid Materials from Organically Modified Ceramic Precursors;" *Chemistry of Materials* **2001**, *13*, 3464-3486.
17. Antonietti, M., Heinz, S., Schmidt, M. and Rosenauer, C.; "Determination of the Micelle Architecture of Polystyrene/Poly(4-vinyl pyridine) Block Copolymers in Dilute Solutions;" *Macromolecules* **1994**, *27*, 3276-2381.
18. Antonietti, M., Forster, S., Hartmann, J. and Oestreich, S.; "Novel Amphiphilic Block Copolymers by Polymer Reactions and Their Use for Solubilization of Metal Salts and Metal Colloids;" *Macromolecules* **1996**, *29*, 3800-3806.
19. Antonietti, M., Thunemann, A. and Wenz, E.; "Synthesis and Characterization of Non-spherical Gold Colloids in Block-Copolymer Micelles;" *Colloid Polymer Science* **1996**, *274*, 795-800.
20. Boontongkong, Y., Cohen, R. E. and Rubner, M. F.; "Selective Electroless Copper Deposition within Block Copolymer Microdomains;" *Chemistry of Materials* **2000**, *12*, 1628-1633.
21. Chan, Y. N. C., Craig, G. S. W., Schrock, R. R. and Cohen, R. E.; "Synthesis of Palladium and Platinum Nanoclusters within Microphase-Separated Diblock Copolymers;" *Chemistry of Materials* **1992**, *4*, 885-894.
22. Chan, Y. N. C., Schrock, R. R. and Cohen, R. E.; "Synthesis of Single Silver Nanoclusters within Spherical Microdomains in Block Copolymer Films;" *Journal of the American Chemical Society* **1992**, *114*, 7295-7296.
23. Chan, Y. N. C., Schrock, R. R. and Cohen, R. E.; "Synthesis of Silver and Gold Nanoclusters within Microphase-Separated Diblock Copolymers;" *Chemistry of Materials* **1992**, *4*, 24-27.
24. Chan, V. Z. H., Hoffman, J., Lee, V. Y., Iatrou, H., Avgeropoulos, A., Hadjichristidis, N., Miller, R. D. and Thomas, E. L.; "Ordered Bicontinuous Nanoporous and Nanorelief Ceramic Films from Self Assembling Polymer Precursors;" *Science* **1999**, *286*, 1716-1719.

25. Ciebien, J. F., Cohen, R. E. and Duran, A.; "Catalytic Properties of Palladium Nanoclusters Synthesized within Diblock Copolymer Films: Hydrogenation of Ethylene and Propylene;" *Supramolecular Science* **1998**, *5*, 31-39.
26. Ciebien, J. F., Clay, R. T., Sohn, B. H. and Cohen, R. E.; "Brief Review of Metal Nanoclusters in Block Copolymer Films;" *New Journal of Chemistry* **1998**, *22*, 685-691.
27. Clay, R. T. and Cohen, R. E.; "Synthesis of Metal Nanoclusters within Microphase-Separated Diblock Copolymers: a "Universal" Approach;" *Supramolecular Science* **1995**, *2*, 183-191.
28. Clay, R. T. and Cohen, R. E.; "Synthesis of Metal Nanoclusters Within Microphase-Separated Diblock Copolymers: ICP-AES Analysis of Metal Ion Uptake;" *Supramolecular Science* **1997**, *4*, 113-119.
29. Clay, R. T. and Cohen, R. E.; "Synthesis of Metal Nanoclusters Within Microphase-Separated Diblock Copolymers: Sodium Carboxylate vs Carboxylic Acid Functionalization;" *Supramolecular Science* **1998**, *5*, 41-48.
30. Cummins, C. C., Schrock, R. R. and Cohen, R. E.; "Synthesis of ZnS and CdS within ROMP Block Copolymer Microdomains;" *Chemistry of Materials* **1992**, *4*, 27-30.
31. Forster, S. and Antonietti, M.; "Amphiphilic Block Copolymer in Structure-Controlled Nanometal Hybrids;" *Advanced Materials* **1998**, *10*, 195-216.
32. Hashimoto, T., Harada, M. and Sakamoto, N.; "Incorporation of Metal Nanoparticles into Block Copolymer Nanodomains via in-Situ Reduction of Metal Ions in Microdomain Space;" *Macromolecules* **1999**, *32*, 6867-6870.
33. Mayer, A. B. R. and Mark, J. E.; "Polymer-Protected, Colloidal Platinum Nanocatalysts;" *Polymer Bulletin* **1996**, *37*, 683-690.
34. Mayer, A. B. R. and Mark, J. E.; "Transition Metal Nanoparticles Protected by Amphiphilic Block Copolymers as Tailored Catalyst Systems;" *Colloid Polymer Science* **1997**, *275*.
35. Mayer, A. B. R.; "Formation of Noble Metal Nanoparticles Within a Polymeric Matrix: Nanoparticle Features and Overall Morphologies;" *Material Science and Engineering C* **1998**, *6*, 155-166.
36. Mayer, A. B. R., Mark, J. E. and Morris, R. E.; "Palladium and Platinum Nanocatalysts Protected by Amphiphilic Block Copolymers;" *Polymer Journal* **1998**, *30*, 197-205.
37. Mayer, A. B. R., Mark, J. E. and Hausner, S. H.; "Palladium and Platinum Nanocatalysts Protected by Polyacids;" *Journal of Applied Polymer Science* **1998**, *70*, 1209-1219.
38. Moller, M. and Lenz, R. W.; "Poly(2-vinyl pyridine) Block Copolymers: Phase Separation and Electric Conduction of Iodine Complexes;" *Makromol Chemistry* **1989**, *190*, 1153-0068.

39. Meiners, J. C., Ritzi, A., Rafailovich, M. H., Sokolov, J., Mlynek, J. and Krausch, G.; "Two-Dimensional Micelle Formation of Polystyrene-poly(vinylpyridine) Diblock Copolymers on Mica Surfaces;" *Applied Physics A* **1995**, *61*, 519-524.
40. Roescher, A. and Moller, M.; "Extraction of Aqueous Gold Sols with Styrene / 2-Vinyl pyridine Block Copolymer in Toluene;" *Advanced Materials* **1995**, *7*, 151-154.
41. Roescher, A. and Moller, M.; "Stabilization of Gold Nanoparticles by Styrene/ethylene oxide Block Copolymers;" *Polymer Preprints* **1996**, *37*, 283-284.
42. Sankaran, V., Cummins, C. C., Schrock, R. R., Cohen, R. E. and Silbey, R. J.; "Small PbS Clusters Prepared via ROMP Block Copolymer Technology;" *Journal of the American Chemical Society* **1990**, *112*, 6858-6859.
43. Sankaran, V., Cohen, R. E., Cummins, C. C. and Schrock, R. R.; "Morphology of Diblock Copolymers of Norbornene and Organometallic Derivatives of Norbornene;" *Macromolecules* **1991**, *24*, 6664-6669.
44. Sankaran, V., Yue, J., Schrock, R. R., Cohen, R. E., Schrock, R. R. and Silbey, R. J.; "Synthesis of Zinc Sulfide Clusters and Zinc Particles within Microphase-Separated Domains of Organometallic Block Copolymers;" *Chemistry of Materials* **1993**, *5*, 1133-1142.
45. Spatz, J. P., Roescher, A., Sheiko, S., Krausch, G. and Moller, M.; "Noble Metal Loaded Block Ionomers: Micelle Organization, Adsorption of Free Chains and Formation of Thin Films;" *Advanced Materials* **1995**, *7*, 731-735.
46. Spatz, J. P., Roescher, A. and Moller, M.; "Gold Nanoparticles in Micellar Poly(Styrene)-b-Poly(ethylene oxide) Films - Size and Interparticle Distance Control in Monoparticulate Films;" *Advanced Materials* **1996**, *8*, 337-340.
47. Spatz, J. P., Mobmer, S. and Moller, M.; "Mineralization of Gold Nanoparticles in Block Copolymer Microemulsion;" *Journal of European Chemistry* **1996**, *2*, 1552-1555.
48. Spatz, J. P., Mobmer, S. and Moller, M.; "Metastable Reverse Globular Micelles and Giant Micellar Wires from Block Copolymers;" *Angewandte Chemie* **1996**, *35*, 1510-1512.
49. Spatz, J. P., Sheiko, S. and Moller, M.; "Ion-Stabilized Block Copolymer Micelles: Film Formation and Intermicellar Interaction;" *Macromolecules* **1996**, *29*, 3220-3226.
50. Spatz, J. P., Mössmer, S., Hartmann, C., Möller, M., Ulm, U., Herzog, T., Krieger, M., Boyen, H.-G., Ziemann, P. and Kabius, B.; "Ordered Deposition of Inorganic Clusters from Micellar Block Copolymer Films;" *Langmuir* **2000**, *16*, 407-415.
51. Spatz, J. P., Herzog, T., Mossmer, S., Ziemann, P. and Moller, M.; "Micellar Inorganic-Polymer Hybrid Systems - A Tool for Nanolithography;" *Advanced Materials* **1999**, *11*, 149-153.

52. Mössmer, S., Spatz, J. P., Möller, M., Aberle, T., Schmidt, J. and Burchard, W.; "Solution Behavior of Poly(styrene)-block-poly(2-vinylpyridine) Micelles Containing Gold Nanoparticles;" *Macromolecules* **2000**, *33*, 4791-4798.
53. Selvan, S. T., Hayakawa, T., Nogami, M. and Möller, M.; "Block Copolymer Mediated Synthesis of Gold Quantum Dots and Novel Gold Polypyrrole Nanocomposites;" *Journal of Physical Chemistry B* **1999**, *103*, 7441-7448.
54. Lengl, G., Plettl, A., Ziemann, P., Spatz, J. P. and Moller, M.; "Excimer Laser Ablation of Gold-Loaded Inverse Polystyrene-block-poly (2-vinylpyridine) Micelles;" *Applied Physics A - Material Science & Processing* **2001**, *72*, 679-685.
55. Heuer, A. H., Fink, D. J., V.J.Laraia, Calvert, P. D., Kendall, K., Messing, G. L., Blackwell, J., Rieke, P. C., Thompson, D. H., Wheeler, A. P., Veis, A. and Calan, A. I.; "Innovative Materials Processing Strategies: A Biomimetic Approach;" *Science* **1992**, *255*, 1098-1105.
56. Weller, H.; "Quantized Semiconductor Particles: A Novel State of Matter for Materials Science;" *Advanced Materials* **1993**, *5*, 88-95.
57. Schmid, G.; "Large Clusters and Colloids. Metals in the Embryonic State;" *Chemistry Review* **1992**, *92*, 1709-1727.
58. Andres, R. P., Averback, R. S., Brown, W. L., Brus, L. E., W. A. Goddard, I., Kaldor, A., Louje, S. G., Moscovits, M., Peercy, P. S., Riley, S. J., Siegel, R. W., Spaepen, F. and Wang, Y. "Research Opportunities on Clusters and Cluster-assembled materials," A Department of Energy, Council on Materials Science Panel Report, 1989.
59. Hache, F., Richard, D. and Ftytzanis, C.; "Optical Nonlinearities of Small Metal Particles: Surface-Mediated Resonance and Quantum Size Effect;" *Journal of the Optical Society of America* **1986**, *3*, 1647-1655.
60. Kreibig, U. and Vollmer, M. *Optical Properties of Metal Clusters*; Springer: Berlin, 1995; Vol. 25.
61. Lee, S.-I., Noh, T. W. and Gains, J. R.; "Optical Studies of Porous Glass Media Containing Silver Particles;" *Physical Review B* **1998**, *37*, 2918-2926.
62. Andrews, M. P. and Ozin, G. A.; "Wrapping Oligomers and Polymers Around Metal Atoms, Metal Clusters and Metal Colloids;" *Chemistry of Materials* **1989**, *1*, 174-187.
63. Maxwell, D. J., Emory, S. R. and Nie, S.; "Nanostructured Thin-Film Materials with Surface-Enhanced Optical Properties;" *Chemistry of Materials* **2001**, *13*, 1082-1088.
64. Manoharan, V. N., Imhof, A., Thorne, J. D. and Pine, D. J.; "Photonic Crystals from Emulsion Templates;" *Advanced Materials* **2001**, *13*, 447-450.

65. Kalinina, O. and Kumacheva, E.; "Polymeric Nanocomposite Material with a Periodic Structure;" *Chemistry of Materials* **2001**, *13*, 35-38.
66. Sharma, V. K. and Baiker, A.; "Superparamagnetic Effects in the Ferromagnetic Resonance of Silical Supported Nickel Particles;" *Journal of Chemical Physics* **1981**, *75*, 5596.
67. Sronstein, L. M., Mirzoeva, E. S., Valetsky, P. M., Solodovnikov, S. P. and Register, R. A.; "Nanodispersed Cobalt Particles in a Thermolysed Poly(acrylonitrile) Matrix;" *Journal of Materials of Chemistry* **1995**, *5*, 1197-1201.
68. Touroude, R., Girard, P., Maire, G., Kizleng, J., Boutonnet-Kizling, M. and Stenius, P.; "Preparation of Colloidal Platinum/Palladium Alloy Particles From Non-ionic Microemulsions: Characterization and Catalytic Behavior;" *Colloids and Surfaces* **1992**, *67*, 9-19.
69. Hirai, H., Nakao, Y. and Toshima, N.; "Preparation of Colloidal Transition Metals in Polymers by Reduction with Alcohols or Ethers;" *Journal of Macromolecular Science & Chemistry* **1979**, *6*, 727-750.
70. Lewis, L. N.; "Chemical Catalysis by Colloids and Clusters;" *Chemistry Review* **1993**, *93*, 2693-2730.
71. Ahmadi, T. S., Wang, Z. L., Green, T. C., Henglein, A. and El-Sayed, M. A.; "Shape-Controlled Synthesis of Colloidal Platinum Nanoparticles;" *Science* **1996**, *272*, 1924-1926.
72. RamachandraRao, V. S., Gupta, R. R., Russell, T. P. and Watkins, J. J.; "Enhancement of Diblock Copolymer Ordering Kinetics by Supercritical Carbon Dioxide Annealing;" *Macromolecules* **2001**, *34*, 7923-7925.
73. Vaia, R. A. and Giannelis, E. P.; "Lattice Model of Polymer Melt Intercalation in Organically-Modified Layered Silicates;" *Macromolecules* **1997**, *30*, 7990-7999.
74. Vaia, R. A. and Giannelis, E. P.; "Polymer Melt Intercalation in Organically-Modified Layered Silicates: Model Predictions and Experiment;" *Macromolecules* **1997**, *30*, 8000-8009.
75. Burnside, S. D., Wang, H.-C. and Giannelis, E. P.; "Direct Polymer Intercalation in Single Crystal Vermiculite;" *Chemistry of Materials* **1999**, *11*, 1055-1060.
76. Schottner, G.; "Hybrid Sol-Gel-Derived Polymers: Applications of Multifunctional Materials;" *Chemistry of Materials* **2001**, *13*, 3422-3435.
77. Rodrigues, D. E., Risch, B. G. and Wilkes, G. L.; "Phase Separation Behavior of Silicate Phases Grown in Poly(methyl methacrylate) by a Sol-Gel Process;" *Chemistry of Materials* **1997**, *9*, 2709-2719.
78. Iler, R. K. *The Chemistry of Silica*; Wiley-Interscience Publication: New York, 1978.

79. Mauritz, K. A., *Sol-Gel Chemistry*, 2002.
80. Ingersoll, C. M. and Bright, F. V.; "Using Sol-Gel-Based Platforms for Chemical Sensors;" *Chemtech* 1997, 27, 26-31.
81. Juangvanich, N. and Mauritz, K. A.; "Polyethersulfone- [Silicon Oxide] Hybrid Materials via In Situ Sol-Gel Reactions for Tetra-Alkoxysilanes;" *Journal of Applied Polymer Science* 1997, 67, 1799-1810.
82. Loy, D. A., Russick, E. M., Yamanaka, S. A., Baugher, B. M. and Shea, K. J.; "Direct Formation of Aerogels by Sol-Gel Polymerizations of Alkoxysilanes in Supercritical Carbon Dioxide;" *Chemistry of Materials* 1997, 9, 2264-2268.
83. Tadros, M. E., Adkins, C. L. J., Russick, E. M. and Youngman, M. P.; "Synthesis of Titanium Dioxide Particles in Supercritical CO₂;" *The Journal of Supercritical Fluids* 1996, 9, 172-176.
84. Hedrick, J. L., Hawker, C. J., Miller, R. D., Twieg, R., Srmivasan, S. A. and Trolisas, M.; "Structure Control in Organic-Inorganic Hybrids Using Hyperbranched High-Temperature Polymers;" *Macromolecules* 1997, 30, 7607-7610.
85. Esumi, K., Tano, T., Torigoe, K. and Meguro, K.; "Preparation and Characterization of Bimetallic Pd-Cu Colloids by Thermal Decomposition of Their Acetate Compounds in Organic Solvents;" *Chemistry of Materials* 1990, 2, 564-567.
86. Nazem, N., *Preparation of Highly Reflective Films by Supercritical Infusion of a Silver Additive into Poly(ether ether ketone)*; Master of Science in Chemical Engineering, Virginia Polytechnic Institute, 1997.
87. Rosenblum, N. *A World History of Photography*; 3rd ed.; Abbeville Press; 1997.
88. Cole, D. H., Shull, K. R., Rehnt, L. and Baldo, P.; "Metal-Polymer Interactions in a Polymer/Metal Nanocomposite;" *Physical Review Letters* 1997, 78, 5006-5009.
89. El-Shall, M. S. and Slack, W.; "Ultrafine Metal Particles in Polymers and the Formation of Periodic Polymer Stripes;" *Macromolecules* 1995, 28, 8456-8458.
90. Miller, T. M. and Whitesides, G. M.; "Isotopic Exchange Reactions Occurring in the Hydrogenation of (1,5-Cyclooctadiene)dialkylplatinum(II) Complexes over Platinum Black;" *Journal of the American Chemical Society* 1988, 110, 3164-3170.
91. Miller, T. M., McCarthy, T. J. and Whitesides, G. M.; "Deuterium-Labeling Experiments Relevant to the Mechanism of Platinum-Catalyzed Hydrogenation of (i)olefin)dialkylplatinum(II) Complexes: Evidence for Isotopic Exchange via Platinum Surface Hydrogen The Stereochemistry of Reduction;" *Journal of the American Chemical Society* 1988, 110, 3156-3163.

92. Miller, T. M., Izumi, A. N., Shib, Y.-S. and Whitesides, G. M.; "Heterogeneous, Platinum-Catalyzed Hydrogenation of (Diolen) dialkylplatinum(II) Complexes: Kinetics;" *Journal of the American Chemical Society* **1988**, *110*, 3146-3156.
93. Blackburn, J. M., Long, D. P. and Watkins, J. J.; "Reactive Deposition of Conformal Palladium Films from Supercritical Carbon Dioxide Solution;" *Chemistry of Materials* **2000**, *12*, 2625-2631.
94. Long, D. P., Blackburn, J. M. and Watkins, J. J.; "Chemical fluid deposition: A hybrid technique for low-temperature metallization;" *Advanced Materials* **2000**, *12*, 913-915.
95. Watkins, J. J., Blackburn, J. M. and McCarthy, T. J.; "Chemical fluid deposition: Reactive deposition of platinum metal from carbon dioxide solution;" *Chemistry of Materials* **1999**, *11*, 213-215.
96. Watkins, J. J. and McCarthy, T.; "Polymer/Metal Nanocomposites in Supercritical CO₂;" *Chemistry of Materials* **1995**, *7*, 1991.
97. Blackburn, J. M., Long, D. P., Cabanas, A. and Watkins, J. J.; "Deposition of Conformal Copper and Nickel Films from Supercritical Carbon Dioxide;" *Science* **2001**, *294*, 141-145.
98. Belluco, U. *Organometallic and Coordination Chemistry of Platinum*; Academic Press: London, 1974.
99. Yue, J. and Cohen, R. E.; "Nanoreactors for Inorganic Cluster Synthesis;" *Supramolecular Science* **1994**, *1*, 117-122.
100. Huang, J., Yang, Y., Yang, B., Liu, S. and Shen, J.; "Preparation and Characterization of Cu₂S/CdS/ZnS Nanocomposite in Polymeric Networks;" *Polymer Bulletin* **1996**, *37*, 679-682.
101. Huo, Q. S., Marogolese, D. I., Ciesla, U., Demuth, D. G., Feng, P. Y., Gier, T. E., Sieger, P., Firouzi, A., Chelka, B. F., Schuth, F. and Stucky, G. D.; "Organization of Organic-Molecules with Inorganic Molecular-Species into Nanocomposite Biphase Arrays;" *Chemistry of Materials* **1994**, *6*, 1176-1191.
102. Moffitt, M., McMahan, L., Pessel, V. and Eisenberg, A.; "Size Control of Nanoparticles in Semiconductor-Polymer Composites. 2. Control via Sizes of Spherical Ionic Microdomains in Styrene-Based Diblock Ionomers;" *Chemistry of Materials* **1995**, *7*, 1185-1192.
103. Moffitt, M. and Eisenberg, A.; "Size Control of Nanoparticles in Semiconductor-Polymer Composites. 1. Control via Multiple Aggregation Numbers in Styrene-Based Random Ionomers;" *Chemistry of Materials* **1995**, *7*, 1178-1184.
104. Yue, J., Sankaran, V., Cohen, R. E. and Schrock, R. R.; "Interconversion of ZnF₂ and ZnS Nanoclusters within Spherical Microdomains in Block Copolymer Films;" *Journal of the American Chemical Society* **1993**, *115*, 4409-4410.

105. Klabunde, K. J., Habdas, J. and Cardenas-Trivino, G.; "Colloidal Metal Particles Dispersed in Monomeric and Polymeric Styrene and Methyl Methacrylate;" *Chemistry of Materials* **1989**, *1*, 481-483.
106. Noguchi, T., Gotoh, K., Yamaguchi, Y. and Deki, S.; "Novel Methods to Disperse Ultrafine Metal Particles into Polymer;" *Journal of Material Science Letters* **1991**, *10*, 477-479.
107. Sayo, K., Deki, S., Noguchi, T. and Goto, K.; "Composite Films Produced by Successive Vapor-Depositions of Nylon-11 and Porphyrin Compounds;" *Thin Solid Films* **1999**, *349*, 276-282.
108. Huang, J., Yang, Y., Yang, B., Liu, S. and Shen, J.; "Synthesis of the CdS Nanoparticles in Polymer Networks;" *Polymer Bulletin* **1996**, *36*, 3237-3340.
109. Saito, R., Okamura, S. I. and Ishizu, K.; "Introduction of Colloid Silver into a Poly(2-vinyl pyridine) Microdomains of Microphase Separated Poly(styrene-b-2-vinyl pyridine) Film;" *Polymer* **1992**, *33*.
110. Wen, J., Dhandapani, B., Oyama, S. T. and Wilkes, G. L.; "Preparation of Highly Porous Silica Gel from Poly(tetramethylene oxide)/Silica Hybrids;" *Chemistry of Materials* **1997**, *9*, 1968-1971.
111. Hedrick, J. L., Miller, R. D., Hawker, C. J., Carter, K. R., Volksen, W., Yoon, D. Y. and Trollsas, M.; "Templating Nanoporosity in Thin-Film Dielectric Insulators;" *Advanced materials* **1998**, *10*, 1049-1053.
112. Nguyen, C. V., Carter, K. R., Hawker, C. J., Hedrick, J. L., Jaffe, R. L., Miller, R. D., Remenar, J. F., Rhee, H.-W., Rice, P. M., Toney, M. F., Trollsas, M. and Yoon, D. Y.; "Low-Dielectric, Nanoporous Organosilicate Films Prepared via Inorganic/Organic Polymer Hybrid Templates;" *Chemistry of Materials* **1999**, *11*, 3080-3085.
113. Moffitt, M. and Eisenberg, A.; "Scaling Relations and Size Control of Block Ionomer Microreactors Containing Different Metal Ions;" *Macromolecules* **1997**, *30*, 4363-4373.
114. Aksay, I. A., Trau, M., Manne, S., Honma, I., Yao, N., Zhou, L., Fenter, P., Eisenberger, P. M. and Gruner, S. M.; "Biomimetic Pathways for Assembling Inorganic Thin Films;" *Science* **1996**, *273*, 892-898.
115. Estroff, L. A. and Hamilton, A. D.; "At the Interface of Organic and Inorganic Chemistry: Bioinspired Synthesis of Composite Materials;" *Chemistry of Materials* **2001**, *13*, 3227-3235.
116. Torrtora, G. j. and Anagnostakos, N. P. *Principles of Anatomy and Physiology*; Sixth ed.; Harper & Row: New York, 1990.
117. Bianconi, P. A., Lin, J. and Strzelecki, A. R.; "Crystallization of an Inorganic Phase Controlled by a Polymer Matrix;" *Nature* **1991**, *349*, 315-317.

118. Lin, J., Cates, E. and Bianconi, P. A.; "A Synthetic Analogue of the Biomineralization Process: Controlled Crystallization of an Inorganic Phase by a Polymer Matrix;" *Journal of the American Chemical Society* **1994**, *116*, 4738-4745.
119. Forster, S.; "Colloids and Polymers; Amphiphilic Block Copolymers;" *Ber. Bunsenges. Phys. Chem.* **1997**, *101*, 1671-1678.
120. Calvert, P. and Rieke, P.; "Biomimetic Mineralization in and on Polymers;" *Chemistry of Materials* **1996**, *8*, 1715-1727.
121. Christiansen, S. C., Zhao, D. Y., Janicke, M. T., Landry, C. C., Stucky, G. D. and Chmelka, B. F.; "Molecularly Ordered Inorganic Frameworks in Layered Silicate Surfactant Mesophases;" *Journal of the American Chemical Society* **2001**, *123*, 4519-4529.
122. Zhao, D., Yang, P., Melosh, N., Feng, J., Chmelka, B. F. and Stucky, G. D.; "Continuous Mesoporous Silica Films with Highly Ordered Large Pore Structures;" *Advanced Materials* **1998**, *10*, 1380-1385.
123. Raman, N. K., Anderson, M. T. and Brinker, C. J.; "Template-Based Approaches to the Preparation of Amorphous Nanoporous Silicates;" *Chemistry of Materials* **1996**, *8*, 1682-1701.
124. Gray, D. H., Hu, S., Juang, E. and Gin, D. L.; "Highly Ordered Polymer - Inorganic Nanocomposites via Monomer Self- Assembly: In-Situ Condensation Approach;" *Advanced Materials* **1997**, *9*, 731-736.
125. Shao, P. L., Mauritz, K. A. and R.B. Moore; "[Perfluorosulfonate Ionomer]/[Mixed Inorganic Oxide] Nanocomposites via Polymer-in Situ Sol-Gel Chemistry;" *Chemistry of Materials* **1995**, *7*, 192.
126. Waller, F. J. and Scoyoc, R. W. V.; "Catalysis with Nafion;" *Chemtech* **1987**, *17*, 438-441.
127. Gierke, T. D., Munn, G. E. and Wilson, F. C.; "The Morphology in Nafion Perfluorinated Membrane Products, as Determined by Wide- and Small-Angle X-Ray Studies;" *Journal of Polymer Science: Polymer Physics Edition* **1981**, *19*, 1687-1704.
128. Mauritz, K. A., Stefanithes, I. D., Daves, S. V., Scheetz, R. W., Pope, R. K., Wilkes, G. L. and Huang, H.-H.; "Microstructural Evolution of a Silicon Oxide Phase in a Perfluorosulfonic Acid Ionomer by an *In Situ* Sol-Gel Reaction;" *Journal of Applied Polymer Science* **1995**, *55*, 181-190.
129. Robertson, M. A. F. and Mauritz, K. A.; "Infrared Investigation of the Silicon Oxide Phase in [Perfluoro-carboxylate/sulfonate(Bilayer)] / [Silicon Oxide] Nanocomposite Membranes;" *Journal of Polymer Science: Part B: Polymer Physics* **1996**, *36*, 595-606.

130. Davis, S. V., Mauritz, K. A. and Moore, R. B.; "Monitoring of pH as a Control in the Initialization of Perfluorosulfonate Ionomer Membranes;" *Polymer Preprints* **1994**, *57*, 419-420.
131. Lodge, T., Hamersky, M. W., Hanley, K. J. and Huang, C.-I.; "Solvent Distribution in Weakly-Ordered Block Copolymer Solution;" *Macromolecules* **1997**, *30*, 6139-6149.
132. Khandpur, A. K., Forster, S., Bates, F. S., Hamley, I. W., Ryan, A. J., Bras, W., Almdal, K. and Mortensen, K.; "Polyisoprene -Polystyrene Diblock Copolymer Phase Diagram near the Order-Disorder Transition;" *Macromolecules* **1995**, *28*, 8796-8806.
133. Bates, F. S., Schulz, M. F., Khandpur, A. K., Foster, S., Rosedale, J. H., Almadal, K. and Mortensen, K.; "Fluctuations, Conformational Asymmetry and Block Copolymer Phase Behavior;" *Faraday Discussions* **1994**, *98*, 7-18.
134. Forster, S., Khandpur, A. K., Zhao, J., Bates, F. S., Hamley, I. W., Ryan, A. J. and Bras, W.; "Complex Phase-Behavior of Polyisoprene-Polystyrene Diblock Copolymers Near the Order-Disorder Transition;" *Macromolecules* **1994**, *27*, 6922-6935.
135. Chen, Z.-R., Kornfield, J. A., Smith, S. D., Grothaus, J. T. and Satkowski, M. M.; "Pathways to Macroscale Order in Nanostructure Block Copolymers;" *Science* **1997**, *277*, 1248-1253.
136. Amundson, K., Helfand, E., Davis, D. D., Quan, X., Patel, S. S. and Smith, S. D.; "Effect of an Electric Field on Block Copolymer Microstructure;" *Macromolecules* **1991**, *24*, 6546-6548.
137. Mansky, P., DeRouchey, J., Russell, T. P., Mayes, J., Pitsikalis, M. and Morkved, T. L.; "Large-Area Domain Alignment in Block Copolymer Thin Films Using Electric Fields;" *Macromolecules* **1998**, *31*, 4399-4401.
138. Morkved, T. L., Lu, M., Urbas, A. M., Ehrichs, E. E., Jaeger, H. M., Mansky, P. and Russell, T. P.; "Local Control of Microdomain Orientation in Diblock Copolymer Thin Films with Electric Fields;" *Science* **1996**, *273*, 931-933.
139. Schmidt-Winkel, P., Lukens, W. W., Zhao, D. Y., Yang, P. D., Chmelka, B. F. and Stucky, G. D.; "Mesocellular Siliceous Foams with Uniformly Sized Cells and Windows;" *Journal of the American Chemical Society* **1999**, *121*, 254-255.
140. Zhao, D., Yang, P., Chmelka, B. F. and Stucky, G. D.; "Multiphase Assembly of Mesoporous-Macroporous Membranes;" *Chemistry of Materials* **1999**, *11*, 1174-1178.
141. Aiken, J. D. and Finke, R. G.; "Nanocluster Formation Synthetic, Kinetic, and Mechanistic Studies. The Detection of, and Then Methods to Avoid, Hydrogen Mass-Transfer Limitations in the Synthesis of Polyoxoanion- and Tetrabutylammonium-Stabilized, Near-Monodisperse 40 +/- 6 Angstrom Rh(0) Nanoclusters;" *Journal of the American Chemical Society* **1998**, *120*, 9545-9554.

142. Watkins, J. J., *Chemistry in Supercritical Fluid-Swollen Polymers : Direct Synthesis of Polymer/Polymer and Polymer/Metal Composites*; Ph.D. in Polymer Science and Engineering, University of Massachusetts at Amherst, 1997.
143. Kane, R. S., Cohen, R. E. and Silbey, R.; "Semiconductor Nanocluster Growth within Polymer Films;" *Langmuir* **1999**, *15*, 39-43.
144. LaMer, V. K. and Dinegar, R. H.; "Theory, Production and Mechanism of Formation of Monodispersed Hydrosols;" *Journal of the American Chemical Society* **1950**, *72*, 4874-4854.
145. Cole, D. H., Shull, K. R., Baldo, P. and Rehnt, L.; "Dynamic Properties of a Model Polymer/Metal Nanocomposite: Gold Particles in Poly(tert-butyl acrylate);" *Macromolecules* **1999**, *32*, 771-779.
146. Green, P. F., Palmstrum, C. J., Mayer, J. W. and Kramer, E. J.; "Marker Displacement Measurements of Polymer-Polymer Interdiffusion;" *Macromolecules* **1985**, *18*, 501-507.
147. Kunz, M. S., Shull, K. R. and Kellock, A. J.; "Colloidal Gold Dispersions in Polymeric Matrices;" *Journal of Colloid and Interface Science* **1993**, *156*, 240-249.
148. Shull, K. R. and Kellock, A. J.; "Metal Particle Adsorption and Diffusion in a Model Polymer/Metal Composite System;" *Journal of Polymer Science: Part B: Polymer Physics* **1995**, *33*, 1417-1422.
149. Kunz, M. S., Shull, K. R. and Kellock, A. J.; "Morphologies of Discontinuous Gold Films on Amorphous Polymer Substrates;" *Journal of Applied Physics* **1992**, *72*, 4458-4460.
150. Tsai, W. H., Boerio, F. J., Clarson, S. J., Parsonage, E. E. and Tirrell, M.; "Characterization of Adsorbed 2-Vinylpyridine/ Styrene Diblock Copolymers on Silver Surfaces Using Surface-Enhanced Raman Scattering;" *Macromolecules* **1991**, *24*, 2538-2545.
151. Odian, G. G. *Principles of Polymerization*; John Wiley & Sons:, 1991.
152. McHugh, M. and Krukoni, V. *Supercritical Fluid Extraction*; Second ed.; Butterworth-Heinemann: Newton, 1994.
153. Johnson, K. P.; "Safer Solutions for Chemists;" *Nature* **1994**, *368*, 187-188.
154. Kaupp, G.; "Reactions in Supercritical Carbon Dioxide;" *Angewandte Chemie* **1994**, *33*, 1452-1455.
155. Wu, B. C., Klein, M. T. and Sandler, S. I.; "Solvent Effects on Reactions in Supercritical Fluids;" *Industrial Engineering Chemical Research* **1991**, *30*, 822-828.
156. Hyatt, J. A.; "Liquid and Supercritical Carbon Dioxide as Organic Solvents;" *Journal of organic Chemistry* **1984**, *49*, 5097-5101.

157. Cansell, F., Cheavlier, B., Demourgues, A., Etourneau, J., Even, C., Garrabos, Y., Pessy, V., Petit, S., Tressaud, A. and Weil, F.; "Supercritical Fluid Processing: A New Route for Material Synthesis;" *Journal of Materials Chemistry* **1999**, *9*.
158. Watkins, J. J. and McCarthy, T. J.; "Polymerization of Styrene in Supercritical CO₂-Swollen Poly(chlorotrifluoroethylene);" *Macromolecules* **1995**, *28*, 4067-4074.
159. NIST, *NIST Chemistry WebBook*, **2002**.
160. Cooper, A. I.; "Polymer Synthesis and Processing Using Supercritical Carbon Dioxide;" *Journa of Materials Chemistry* **2000**, *10*, 207-234.
161. Lee, M. H., Tzoganakis, C. and Park, C. B.; "Extrusion of PE/PS blends with Supercritical Carbon Dioxide;" *Polymer Engineering and Science* **1998**, *38*, 1112-1120.
162. Lee, M. H., Park, C. B. and Tzoganakis, C.; "Measurements and Modeling of PS/Supercritical CO₂ Solution Viscosities;" *Polymer Engineering and Science* **1999**, *39*, 99-109.
163. Stafford, C. M., Russell, T. P. and McCarthy, T. J.; "Expansion of Polystyrene Using Supercritical Carbon Dioxide: Effects of Molecular Weight, Polydispersity, and Low Molecular Weight Components;" *Macromolecules* **1999**, *32*, 7610-7616.
164. Shiho, H. and DeSimone, J. M.; "Dispersion Polymerization of Acrylonitrile in Supercritical Carbon Dioxide;" *Macromolecules* **2000**, *33*, 1565 -1569.
165. Canelas, D. A., Betts, D. E., DeSimone, J. M., Yates, M. Z. and Johnston, K. P.; "Poly(vinyl acetate) and Poly(vinyl acetate-co-ethylene) Latexes via Dispersion Polymerizations in Carbon Dioxide;" *Macromolecules* **1998**, *31*, 6794-6805.
166. Quadir, M. A., DeSimone, J. M., Herk, A. M. v. and German, A. L.; "Pulsed-Laser Polymerization of Methyl Methacrylate in Liquid and Supercritical Carbon Dioxide;" *Macromolecules* **1998**, *31*, 6481 -6485.
167. Triolo, R., Triolo, A., Triolo, F., Steytler, D. C., Lewis, C. A., Heenan, R. K., Wignall, G. D. and DeSimone, J. M.; "Structure of Diblock Copolymers in Supercritical Carbon Dioxide and Critical Micellization Pressure;" *Physical Review E* **2000**, *61*, 4640-4643.
168. Berens, A. R., Huvad, G. S., Richard, W. K. and Kunig, F. W.; "Application of Compress Carbon Dioxide in the Incorporation of Additives into Polymers;" *Journal of Applied Polymer Science* **1992**, *46*, 231-242.
169. Mokdad, A., Dubault, A. and Monnerie, L.; "Sorption and Diffusion of Carbon Dioxide in Single-Phase Polystyrene/Poly(vinyl methylether) Blends;" *Journal of Polymer Science: Part B: Polymer Physics* **1996**, *34*, 2723-3730.

170. Wissinger, R. G. and Paulatis, M. E.; "Swelling and Sorption in Polymer-CO₂ Mixtures at Elevated Pressures;" *Journal of Polymer Science: Part B: Polymer Physics* **1987**, *25*, 2497-2510.
171. Wang, W.-C. V., Kramer, E. J. and Sachse, W. H.; "Effects of High-Pressure CO₂ on the Glass Transition Temperature and Mechanical Properties of Polystyrene;" *Journal of Polymer Physics: Polymer Physics Edition* **1982**, *20*, 1371-1384.
172. Chiou, J. S., Barlow, J. W. and Paul, D. R.; "Plasticization of Glassy Polymers by CO₂;" *Journal of Applied Polymer Science* **1985**, *30*, 2633-2642.
173. Kwag, C., Gerhardt, L. J., Khan, V., Gulari, E. and Manke, C. W.; "Plasticization of Polymer Melts with Dense or Supercritical Carbon Dioxide;" *Polymeric Materials: Science & Engineering* **1996**, *74*, 183.
174. RamachandraRao, V. S. and Watkins, J. J.; "Phase Separation in Polystyrene-Poly(vinyl methyl ether) Blends Dilated with Compressed Carbon Dioxide;" *Macromolecules* **2000**, *33*, 5143-5152.
175. Bae, Y. C. and Gulari, E.; "Viscosity Reduction of Polymeric Liquid by Dissolved Carbon Dioxide;" *Journal of Applied Polymer Science* **1997**, *64*, 459-466.
176. Wissinger, R. G. and Paulatis, M. E.; "Glass Transitions in Polymer/CO₂ Mixtures at Elevated Pressures;" *Journal of Polymer Science: Part B: Polymer Physics* **1991**, *29*, 631-633.
177. Mansky, P., Tsui, O. K. C., Russell, T. P. and Gallot, Y.; "Phase Coherence and Microphase Separation Transitions in Diblock Copolymer Thin Films;" *Macromolecules* **1999**, *32*, 4832-4837.
178. Dooley, K. M., Launey, D., Becnel, J. M. and Caines, T. L. *Measurement and Modeling of Supercritical Fluid Extraction from Polymeric Matrices*, 1995; Vol. 608.
179. Chapman, B. R., Gochanour, C. R. and Paulaitis, M. E.; "CO₂-Enhanced Diffusion of Azobenzene in Glassy Polystyrene Near the Glass Transition;" *Macromolecules* **1996**, *29*, 5635-5649.
180. Gupta, R. R., RamachandraRao, V. S., Russell, T. P. and Watkins, J. J.; "Interaction of Polymer Thin Films with Supercritical Carbon Dioxide: A High-Pressure Neutron Reflectivity Study;" *Polymeric Materials: Science & Engineering* **2000**, *84*, 221-222.
181. Russell, T. P., Karis, T. E., Gallot, Y. and Mayes, A. M.; "A Lower Critical Ordering Transition in a Diblock Copolymer Melt;" *Nature* **1994**, *368*, 729-731.
182. Lodge, T. P., Hanley, K. J., Huang, C. I. and Ryu, C. Y.; "Order-Order and Order-Disorder Transitions in Block Copolymer Solutions and Melts;" *Polymeric Materials: Science & Engineering* **2001**, *78*, 113.

183. Ryu, C. Y. and Lodge, T. P.; "Thermodynamic Stability and Anisotropic Fluctuations in the Cylinder-to-Sphere Transition of a Block Copolymer;" *Macromolecules* **1999**, *32*, 7190-7201.
184. Dormidontova, E. E. and Lodge, T. P.; "The Order-Disorder Transition and the Disordered Micelle Regime in Sphere-Forming Block Copolymer Melts;" *Macromolecules* **2001**, *34*, 9143-9155.
185. Watkins, J. J., Brown, G. D., RamachandraRao, V. S., Pollard, M. A. and Russell, T. P.; "Phase Separation in Polymer Blends and Diblock Copolymers Induced by Compressible Solvents;" *Macromolecules* **1999**, *32*, 7737-7740.
186. Watkins, J. J., Brown, G. D., Pollard, M. A., RamachandraRao, V. S. and Russell, T. P.; "Transitions in Polymer Blends and Block Copolymers Induced by Phase-Selective Dilation with Supercritical CO₂;" *Polymeric Materials: Science & Engineering* **1998**, *216*, 310-311.
187. Watkins, J. J., Brown, G. D., Pollard, M. A., RamachandraRao, V. S. and Russell, T. P.; "Phase Transitions in Polymer Blends and Block Copolymers Induced by Dilation with Supercritical CO₂;" *Polymeric Materials: Science & Engineering* **1998**, *215*, 70-71.
188. Vogt, B. D., Brown, G. D., RamachandraRao, V. S. and Watkins, J. J.; "Phase Behavior of Nearly Symmetric Polystyrene-Block-Polyisoprene Copolymers in the Presence of CO₂ and Ethane;" *Macromolecules* **1999**, *32*, 7907-7912.
189. Russell, T. P., Watkins, J. J., RamachandraRao, V. S., Brown, G. D. and Pollard, M. A.; "The Influence of Supercritical Fluids on Polymer Mixtures and Block Copolymers;" *Polymeric Materials: Science & Engineering* **1998**, *216*.
190. Li, D. and Han, B.; "Phase Behavior of Supercritical CO₂/Styrene/Poly(vinyl chloride) System and Synthesis of Polystyrene/Poly(vinyl chloride) Composites;" *Macromolecules* **2000**, *33*, 4555-4560.
191. Kordikowski, A., York, P. and Latham, D.; "Resolution of Ephedrine in Supercritical CO₂: A Novel Technique for the Separation of Chiral Drugs;" *Journal of Pharmaceutical Sciences* **1999**, *88*, 768.
192. Park, Y., Curtis, C. W. and Roberts, C. B.; "Formation of Nylon Particles and Fibers Using Precipitation with a Compressed Antisolvent;" *Industrial & Engineering Chemistry Research* **2002**, *41*, 1504-1510.
193. Jung, J. and Perrut, M.; "Particle Design Using Supercritical Fluids: Literature and Patent Survey;" *Journal of Supercritical Fluids* **2001**, *20*, 179-219.
194. Cabanas, A., Darr, J. A., Lesterb, E. and Poliakoff, M.; "A Continuous and Clean One-Step Synthesis of Nano-Particulate Ce_{1-x}Zr_xO₂ Solid Solutions in Near-Critical Water;" *Chemical Communications* **2000**, *11*, 901-902.

195. Shah, P. S., Holmes, J. D., Doty, R. C., Johnston, K. P. and Korgel, B. A.; "Steric Stabilization of Nanocrystals in Supercritical CO₂ Using Fluorinated Ligands;" **2000**, *122*, 4245-4246.
196. Nandi, M., Conklin, J. A., Salvati, L. and Sen, A.; "Molecular Level Ceramic/Polymer Composites. 2. Synthesis of Polymer-Trapped Silica and Titania Nanoclusters;" *Chemistry of Materials* **1991**, *3*, 201-296.
197. Mark, J. E.; "Ceramic-Reinforced Polymers and Polymer-Modified Ceramics;" *Polymer Engineering and Science* **1996**, *36*, 2905-2920.
198. Monnier, A., Schuth, F., Huo, Q., Kumar, D., Maroglese, D., Maxwell, R. S., Stucky, G. D., Krishnamurty, M., Petroff, P., Firouzi, A., Janicke, M. and Chmelka, B. F.; "Cooperative Formation of Inorganic-organic Interfaces in the Synthesis of Silicate Mesostructures;" *Science* **1993**, *261*, 1299-1303.
199. Wen, J. and Wilkes, G. L.; "Organic/Inorganic Hybrid Network Materials by the Sol-Gel Approach;" *Chemistry of Materials* **1996**, *8*, 1667-1681.
200. Coan, C. R. and King, A. D.; "Solubility of Water in Compressed Carbon Dioxide, Nitrous Oxide, and Ethane. Evidence for Hydration of Carbon Dioxide and Nitrous Oxide in the Gas Phase;" *Journal of the American Chemical Society* **1971**, *93*, 1847-1862.
201. Wenzel, H. and Rupp, W.; "Calculation of Phase Equilibria in Systems Containing Water and Supercritical Components;" *Chemical Engineering Science* **1978**, *33*, 683-687.
202. Houghton, G., McLean, A. M. and Ritchie, P. D.; "Compressibility, Fugacity, and Water-Solubility of Carbon Dioxide in the Region 0-36 atm and 0-100 °C;" *Chemical Engineering Science* **1957**, *6*, 132-137.
203. ASTM *X-Ray Powder Data File, Inorganic*; American Society for Testing Materials: Philadelphia, 1960; Vol. 2.
204. Moffitt, M., Vali, H. and Eisenberg, A.; "Spherical Assemblies of Semiconductor Nanoparticles in Water-Soluble Block Copolymer;" *Chemistry of Materials* **1998**, *10*, 1021-1028.
205. Jenkins, R. and Snyder, R. L. *Introduction to X-Ray Powder Diffraction*; Wiley: New York, 1996.
206. Blackburn, J. M., *Chemical Fluid Deposition: Reactive Deposition of Thin Metal Films From Supercritical Carbon Dioxide Solutions*; Ph.D. in Chemical Engineering, University of Massachusetts, 2001.
207. Long, D. P., *Unpublished Results*.
208. Vogel, A. I. *Vogel's Qualitative Inorganic Analysis*; Wiley: New York, 1987.

209. Schulz, M. F., Khandpur, A. K., Bates, S. F., Almdal, K., Mortensen, K., Hajduk, D. A. and Gruner, S. M.; "Phase Behavior of Polystyrene-Poly(2-vinylpyridine) Diblock Copolymers;" *Macromolecules* **1996**, *29*, 2857-2867.
210. Liu, Y., Quinn, J., Rafailovich, M. H., Sokolov, J., Zhong, X. and Eisenberg, A.; "Neutron Reflectivity Study of Poly(4-vinylpyridine) - Deuterated Polystyrene (P4VP-dPS) Diblock Brushes;" *Macromolecules* **1995**, *28*, 6347-6348.
211. Han, C. D., Vaidya, N. Y., Kim, D., Shin, G., Yamaguchi, D. and Hashimoto, T.; "Lattice Disordering/Ordering and Demicellization/Micellization Transitions in Highly Asymmetric Polystyrene-block-Polyisoprene Copolymers;" *Macromolecules* **2000**, *33*, 3767-3780.

